Computational Intelligence and Neuroscience

EEG-Based Biometrics: Challenges and Applications

Lead Guest Editor: Victor Hugo C. De Albuquerque
Guest Editors: Robertas Damaševičius, João Manuel R. S. Tavares, and Plácido R. Pinheiro

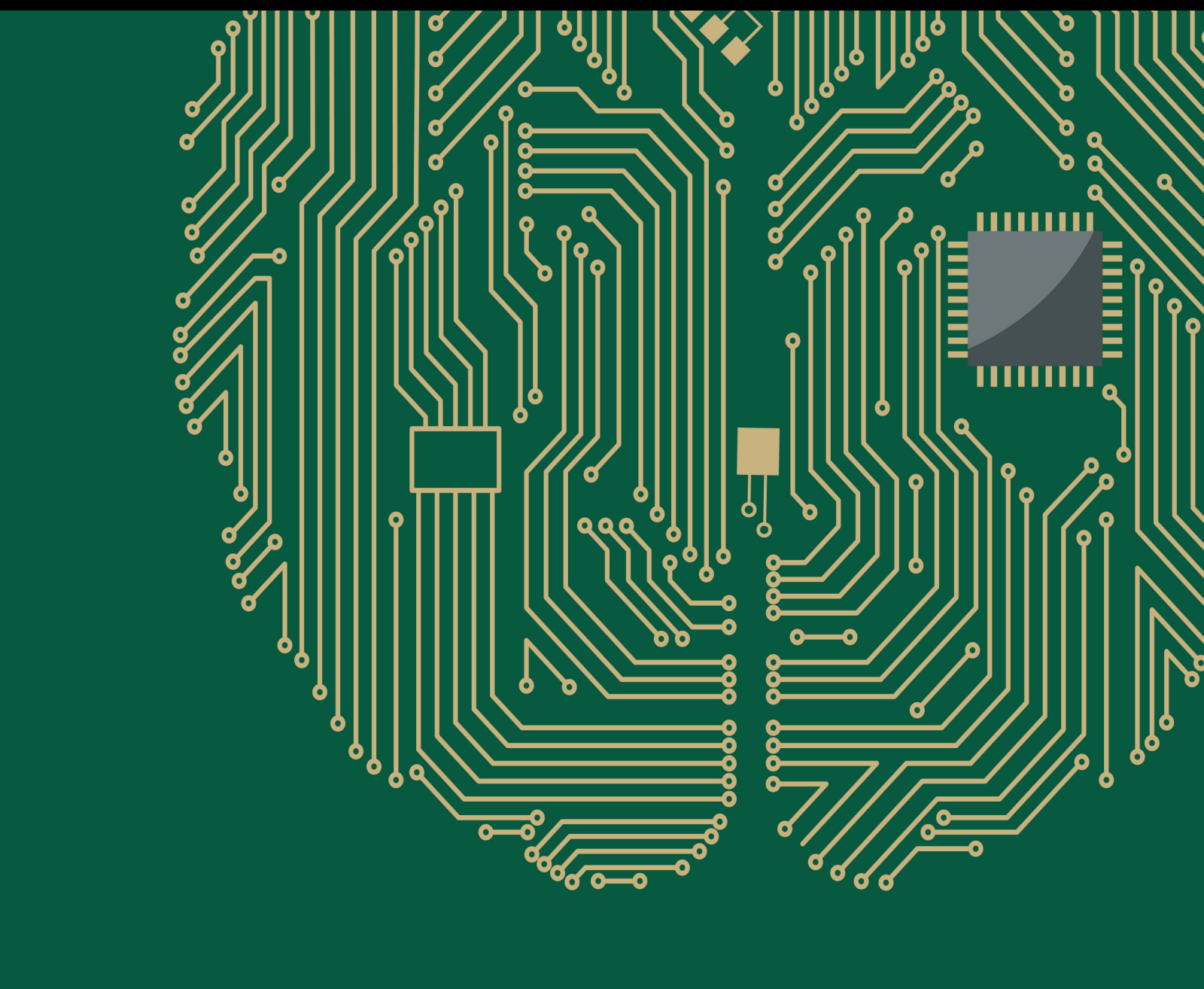

EEG-Based Biometrics: Challenges and Applications

Computational Intelligence and Neuroscience

EEG-Based Biometrics: Challenges and Applications

Lead Guest Editor: Victor Hugo C. De Albuquerque
Guest Editors: Robertas Damaševicius, João Manuel R. S. Tavares, and Plácido R. Pinheiro

Editorial Board

Contents

Hindawi
Computational Intelligence and Neuroscience
Volume 2018, Article ID 5483921, 2 pages
https://doi.org/10.1155/2018/5483921

Editorial

EEG-Based Biometrics: Challenges And Applications

Victor Hugo C. de Albuquerque,[1] **Robertas Damaševičius**,[2] **João Manuel R. S. Tavares**,[3] **and Plácido R. Pinheiro**[1]

[1]*Programa de Pós Graduação em Informática Aplicada, Laboratório de Bioinformática, Universidade de Fortaleza, Fortaleza, CE, Brazil*
[2]*Department of Software Engineering, Kaunas University of Technology, Kaunas, Lithuania*
[3]*Instituto de Ciência e Inovação em Engenharia Mecânica e Engenharia Industrial, Departamento de Engenharia Mecânica, Faculdade de Engenharia, Universidade do Porto, Porto, Portugal*

Correspondence should be addressed to Victor Hugo C. de Albuquerque; victor.albuquerque@unifor.br

Received 13 May 2018; Accepted 13 May 2018; Published 7 June 2018

1. Introduction

Biometrics is aimed at recognizing individuals based on physical, physiological, or behavioural characteristics of a human body such as fingerprint, gait, voice, iris, and gaze. Currently, the state-of-the-art methods for biometric authentication are being incorporated in various access control and personal identity management applications. While the hand-based biometrics (including fingerprint) have been the most often used technology so far, there is growing evidence that electroencephalogram (EEG) signals collected during a perception or mental task can be used for reliable person recognition. However, the domain of EEG-based biometry still faces the problems of improving the accuracy, robustness, security, privacy, and ergonomics of the EEG-based biometric systems and substantial efforts are needed towards developing efficient sets of stimuli (visual or auditory) that can be used of person identification in Brain-Computer Interface (BCI) systems and applications.

There are still many challenging problems involved in improving the accuracy, efficiency, and usability of EEG-based biometric systems and problems related to designing, developing, and deploying new security-related BCI applications, for example, for personal authentication on mobile devices, augmented and virtual reality, headsets, and Internet.

This special issue is aimed to introduce the recent advances of EEG-based biometrics and addresses the challenges in developing the EEG-based biometry systems for various practical applications, while proposing new ideas and directions for future development, such as data preprocessing, feature extraction, recognition, and matching; signal processing and machine learning techniques; EEG biometric based passwords and encryption; cancellable EEG biometrics; multimodal (EEG, EMG, ECG, and other biosignals) biometrics; pattern recognition techniques; protocols, standards, and interfaces; security and privacy; information fusion for biometrics involving EEG data, virtual environment applications, stimuli sets, and passive BCI technology.

2. Computational Intelligence Techniques

This special issue 6 published original works selected from 13 submitted articles, addressing new trends in the field from several novel methods and techniques used in different applications, for instance, A. Gumaei et al. proposed a novel method based on autoencoder and regularized extreme learning machine to make recognition faster by reducing the number of palmprint features without degrading the accuracy of the classifier, in which the results were high compared to the recent studies and proved the robustness and efficiency of the proposed technique.

R. Damaševičius et al. presented a cryptographic authentication approach (using a dataset of electroencephalography data collected from 42 subjects) based on the discrete logarithm problem and Bose-Chaudhuri-Hocquenghem codes

for security analysis, showing that the proposed biometric user authentication method presented satisfactory results.

K. A. A. Cruz et al. evaluated n-iterative exponential forgetting factor for EEG signals parameter estimation, showing the effectiveness of technique thought of the comparison of three forms of iterative-recursive uses of the Exponential Forgetting Factor combined with a linear function to identify a synthetic stochastic signal.

M. Fazlyyyakhmatov et al. investigated a cortical activity during the cognitive task consisted of binocular viewing of a false image, which is observed when the eyes are refocused out of the random-dot stereogram plane (3D phenomenon) and concluded that during stereo perception of the false image the power of alpha-band activity decreased in the left parietal area and bilaterally in frontal areas of the cortex, while activity in beta-1, beta-2, and delta frequency bands remained unchanged.

N. Yu et al. evaluated a new sparse coding algorithm using p-norm optimization in single-trial evoked potentials (EPs) estimating, in which we can track the underlying EPs corrupted by α-stable distribution noise, trial-by-trial, without the need to estimate the α value. Simulations and experiments on human visual evoked potentials and event-related potentials are carried out to examine the performance of the proposed approach, concluding that the proposed method is effective in estimating single-trial EPs under impulsive noise environment.

R. D. de C. Silva et al. proposed a novel tool based on augmented reality to reduce the stigma related to schizophrenia, simulating the psychotic symptoms typical of schizophrenia and simulating sense perception changes in order to create an immersive experience capable of generating pathological experiences of a patient with schizophrenia, presenting a robust tool, quite realistic and, thus, very promising to reduce stigma associated with schizophrenia by instilling in the observer a greater comprehension of any person during a schizophrenic outbreak, whether a patient or a family member.

Acknowledgments

The guest editors wish to thank all the authors and reviewers for helping to improve the works published here.

Victor Hugo C. de Albuquerque
Robertas Damaševičius
João Manuel R. S. Tavares
Plácido R. Pinheiro

Hindawi
Computational Intelligence and Neuroscience
Volume 2018, Article ID 8041609, 13 pages
https://doi.org/10.1155/2018/8041609

Research Article

An Improved Multispectral Palmprint Recognition System Using Autoencoder with Regularized Extreme Learning Machine

Abdu Gumaei,[1] **Rachid Sammouda**,[1] **Abdul Malik S. Al-Salman**,[1] **and Ahmed Alsanad**[2]

[1]*Department of Computer Science, King Saud University, Riyadh, Saudi Arabia*
[2]*Department of Information Systems, King Saud University, Riyadh, Saudi Arabia*

Correspondence should be addressed to Abdu Gumaei; abdugumaei@gmail.com

Received 29 December 2017; Revised 31 March 2018; Accepted 19 April 2018; Published 27 May 2018

Academic Editor: Plácido R. Pinheiro

Multispectral palmprint recognition system (MPRS) is an essential technology for effective human identification and verification tasks. To improve the accuracy and performance of MPRS, a novel approach based on autoencoder (AE) and regularized extreme learning machine (RELM) is proposed in this paper. The proposed approach is intended to make the recognition faster by reducing the number of palmprint features without degrading the accuracy of classifier. To achieve this objective, first, the region of interest (ROI) from palmprint images is extracted by David Zhang's method. Second, an efficient normalized Gist (NGist) descriptor is used for palmprint feature extraction. Then, the dimensionality of extracted features is reduced using optimized AE. Finally, the reduced features are fed to the RELM for classification. A comprehensive set of experiments are conducted on the benchmark MS-PolyU dataset. The results were significantly high compared to the state-of-the-art approaches, and the robustness and efficiency of the proposed approach are revealed.

1. Introduction

Biometrics is an effective technology used for security purposes in many applications [1]. Recently, it has gained more and more attention of researchers throughout the world. A number of biometric traits, including fingerprint, face, iris, gait, key-stroke, and palmprint, have been widely used according to the suitability of the applications [2–4]. Comparing to other biometric traits, palmprint has a strong stability, low distortion, and high uniqueness [5]. Unfortunately, palmprint patterns may be affected by some factors, such as variations in illumination, changes in orientation, and sensor noise that may lead to misclassification. Variations in illumination and changes in orientation of multispectral palmprint images can extremely affect the capability of such systems to recognize the individuals.

Several works have been proposed to solve these issues by using different feature extraction, reduction, and matching methods. These works can be categorized into four groups: line-based, statistic-based, subspace-based, and coding-based approaches.

The line-based approaches are proposed to detect the palmprint lines by using edge detector methods. For example, Han et al. [6] have proposed a method based on Sobel edge detector with morphological operations to extract the line features from palmprint images. Wu et al. [7] used the Sobel mask to compute the magnitudes of palmprint lines and project these magnitudes along both the x- and y-axes for generating the histograms as discriminative features.

Statistic-based approaches are also proposed in different studies and attained reasonable results [8–10]. There are several statistics that have been used in this group of approaches, such as Hu moments, Zernike moments, variance, mean, standard deviation, energy and histograms of local binary patterns. A number of transforms have also been utilized to extract the useful features from palmprint images. For example, Gan and Zhou [11] used a wavelet transform to convert the palmprint image into a small number of wavelet coefficients, then compute the variance and mean of these coefficients, and generate a feature vector of palmprint image. Li et al. [12] proposed a two-phase test sample representation (TPTSR) method as feature extractor for effective palmprint

recognition. A Coarse to Fine K-Nearest Neighbor Classifier (CFKNNC) is proposed by Xu et al. [13] to improve the accuracy of palmprint recognition system. However, the CFKNNC is a more complicated than FKNNC because it consists of a large number of steps. Zhang and Gu [14] proposed a novel palmprint recognition method based on RBF kernel mapping function. In this method, a linear combination of all training dataset in the feature space is used to represent the testing dataset. A different set of methods based on texture features of palmprint is also introduced by some researchers in the area of palmprint recognition. These methods are proposed to compute the statistical features after extracting the palmprint textures using some filters and transforms such as Gabor wavelet, Gaussian derivative filters, wavelet transform, and Fourier transform. In this context, Xu et al. [15] proposed a method for palmprint recognition based on a quaternion matrix. This method utilized the principal components analysis (PCA) and wavelet transform for extracting the palmprint texture features from the quaternion matrix. For palmprint matching, the Euclidean distance classifier is used to compute the similarity between the extracted features.

Subspace-based methods are used to extract subspace features for improving the palmprint recognition system. Various representative subspace learning approaches such as principal components analysis (PCA), linear discriminant analysis (LDA), and independent component analysis (ICA). Lu et al. [16] proposed an approach to transform the original palmprint images into a small feature space set, called eigenpalms. In fact, the eigenpalms are the eigenvectors of the PCA, representing the training dataset of the palmprint images. In this method, Euclidean distance classifier is used for matching. In [17], a vertical and horizontal two-dimensional LDA (2DLDA) are applied to extract the Gabor features, then a distance-based adaptive method is employed to merge the vertical and horizontal features. Recently, Xu et al. [18] proposed a multispectral palmprint recognition approach using digital Shearlet transform and multiclass projection extreme learning machine. The approach used the singular value decomposition (SVD) to compute the projection matrix from the training dataset, after that, kth singular vector is extracted depending on the largest values in the singular matrix. Lu et al. [19] presented a multispectral palmprint recognition approach using fast and adaptive bidimensional empirical mode decomposition (FABEMD) method with tensor flow extreme learning machine (TFELM) classifier. In this approach, the multispectral images are decomposed into their bidimensional intrinsic mode functions by the FABEMD method; then the fusion coefficients are constructed at the decomposition level by using weighted Fisher criterion method. The experimental results of [18, 19] have demonstrated the capability of ELM classifier to recognize the palmprint patterns. However, ELM is not robust to translation, rotation, and other changes of palmprint templates and needs some regularization parameters for generality during the training phase. El-Tarhouni et al. [20] proposed a method for multispectral palmprint feature extraction. In this method, a kernel discriminant analysis (KDA) is used to reduce the dimensionality of features. For classification, a KNN classifier is used; however, it is not robust to inter- and intraclass variations of palmprint.

Coding-based approaches are the fourth group which is usually widely used in many works of palmprint recognition. Some coding methods are used to generate palmprint codes such as palm code [5], fusion code [21], ordinal code [22], competitive code [23], and Log-Gabor code [24]. For instance, Kong et al. [21] proposed a method for encoding the phases and responses of the six Gabor filters as a fusion code which is used later for competition. Jia et al. [25] proposed a robust line orientation code (RLOC) method to extract the orientation features of palmprint. A modified finite Radon transform is used in this method and the extracted feature vector is utilized as a competitive code. The classification step is performed using KNN classifier. However, the large size of features may lead to overfitting of palmprint classification. Hong et al. [26] proposed an approach to extract the palmprint orientation features. In this approach, rough feature and fine feature are extracted using Block Dominant Orientation Code (BDOC) and Block-based Histogram of Oriented Gradient (BHOG), respectively. Unfortunately, this approach may be affected by changes in illumination and shadowing of palmprint images. Fei et al. [27] proposed a half orientation code (HOC) for palmprint feature extraction. The authors used the half of Gabor filters to represent the HOC. Another method in [28] is introduced to extract the palmprint features based on a double orientation code (DOC) of Gabor filters with nonlinear classifier for matching. For evaluation, the methods in [27, 28] are tested using MS-PolyU database of multispectral palmprint images.

To improve the efficiency and performance of palmprint recognition system, we propose a novel multispectral palmprint recognition approach based on AE and RELM with efficient NGist descriptor. NGist is an extended version of Gist descriptor, used for describing the spatial envelope of the palmprint image. In NGist descriptor, we added a new step, named a variation tolerance step to cancel out the variation of average intensity values computed from different blocks of different scales and orientations. The variation tolerance step normalizes the palmprint features using Euclidean norm reducing the variations of features values due to changes in illumination, shadowing, and orientations. Hence, it can summarize the normalized features of scales and orientations for different parts of an image, providing a normalized rough description of the palmprint image. The NGist feature vector has a high dimension of features that increases the complexity of the classifier. To overcome this, we use the AE which not only help in dimensionality reduction but also address the nonlinearity of features. For recognition, a fast and robust regularized extreme learning machine (RELM) classifier is applied for palmprint recognition. In RELM classifier, a Frobenius norm is adopted as a regularization parameter to a trade-off between the approximated error and the regularized degree of the training samples.

The remainder of the paper is organized as follows: Section 2 explains the proposed multispectral palmprint recognition approach. The main steps of the approach based on NGist and AE with RELM are also introduced in this section. Section 3 demonstrates the applicability of the

proposed approach by a number of experimental models on a public database of multispectral palmprint images, named MS-PolyU. Finally, the conclusion and future work are summarized in Section 4.

2. Proposed Approach for Multispectral Palmprint Recognition

The improved palmprint recognition system is based on the optimal spectral band which attains the highest recognition rate. The proposed approach starts after segmenting the region of interests (ROIs) from all spectral bands images by using Zhang et al.'s method [5]. The main steps of the proposed approach can be labeled as follows: NGist-based feature extraction, feature reduction using AE, and multispectral palmprint classification based on RELM. Figure 1 shows the diagram of the proposed approach and its fundamental steps.

In NGist-based feature extraction, we extract the palm features by using effective NGist descriptor. Then, an optimized AE method is adopted to reduce the size of the extracted NGist feature vector (i.e., dimensionality of features).

Finally, in the classification step, the correct recognition of a person is accomplished when its palmprint image matches a palmprint image of the same person in the training dataset. While the incorrect recognition of a person may happen when its palmprint image does not match any palmprint image either for the same person or not or matches the palmprint image of another person in the training dataset. The classification step of the proposed approach is based on the RELM classifier. The advantages of RELM such as the speed for training and testing and the generality achieved by the regularization are exploited for improving the palmprint recognition system.

2.1. NGist-Based Feature Extraction. Global image features can be summarized by characterizing several substantial statistics of the input image. One of the methods used for feature extraction is the convolution process of the Gabor filter with an image at different scales and orientations. Consequently, the high and low frequency responses of gradient directions are measured as discriminative features. Taking the average intensity values of the convolution filter at each scale and orientation generates the Gist feature vector of an image. This feature vector is commonly being utilized for the image classification [29–31]. The first step of the proposed feature extraction method is converting the input image into a grayscale image. Then, the grayscale image is processed by a whitening filter and normalized according to the local contrast for preserving the main structural details. After that, it passed through a number of 2D Gabor filters of m scales with n orientations. The 2D Gabor filter function, $g(x, y)$, and its Fourier function transform, $G(u, v)$, can be calculated using (1) and (2), respectively:

$$g(x,y) = \left(\frac{1}{2\pi\sigma_x\sigma_y}\right)\exp\left[-\frac{1}{2}\left(\frac{x^2}{{\sigma_x}^2}+\frac{x^2}{{\sigma_y}^2}\right)+2\pi jWx\right], \quad (1)$$

where $j = \sqrt{-1}$ and W is the radial frequency of the Gabor function.

$$G(u,v) = \exp\left\{-\frac{1}{2}\left[\frac{(u-W)^2}{\sigma_u^2}+\frac{v^2}{\sigma_v^2}\right]\right\}, \quad (2)$$

where $\sigma_u = (1/2)\pi\sigma_x$, $\sigma_v = (1/2)\pi\sigma_y$; with the Gabor functions, a complete and nonorthogonal basis set can be formed. Using this basis set, the signals can be expanded to provide with the best description of the localized frequency. Consider $g(x, y)$ as a mother Gabor wavelet. Subsequently, self-similar filter dictionary can be obtained by suitable rotation and dilation parameters (orientation θ and scaling factor α) of following function:

$$g_{mn}(x,y) = \alpha^{-m} g\left(x', y'\right), \quad (3)$$

where $\alpha > 1, m, n$ are integers and x' and y' are given by (4) as

$$\begin{aligned} x' &= \alpha^{-m}\left(x\cos\theta + y\sin\theta\right), \\ y' &= \alpha^{-m}\left(x\sin\theta + y\cos\theta\right), \end{aligned} \quad (4)$$

where $\theta = n\pi/K$ and K represents the number of orientations. The scale α^{-m} in (3) is aimed to guarantee that the energy is independent of m. The Gabor wavelets nonorthogonality indicates that there is a small redundancy among information of the filtered images, and the following strategy can be applied to reduce this redundancy of information. Consider the lower and upper center interest frequencies are indicated by U_l and U_h. K and S represent the number of orientations and the number of scales in the multiresolution decomposition, respectively. Using (5), the projection of filters in the design strategy can be used to ensure that filter responses in the half-peak magnitude of the frequency spectrum touch one another.

$$\begin{aligned} \alpha &= \left(\frac{U_h}{U_l}\right)^{1/(S-1)}, \\ \sigma_u &= \frac{(\alpha-1)U_h}{(\alpha+1)\sqrt{2\ln 2}}, \\ \sigma_v &= \tan\left(\frac{\pi}{2K}\right)\left(U_K - 2\ln\left(\frac{2\sigma_u^2}{U_h}\right)\right) \\ &\quad\cdot\left(2\ln 2 - \frac{(2\ln 2)^2\sigma_u^2}{U_h^2}\right)^{-1/2}, \end{aligned} \quad (5)$$

where $W = U_h$ and $m = 0, 1, \ldots, S-1$. For multispectral palmprint feature extraction, Gabor filters with different scales and orientations can be used for ensuring maximum information with minimum redundancy. The proposed method uses 4 scales ($m = 0, 1, 2, 3$) and 8 orientations ($n = 0, 1, \ldots, 7$) of the Gabor wavelet, resulting in a total of 32 Gabor images for each input image. These generated images are divided into a 4-by-4 block. For each block, the average intensity value is calculated to represent the feature of

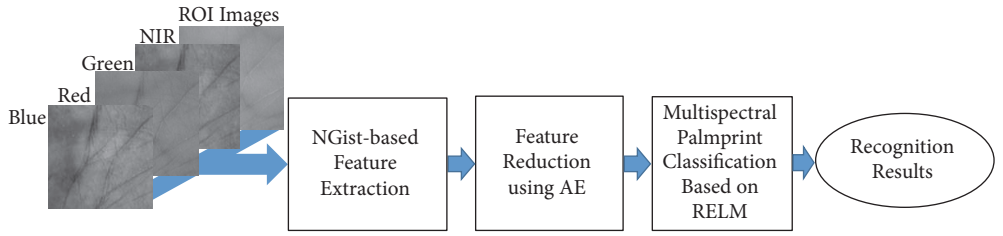

Figure 1: A diagram of the proposed approach for multispectral palmprint recognition.

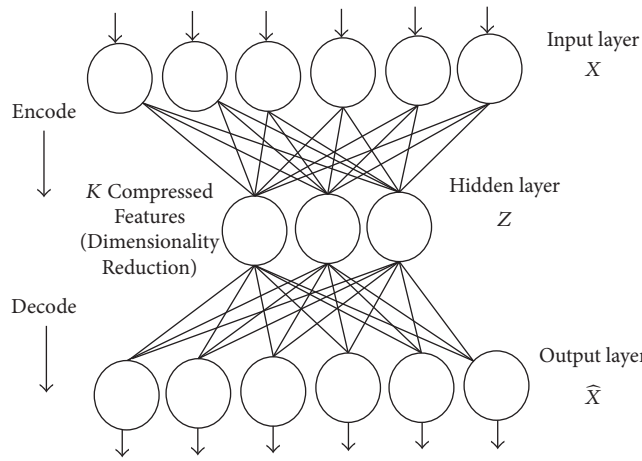

Figure 2: A simple autoencoder consists of a single hidden layer, input layer, and output layer.

that block. The final output is a concatenated features vector, named Gist of $32 \times 4 \times 4 = 512$ dimensions.

To cancel out the variation of average intensity values for blocks computed from different scales and orientations, we extend the traditional Gist descriptor by adding a new step, called variation tolerance step. In this step, the Gist features are normalized by using Euclidean norm as in Eq. (6). This extended version of Gist descriptor is named a normalized Gist (NGist) descriptor.

$$\text{NGist} = \frac{\text{Gist}}{\sqrt{\sum_{i=1}^{512} |\text{Gist}(i)|^2}} \tag{6}$$

It is worth mentioning that we chose the Euclidean norm because it is the natural norm associated with the dot-product that measures the similarity between objects.

2.2. Feature Reduction Using AE. AE is a feedforward neural network (FNN), utilized for unsupervised learning as an efficient encoding algorithm [32, 33]. The goal of AE is to learn the feature representation, especially for feature dimensionality reduction. Figure 2 shows a simple form of AE consists of a single hidden layer, input layer, and output layer and.

In this subsection, a nonlinear AE is practically utilized to reduce the dimensionality of the NGist feature vector. New features from the extracted features of training and testing data samples are produced, separately. There are several parameters for AE should be tuned and prepared through this step. The key parameters of AE include the activation function, the number of hidden nodes, the weight decay and regularization parameter, the weights of hidden nodes, the amount of epochs to be iterated, and the learning rate.

Now, suppose that the structure of the AE as shown in Figure 1, the input vector, $X \in \mathscr{R}^{512}$, represents the extracted NGist feature vector, and the output, $\widehat{X} \in \mathscr{R}^{512}$, represents the reconstructed feature vector. Because we have only K hidden nodes, the AE is subjected to learn a compressed feature vector, $Z \in \mathscr{R}^{K}$ (new feature vector), to recover 512-features of input, X. This new feature vector will be the input to the RELM for the classification task.

2.3. Multispectral Palmprint Classification Based on RELM. RELM is a feedforward neural network (FNN) consists of a single hidden layer, input layer and output layer. The weights of the input layer will be initialized randomly and the weights of the output layer can be computed arithmetically [34].

Suppose that $X \in \mathscr{R}^{N \times K}$ is a matrix of training dataset. The RELM with K hidden nodes and activation function, $g(x)$, can be modeled by the following equation:

$$o_j = \sum_{i=1}^{K} \beta_i g\left(w_i \cdot x_j + b_i\right), \quad j = 1, \ldots, N, \tag{7}$$

where $w_i = [w_{i1}, w_{i2}, \ldots, w_{iK}]^T$ is a weight vector which connects each hidden node i with all input nodes, $w_i \cdot x_j$ represents an inner product of w_i and x_j, b_i is a threshold of

the ith hidden nodes, and $\beta_i = [\beta_{i1}, \beta_{i2}, \ldots, \beta_{iN}]^T$ is a weight vector between the ith hidden nodes and the output nodes. The N data samples can be approximated with zero error by

$$\sum_{j=1}^{N} \left\| o_j - t_j \right\| = 0, \tag{8}$$

where t_j is an encoding of the user's ID as a target vector. In order to represent this encoding uniformly, we define the target vector corresponding to users' IDs (id_j) as

$$t_j = (b_1, \ldots, b_i, \ldots, b_m)^T, \tag{9}$$

where m is a number of users in the training set and b_i is equal to 1 or −1 depending on whether the related user's ID belongs to the corresponding IDs or not.

For example, suppose that there are three users ($m = 3$); the users' IDs, $t_{j\in(1,2,3)} = (1, 2, 3)$, and the related target vectors are as follows: $t_1 = (1, -1, -1)^T$ belongs to the first user, $t_2 = (-1, 1, -1)^T$ belongs to the second user, and $t_3 = (-1, -1, 1)^T$ belongs to the third user.

Equation (7) can be reformulated shortly as matrices by

$$T = H\beta, \tag{10}$$

where

$$H = \begin{bmatrix} g(w_1 \cdot x_1 + b_1) & \cdots & g(w_K \cdot x_1 + b_K) \\ \vdots & \cdots & \vdots \\ g(w_1 \cdot x_N + b_1) & \cdots & g(w_K \cdot x_N + b_K) \end{bmatrix}_{N\times K} \tag{11}$$

$$\beta = \begin{bmatrix} \beta_1^T \\ \vdots \\ \beta_K^T \end{bmatrix}_{K\times N}, \qquad T = \begin{bmatrix} t_1^T \\ \vdots \\ t_N^T \end{bmatrix}_{N\times K}, \tag{12}$$

where H is an output matrix of the hidden layer where each i column of H represents the output of the i hidden node related to the inputs, $x_1, x_2, \ldots, x_N$. The parameters of hidden nodes with nonzero activation functions, $g(\cdot)$, can be fixed randomly and the output weights can be computed on any input data sets [34, 35].

For testing phase, the output target matrix can be computed by

$$Y = \widehat{H}\widehat{\beta}, \tag{13}$$

where $\widehat{H}$ is an output matrix of the hidden layer for the testing dataset and $\widehat{\beta}$ is a matrix of weights for the testing dataset which is computed as

$$\widehat{\beta} = \left(H^T H + \lambda I\right)^{-1} H^T T, \tag{14}$$

where I is an identity matrix, H^T is a transpose matrix of H, T is a target output matrix, and λ is a regularizer parameter to trade-off between the regularized degree and the estimated error [36]. Frobenius norm is adopted as a regularization method in our work. This is because its efficiency to deal with sparse weights values.

For encoding the users' IDs (multilabel), we define each user's ID by using a discriminative target function written as

$$t_j = \arg\max_i (Y). \tag{15}$$

Algorithm 1 describes the phases and steps of the classification task of the proposed approach.

3. Experimental Models and Discussion

A complete set of experimental models are done on the public database of multispectral palmprint, created by Hong Kong Polytechnic University (MS-PolyU) [5]. To evaluate and validate the robustness and efficiency of the proposed approach, we systematically establish three different experimental models during our experiments.

3.1. MS-PolyU Database Description. The database consists of 24000 multispectral images of 250 people, each with two different palms, taken under four varied illuminations: red, green, blue, and NIR spectral bands. The images were acquired from 55 females and 195 males in two separated sessions. In every session, six images were collected for each spectrum of each palm. The average interval time between the two sessions was about nine days. So, there is in total 250 (volunteers) × 2 (different palms) × 4 (different spectra) × 6 (images) × 2 (sessions) = 24,000 images within the MS-PolyU database. Figure 3 shows the ROI images of a palm sample taken from the MS-PloyU database.

3.2. Parameters Setup. The number of hidden nodes in AE, K_{AE}, is fixed to 250, since it is enough to represent the most important extracted features of palmprint. Another most important parameter is the number of hidden nodes within the RELM, K_{RELM}. This parameter is selected using a grid search technique depending on the maximum accuracy. The grid search technique is done by using 71 different numbers of hidden nodes, ranging from 800 to 1500 with a common nonlinear sigmoid activation function. Table 1 states all parameters which are initialized in our experiments.

3.3. Experimental Model I. In this experimental model, six samples images of each palm from the first session are taken as a training dataset, while the six samples images of each palm from the second session are taken as a testing dataset. So, there is in total 3000 (500 × 6) training images and 3000 (500 × 6) testing images for each spectral band (red, green, blue, and NIR illuminations). The results of recent previous works, such as TPTSR [12], NFS [13], DWT [15], FABEMD + TELM [19], LBP-HF + Gabor [20], Log-Gabor + D_{Hamm} [24], and Log-Gabor + D_{KL} [24] are used to compare and evaluate the results of the proposed approach according to this model.

Input: the compressed features of AE for training and testing sets and parameters' values
Output: the users' IDs of the testing dataset
Training phase:
(1) Initialization step:
(i) Assign random values for the weights and biases of RELM
(2) Computational step:
(i) Compute the matrix, H of the hidden layer using Eq. (11)
(ii) Compute the matrix, T of the training set using Eq. (10)
(iii) Compute the output weights, $\widehat{\beta}$ using Eq. (14)
Testing phase:
(1) Computational step:
(i) Compute the matrix, $\widehat{H}$ of the hidden layer using Eq. (11)
(ii) Compute the output target value, Y using Eq. (13)
(2) Classification step:
(i) Classify the testing user's ID using Eq. (15) depending on whether this ID belongs to the user ID in the training set.

Algorithm 1: Multispectral palmprint classification based on RELM.

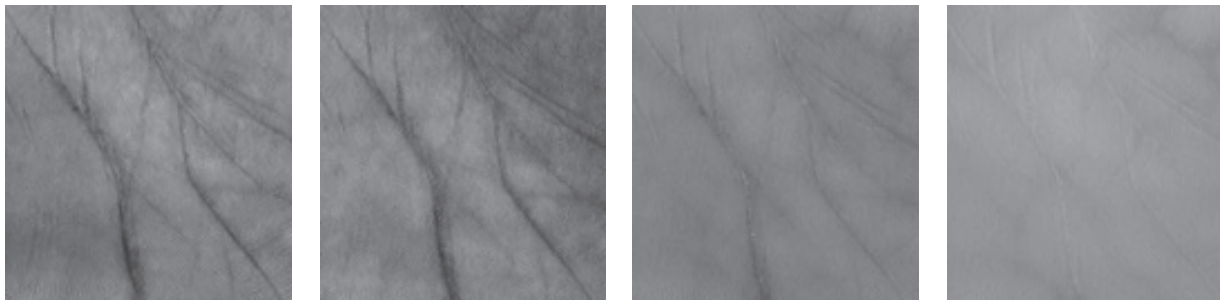

Figure 3: ROI images of a palm sample from the MS-PloyU database: (a) blue, (b) green, (c) red, and (d) NIR.

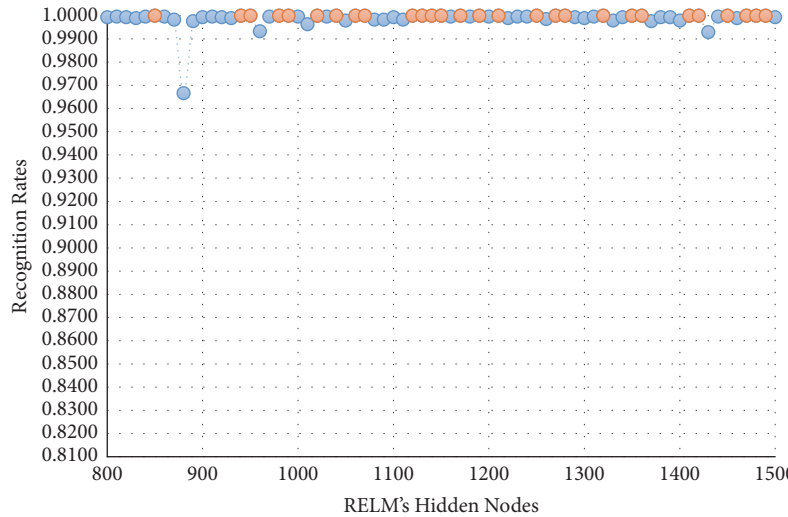

Figure 4: Recognition rates of blue spectral band using different numbers of RELM's hidden nodes.

In this experimental model, we study the influence of the number of hidden nodes on the recognition accuracy. As we see in Figures 4–7, the highest recognition rates are highlighted and marked as orange and red circles. Orange circles mean that the highest accuracy value is equal to the maximum accuracy (100%). In Figures 4 and 5, there are a large number of high accuracy values, reaching the maximum value for both blue and green spectral bands. For red spectral band, there is only one maximum recognition rate when the number of hidden nodes is 1270. Nevertheless,

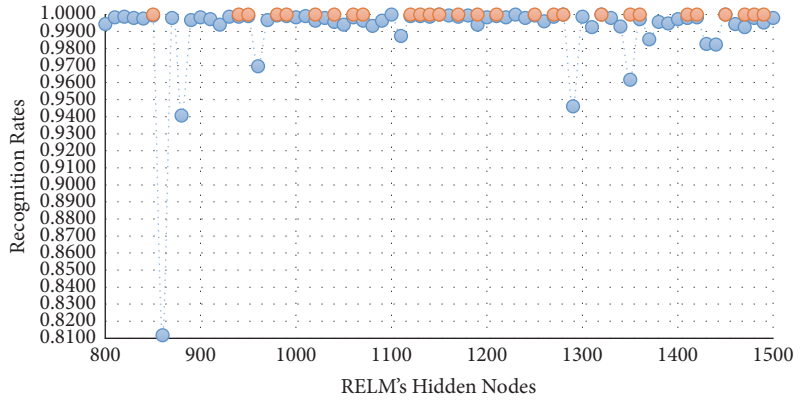

Figure 5: Recognition rates of green spectral band using different numbers of RELM's hidden nodes.

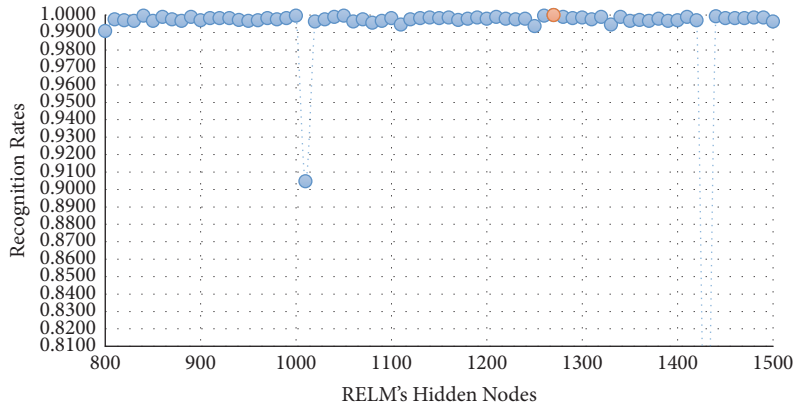

Figure 6: Recognition rates of red spectral band using different numbers of RELM's hidden nodes.

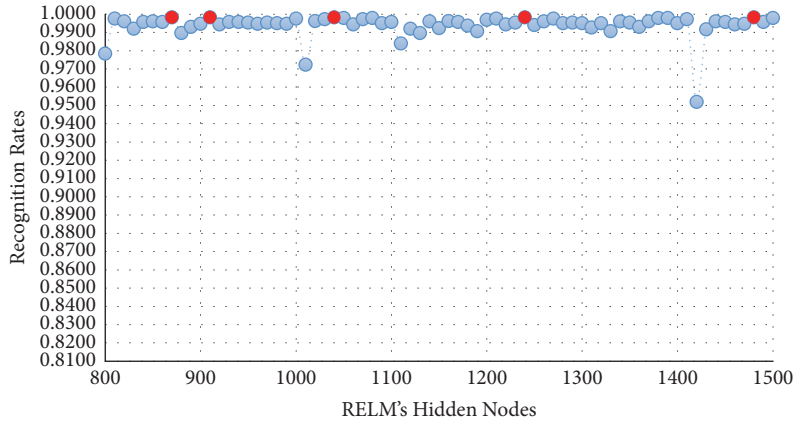

Figure 7: Recognition rates of NIR spectral band using different numbers of RELM's hidden nodes.

the recognition rate, 99.97%, is also obtained with different numbers of hidden nodes. For NIR spectral band in Figure 7, the highest accuracy value is 99.83% which is repeated five times with five different numbers of hidden nodes (870, 910, 1040, 1240, and 1480). Although this accuracy value did not attain the maximum accuracy (100%), most of recognition rates are higher than 99.50%.

To show the effectiveness of the proposed approach based on AE and RELM using NGist features over the features of the original Gist, we computed the recognition rates using extracted features of both descriptors at different numbers of RELM's hidden nodes. Figures 8–11 reveal the improvements of the proposed approach using NGist features over Gist features. For NGist features, we notice that the proposed approach achieves the maximum value of recognition rate (100%) or nearest to this value at different numbers of RELM's hidden nodes demonstrated in Figures 4–7. On the contrary, we note that the Gist features did not achieve the maximum

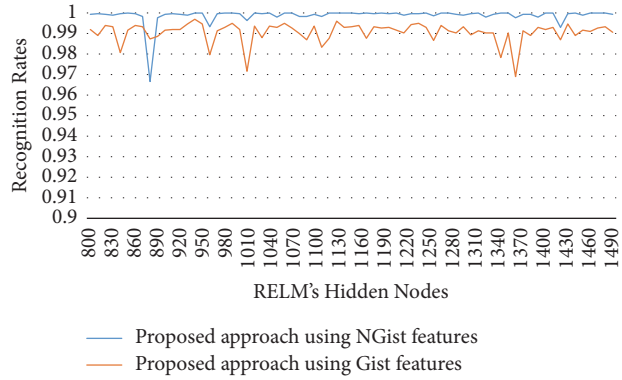

Figure 8: Recognition rates of blue spectral band using extracted features of NGist and Gist at different numbers of RELM's hidden nodes.

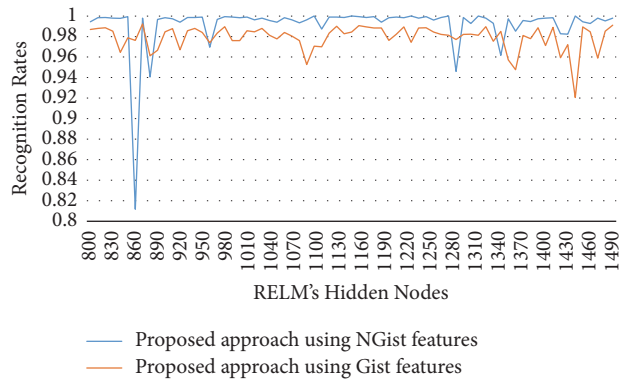

Figure 9: Recognition rates of green spectral band using extracted features of NGist and Gist at different numbers of RELM's hidden nodes.

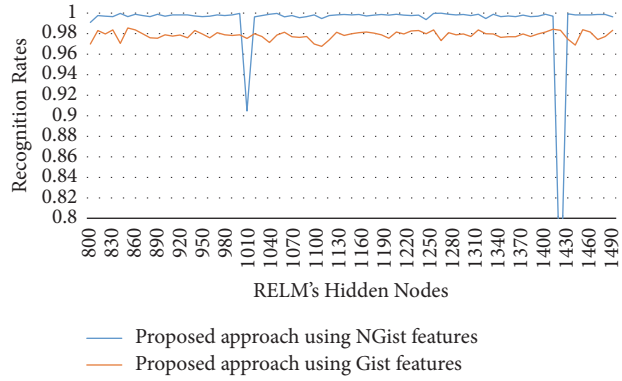

Figure 10: Recognition rates of red spectral band using extracted features of NGist and Gist at different numbers of RELM's hidden nodes.

value of recognition rate at any number of RELM's hidden nodes. The reason of this improvement is due to the ability of the proposed approach to cancel out the variations of extracted features computed from different blocks of different scales and orientations and improve the generalization to changes in palmprint images.

Moreover, we can see in Table 2 and Figure 12 that the proposed approach yields a highest recognition rate (100%) for the blue, green, and red spectral bands. Also, it achieves a recognition rate of 99.83% for the NIR spectral band. These results are highlighted in bold font in Table 2. Consequently, in the case of the blue spectral band, there is an improvement of 21.87% compared to TPTSR, 2.7% compared to NFS, 6.17% compared to DWT, 3.27% compared to FABEMD + TELM, 1.98% compared to LBP-HF + Gabor, 0.77% compared to Log-Gabor + D_{Hamm}, and 0.97% compared to Log-Gabor + D_{KL}.

In the case of the red spectral band, the results indicate that the proposed approach achieves also impressive improvements compared to the state-of-the-art approaches. Even though this experimental model mimics the real life situation where the system may be exposed to different

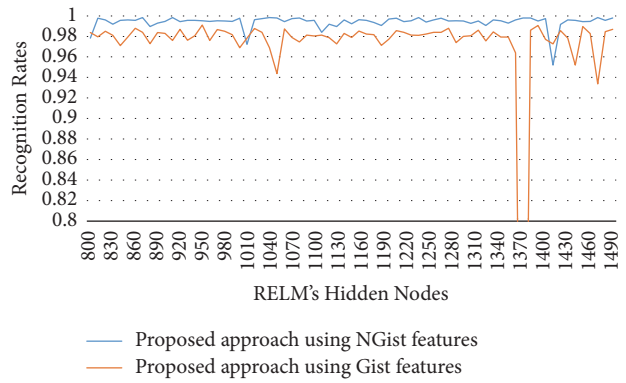

Figure 11: Recognition rates of NIR spectral band using extracted features of NGist and Gist at different numbers of RELM's hidden nodes.

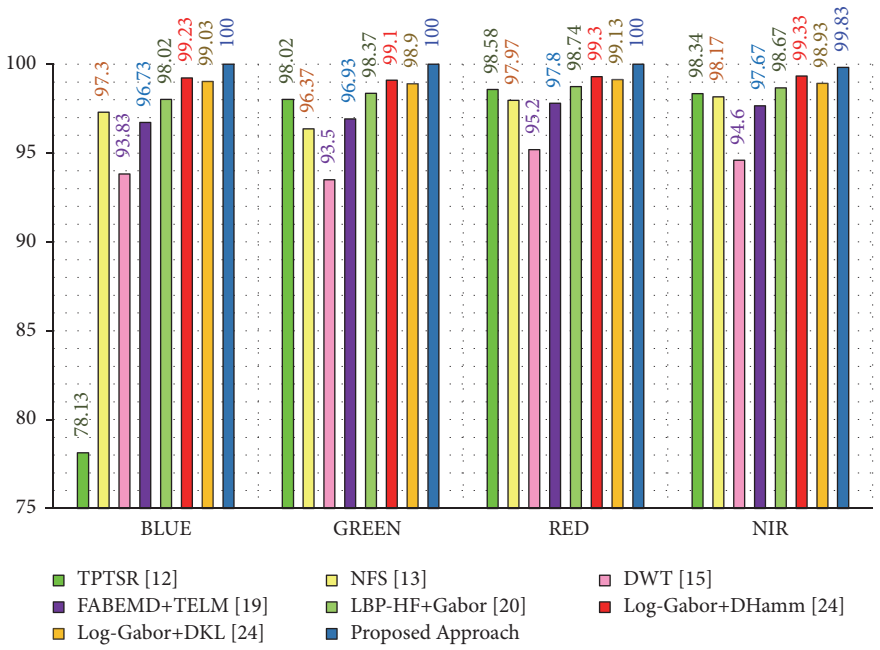

Figure 12: Recognition rates of experimental model I.

Table 1: Parameters setup.

Network Model	Parameters
AE	A number of hidden nodes of AE is $K_{AE} = 250$. Encoder and Decoder transfer function is a logistic sigmoid function. Maximum epochs = 10. L2WeightRegularization = 0.004. A loss function is a mean squared error function. Training algorithm is a conjugate gradient descent.
RELM	A number of hidden nodes of RELM, is $K_{RELM} \in \{800, 810, 820, \ldots, 1500\}$. A regularization parameter $(\lambda) = \exp(val)$, where $val \in \{-1, -0.9, -0.8, \ldots, 0.9, 1\}$ An activation function is a nonlinear sigmoid function, $g(x) = (1/(1 + e^{-x}))$

Table 2: Comparison of recognition rates for the proposed approach with the state-of-the-art approaches for different spectral bands: blue, green, red, and NIR according to experimental model I.

Method [Ref.]	Recognition Rate (%)			
	Blue	Green	Red	NIR
TPTSR [12]	78.13	98.02	98.58	98.34
NFS [13]	97.30	96.37	97.97	98.17
DWT [15]	93.83	93.50	95.20	94.60
FABEMD + TELM [19]	96.73	96.93	97.80	97.67
LBP-HF + Gabor [20]	98.02	98.37	98.74	98.67
Log-Gabor + D_{Hamm} [24]	99.23	99.10	99.30	99.33
Log-Gabor + D_{KL} [24]	99.03	98.90	99.13	98.93
Proposed Approach	**100**	**100**	**100**	**99.83**

Table 3: The EERs (%) of the proposed approach against some orientation-based methods.

Method [Ref.]	ERRs (%)			
	Blue	Green	Red	NIR
Palm code [5]	0.0463	0.0507	0.0297	0.0332
Fusion code [21]	0.0212	0.0216	0.0179	0.0213
Ordinal code [22]	0.0202	0.0202	0.0161	0.0180
Competitive code [23]	0.0170	0.0168	0.0145	0.0137
RLOC [25]	0.0203	0.0249	0.0223	0.0208
BDOC–BHOG [26]	0.0487	0.0418	0.0160	0.0278
HOC [27]	0.0147	0.0144	0.0131	0.0139
DOC [28]	0.0146	0.0146	0.0119	0.0121
Proposed approach	**0.0001**	**0.0003**	**0.0007**	**0.0017**

conditions, the proposed approach attains an interesting result.

This is due to the strength of the proposed NGist descriptor for feature extraction. The approach has a high independency to changes in illumination and orientation problems. Moreover, the advantages of AE to deal with the nonlinearity of features and RELM to solve the overfitting problem made the power of the proposed approach.

For further evaluation of the proposed approach, the Equal Error Rate (EER) [5] is also used to assess the performance of the experimental results. It can be calculated according to the average of False Accepted Rates (FARs) and False Rejected Rates (FRRs) in different thresholds between 0 and 1. Usually, FAR is used to measure the possibility that the biometric approach accepts incorrectly an attempt by a user which is not registered as an authorized user. It is arithmetically computed as the ratio of the number of false acceptances divided by the number of recognition attempts. Contrarily, the FRR metric is used to measure the possibility that the biometric approach rejects incorrectly an attempt by a user who is indeed registered as an authorized user. FRR is computed as the ratio of the number of false rejections divided by the number of recognition attempts. Table 3 exhibits the EERs of the proposed approach against the orientation based methods in the literature review, including competitive code, palm code, fusion code, ordinal code, and recent methods such as RLOC, BDOC–BHOG, HOC, and DOC on the four types of spectral bands. From Table 3, we can see that the proposed approach achieves the lowest EERs compared to the other methods in the state of the art on all spectral bands.

Additionally, we notice that the proposed approach achieves smaller EERs for the blue and green spectral bands than the red and NIR bands. The main possible reason is that the features of the palmprint in the red and NIR bands are very fine and need some level of sharpness to be more useful for recognition.

3.4. Experimental Model II. To demonstrate the robustness and efficiency of the proposed approach, we compare its results with some state-of-the-art approaches that follow this experimental model, namely, NFS [13], RBF [14], and LBP-HF + Gabor [20] on the same benchmark database. In this experimental model, the first three samples images of each palm from the first session are taken as a training dataset to form 1500 (500 × 3) images for each spectral band, and the other six samples images of each palm from the second session are used as a testing dataset of 3000 (500 × 6). This is done for red, green, blue, and NIR spectral bands, separately.

The results in Table 4 obviously demonstrate the advantage of the proposed approach in terms of effectiveness and robustness over other reported approaches. It offers attractive recognition rates of 99.70% to 100%, which are highlighted in a bold font in Table 4. With regard to the recognition rates of blue, green, red, and NIR spectral bands, it can be

Table 4: Comparison of recognition rates for the proposed approach with the state-of-the-art approaches for different spectral bands: blue, green, red, and NIR according to experimental model II.

Method [Ref.]	Recognition Rate (%)			
	Blue	Green	Red	NIR
NFS [13]	95.10	92.87	95.40	95.63
RBF [14]	96.70	96.50	98.20	98.40
LBP-HF + Gabor [20]	97.70	97.44	98.24	98.57
Proposed Approach	**100**	**99.93**	**99.93**	**99.70**

Table 5: Comparison of average recognition rates for the proposed approach with the state-of-the-art approaches for different spectral bands: blue, green, red, and NIR according to experimental model III.

Method [Ref.]	Average Recognition Rate (%)			
	Blue	Green	Red	NIR
MPELM [18]	98.58	99.05	99.45	99.21
ELM [18]	95.02	95.93	98.08	96.87
LPP + SMOSVM [18]	96.09	97.71	98.21	98.78
LPP + LSSVM [18]	95.75	97.45	97.96	98.22
Proposed Approach	**100**	**99.97**	**99.99**	**99.93**

observed that the proposed approach yields improvements of 2.3%, 2%, 1.69%, and 1.13% compared to the LBP-HF + Gabor approach, which has the highest recognition rates against other approaches.

In addition to the recognition rates of our approach, the simplicity and efficiency compared to the LBP-HF + Gabor approach make it a robust and efficient approach. Furthermore, the small simple size of training dataset which are taken at different sessions and tested by a new test case is a rigorous challenge. Actually, the robustness of NGist descriptor with AE and RELM handles this challenge effectively. Figure 13 visualizes the recognition rates of this work compared to the recent works that have high recognition rates.

3.5. Experimental Model III. Here, we take randomly three images of each different palm from the two sessions as a training dataset to form 1500 (500 × 3) images and the other nine images are taken as a testing dataset with 4500 (500 × 9) images. This model is done for each spectral band (blue, green, red, and NIR). The results are evaluated repeatedly for 30 times of random selection of the images in training and testing phases. The average recognition rates will be had as final results. The results of this model are compared with results of recent work given in [18].

As we see in Table 5 and Figure 14, the proposed approach achieves high average recognition rates of 100%, 99.97%, 99.99%, and 99.93%, regarding blue, green, red, and NIR spectral bands, respectively. Similarly, it can be observed that the proposed approach yields improvements of 1.42%, 0.92%, 0.54%, and 0.72%, compared to the MPELM approach. These results indicate that the blue spectral band outperforms all other spectral bands effectively, whereas the red spectral band performs better than the green and NIR spectral bands.

3.6. Computational Cost. All experimental models have been implemented using MATLAB R2015a on a laptop with Windows 10 (x64), Intel Core i7-7500U with 2.7 GHz CPU processor, and 16 GB RAM. Execution time of feature extraction, feature reduction, and classification is shown in Table 6.

Table 6: Average execution time of the proposed approach steps for one test sample (in seconds).

Step	Average execution time (s)
Feature extraction	0.237
Feature reduction	0.000024294
Classification	0.000317

We notice that the average execution time of all steps is very small which makes the proposed approach is efficient and fast enough for real time condition.

4. Conclusion and Future Work

A novel multispectral palmprint recognition approach is proposed based on AE and RELM with an efficient extended version of Gist descriptor, named NGist. The NGist descriptor was applied to extract the features of palmprint, while AE was used to solve the problem of high dimensionality associated with the NGist features.

Recognition rate of the proposed approach has been evaluated using the public MS-PolyU database of multispectral palmprint images. The experiments were performed through three different experimental models, proving that the proposed approach attains higher recognition rates compared to the recent methods in the state of the art. Moreover, it has been observed that the blue spectral band outperforms all other bands effectively, whereas the red and green bands perform better than the NIR band in all three procedures.

Our next step is to extend the approach to handle spoofing problem by using multispectral palmprint fusion

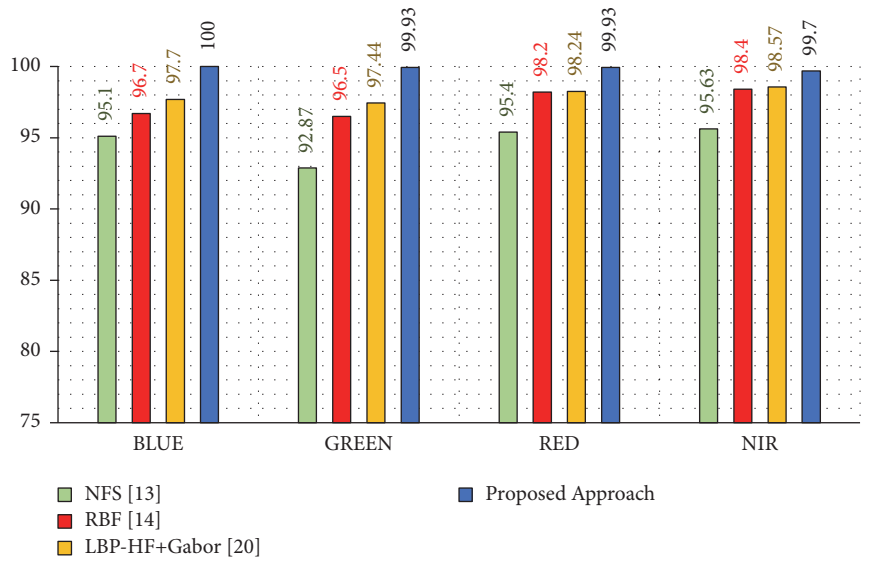

Figure 13: Recognition rates of experimental model II.

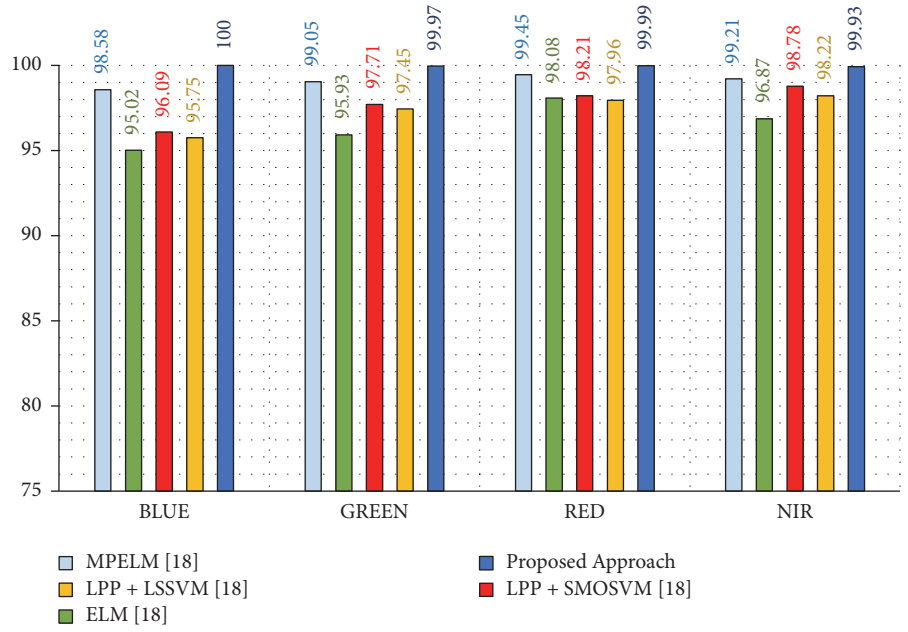

Figure 14: Recognition rates of experimental model III.

techniques. Additionally, we will investigate the applicability of pretrained deep learning models and transfer learning concept for biometric multispectral palmprint recognition.

Conflicts of Interest

The authors declare that there are no conflicts of interest regarding the publication of this paper.

Acknowledgments

This work was supported by the Deanship of Scientific Research at King Saud University through Research Group no. RG-1438-063.

References

[1] A. K. Jain, "Technology: biometric recognition," *Nature*, vol. 449, no. 7158, pp. 38–40, 2007.

[2] A. Gomai, A. El-Zaart, and H. Mathkour, "An efficient iris segmentation approach," in *Proceedings of the International Conference on Graphic and Image Processing (ICGIP '2011)*, vol. 8285, p. 82851T, Cairo, Egypt, September 2011.

[3] H. Jaafar, S. Ibrahim, and D. A. Ramli, "A robust and fast computation touchless palm print recognition system using LHEAT and the IFkNCN classifier," *Computational Intelligence and Neuroscience*, vol. 2015, Article ID 360217, 17 pages, 2015.

[4] L. Binh Tran and T. H. Le, "Multimodal Personal Verification Using Likelihood Ratio for the Match Score Fusion," *Computational Intelligence and Neuroscience*, vol. 2017, pp. 1–9, 2017.

[5] D. Zhang, Z. Guo, G. Lu, L. Zhang, and W. Zuo, "An online system of multispectral palmprint verification," *IEEE Transactions on Instrumentation and Measurement*, vol. 59, no. 2, pp. 480–490, 2010.

[6] C. Han, H. Cheng, C. Lin, and K. Fan, "Personal authentication using palm-print features," *Pattern Recognition*, vol. 36, no. 2, pp. 371–381, 2003.

[7] X. Wu, K. Wang, and D. Zhang, "HMMs Based Palmprint Identification," in *Biometric Authentication*, vol. 3072 of *Lecture Notes in Computer Science*, pp. 775–781, Springer Berlin Heidelberg, Berlin, Heidelberg, 2004.

[8] R. Raghavendra, B. Dorizzi, A. Rao, and G. Hemantha Kumar, "Designing efficient fusion schemes for multimodal biometric systems using face and palmprint," *Pattern Recognition*, vol. 44, no. 5, pp. 1076–1088, 2011.

[9] S. C. Chen, H. G. Fu, and Y. Wang, "Application of improved graph theory image segmentation algorithm in tongue image segmentation," *Computer Engineering and Applications*, vol. 48, no. 5, pp. 201–203, 2012.

[10] G. S. Badrinath, N. K. Kachhi, and P. Gupta, "Verification system robust to occlusion using low-order Zernike moments of palmprint sub-images," *Telecommunication Systems*, vol. 47, no. 3-4, pp. 275–290, 2011.

[11] J. Gan and D. Zhou, "A Novel Method for Palmprint Recognition Based on Wavelet Transform," in *Proceedings of the 2006 8th international Conference on Signal Processing*, Guilin, China, November 2006.

[12] J. Li, J. Cao, and K. Lu, "Improve the two-phase test samples representation method for palmprint recognition," *Optik - International Journal for Light and Electron Optics*, vol. 124, no. 24, pp. 6651–6656, 2013.

[13] Y. Xu, Q. Zhu, Z. Fan, M. Qiu, Y. Chen, and H. Liu, "Coarse to fine K nearest neighbor classifier," *Pattern Recognition Letters*, vol. 34, no. 9, pp. 980–986, 2013.

[14] S. Zhang and X. Gu, "Palmprint recognition based on the representation in the feature space," *Optik - International Journal for Light and Electron Optics*, vol. 124, no. 22, pp. 5434–5439, 2013.

[15] X. Xu, Z. Guo, C. Song, and Y. Li, "Multispectral palmprint recognition using a quaternion matrix," *Sensors*, vol. 12, no. 4, pp. 4633–4647, 2012.

[16] G. Lu, D. Zhang, and K. Wang, "Palmprint recognition using eigenpalms features," *Pattern Recognition Letters*, vol. 24, no. 9-10, pp. 1463–1467, 2003.

[17] F. Du, P. Yu, H. Li, and L. Zhu, "Palmprint recognition using gabor feature-based bidirectional 2dlda," *Communications in Computer and Information Science*, vol. 159, no. 2, pp. 230–235, 2011.

[18] X. Xu, L. Lu, X. Zhang, H. Lu, and W. Deng, "Multispectral palmprint recognition using multiclass projection extreme learning machine and digital shearlet transform," *Neural Computing and Applications*, vol. 27, no. 1, pp. 143–153, 2016.

[19] L. Lu, X. Zhang, X. Xu, and D. Shang, "Multispectral image fusion for illumination-invariant palmprint recognition," *PLoS ONE*, vol. 12, no. 5, Article ID e0178432, 2017.

[20] W. El-Tarhouni, L. Boubchir, N. Al-Maadeed, M. Elbendak, and A. Bouridane, "Multispectral palmprint recognition based on local binary pattern histogram fourier features and gabor filter," in *Proceedings of the 6th European Workshop on Visual Information Processing, EUVIP 2016*, fra, October 2016.

[21] A. Kong, D. Zhang, and M. Kamel, "Palmprint identification using feature-level fusion," *Pattern Recognition*, vol. 39, no. 3, pp. 478–487, 2006.

[22] Z. N. Sun, T. Tan, Y. Wang, and S. Z. Li, "Ordinal palmprint represention for personal identification [represention read representation]," in *Proceedings of the IEEE Computer Society Conference on Computer Vision and Pattern Recognition (CVPR '05)*, vol. 1, pp. 279–284, June 2005.

[23] A. W.-K. Kong and D. Zhang, "Competitive coding scheme for palmprint verification," in *Proceedings of the 17th International Conference on Pattern Recognition (ICPR '04)*, vol. 1, pp. 520–523, The British Machine Vision Association, Cambridge, UK, August 2004.

[24] M. D. Bounneche, L. Boubchir, A. Bouridane, B. Nekhoul, and A. Ali-Chérif, "Multi-spectral palmprint recognition based on oriented multiscale log-Gabor filters," *Neurocomputing*, vol. 205, pp. 274–286, 2016.

[25] W. Jia, D.-S. Huang, and D. Zhang, "Palmprint verification based on robust line orientation code," *Pattern Recognition*, vol. 41, no. 5, pp. 1521–1530, 2008.

[26] D. Hong, W. Liu, J. Su, Z. Pan, and G. Wang, "A novel hierarchical approach for multispectral palmprint recognition," *Neurocomputing*, vol. 151, no. 1, pp. 511–521, 2015.

[27] L. Fei, Y. Xu, and D. Zhang, "Half-orientation extraction of palmprint features," *Pattern Recognition Letters*, vol. 69, pp. 35–41, 2016.

[28] L. Fei, Y. Xu, W. Tang, and D. Zhang, "Double-orientation code and nonlinear matching scheme for palmprint recognition," *Pattern Recognition*, vol. 49, pp. 89–101, 2016.

[29] A. Oliva and A. Torralba, "Modeling the shape of the scene: a holistic representation of the spatial envelope," *International Journal of Computer Vision*, vol. 42, no. 3, pp. 145–175, 2001.

[30] C. Siagian and L. Itti, "Comparison of gist models in rapid scene categorization tasks," *Journal of Vision*, vol. 8, no. 6, pp. 734-734, 2008.

[31] B. Li, K. Cheng, and Z. Yu, "Histogram of oriented gradient based GIST feature for building recognition," *Computational Intelligence and Neuroscience*, vol. 2016, Article ID 6749325, 9 pages, 2016.

[32] C.-Y. Liou, J.-C. Huang, and W.-C. Yang, "Modeling word perception using the Elman network," *Neurocomputing*, vol. 71, no. 16-18, pp. 3150–3157, 2008.

[33] C.-Y. Liou, W.-C. Cheng, J.-W. Liou, and D.-R. Liou, "Autoencoder for words," *Neurocomputing*, vol. 139, pp. 84–96, 2014.

[34] G. B. Huang, Q. Y. Zhu, and C. K. Siew, "Extreme learning machine: a new learning scheme of feedforward neural networks," in *Proceedings of the IEEE International Joint Conference on Neural Networks*, vol. 2, pp. 985–990, July 2004.

[35] G. B. Huang, Q. Y. Zhu, and C. K. Siew, "Extreme learning machine: theory and applications," *Neurocomputing*, vol. 70, no. 1–3, pp. 489–501, 2006.

[36] J. Xu, W.-Q. Zhang, J. Liu, and S. Xia, "Regularized minimum class variance extreme learning machine for language recognition," *EURASIP Journal on Audio, Speech, and Music Processing*, vol. 2015, no. 1, article no. 22, 2015.

Hindawi
Computational Intelligence and Neuroscience
Volume 2018, Article ID 1867548, 11 pages
https://doi.org/10.1155/2018/1867548

Research Article

Combining Cryptography with EEG Biometrics

Robertas Damaševičius[1], **Rytis Maskeliūnas**[2], **Egidijus Kazanavičius**[2] **and Marcin Woźniak**[3]

[1]*Department of Software Engineering, Kaunas University of Technology, Studentų 50-415, Kaunas, Lithuania*
[2]*Centre of Real Time Computer Systems, Kaunas University of Technology, K. Baršausko 59-A338, Kaunas, Lithuania*
[3]*Institute of Mathematics, Silesian University of Technology, Kaszubska 23, 44-100 Gliwice, Poland*

Correspondence should be addressed to Robertas Damaševičius; robertas.damasevicius@ktu.lt

Received 22 December 2017; Revised 20 March 2018; Accepted 18 April 2018; Published 22 May 2018

Academic Editor: Ivan Volosyak

Cryptographic frameworks depend on key sharing for ensuring security of data. While the keys in cryptographic frameworks must be correctly reproducible and not unequivocally connected to the identity of a user, in biometric frameworks this is different. Joining cryptography techniques with biometrics can solve these issues. We present a biometric authentication method based on the discrete logarithm problem and Bose-Chaudhuri-Hocquenghem (BCH) codes, perform its security analysis, and demonstrate its security characteristics. We evaluate a biometric cryptosystem using our own dataset of electroencephalography (EEG) data collected from 42 subjects. The experimental results show that the described biometric user authentication system is effective, achieving an Equal Error Rate (ERR) of 0.024.

1. Introduction

Brain computer interface (BCI) is a highly growing field of research with application in healthcare systems (from fall prevention to neuronal rehabilitation) to educational, self-regulation, production, marketing, and security as well as games and entertainment. BCI aims to provide a channel of communication that does not depend on the usual use of peripheral nerves and muscles [1]. While the main intended target application for BCI research is the development of motor function independent prosthetic devices for impaired patients, other applications of BCI, such as those for learning [2], gaming [3, 4], or entertainment [5], raise the need for ensuring the security and privacy of subjects using BCI systems. BCI systems are based on measurement of brain activity on the surface (in case of noninvasive BCI) or inside (in case of invasive BCI) of the human skull using electrodes. The results of the measurement represent the sum of electrical impulses emitted by a large number of brain's neurons. Noninvasive EEG signal is recorded by attaching the electrodes to the head of a subject according to a given map such as the 10–20 international system for the placement of EEG electrodes.

Recently, BCI applications for biometrics have attracted increased attention from the researchers. Biometrics provides means for identifying people based on their physiological characteristics [6]. Recently, there has been tremendous growth in research on cryptography and biometric frameworks because of incredible need for data security in numerous applications, such as e-commerce, e-health, e-government, e-voting, blockchain, law enforcement, digital forensics, and homeland security. The goal is to verify the identity of a subject using some characteristic of a subject. In cryptographic frameworks, users use their passwords or secret keys to protect their confidential data. However, the use of passwords for identification has some well-known drawbacks: textual passwords can be spied over or cracked, and secret keys are too long and difficult to memorize and can be stolen if stored somewhere. The downside of cryptography is that verification strategies are not unequivocally connected to the person identity. Unlike cryptography based authentication methods, biometrics using behavioural and physiological characteristics such as iris, fingerprints, electroencephalography (EEG) data, face, palm, voice, and gait, is convenient and cannot be forgotten or lost.

The EEG-based subject identification is relatively new. The advantages of using EEG for biometrics are its low exposability (cannot be casually obtained or stolen by external observers) and resistance to forced extraction because understress brain activity changes [7]. They also can be used by disabled patients or users missing some physical trait. Efforts to develop biometric methods and systems based on the EEG have targeted the development of subject condition monitoring tools, for example, for detection of sleep apnea [8], schizophrenia [9], or epilepsy [10]; the creation of BCI systems to assist disabled people [11]; and marketing [12]. Analysts predict that the global EEG and electrocardiography (ECG) biometrics market is to expand at a compound annual growth rate of 12.37% during the period 2016–2020 [13].

The suitability of using EEG for privacy and security applications can be attributed to morphological, anatomical, and functional plasticity (behaviour-related lasting changes in functional connections) traits [14], which contribute to discriminability between subjects [15]. Several studies (mainly from the fields of human physiology and genetics) have confirmed that the spectral characteristics of the EEG alpha waves (in the 8–12 Hz range, which reflect relaxation and disengagement) and the beta waves (in the 12–30 Hz range, related to action and concentration) of EEG show the strongest heritability relationship [16].

The difficulties related to using EEG data are its instability over time (the EEG permanence problem [17]). It is still difficult to achieve high accuracy of EEG-based biometric systems, which motivate researchers to explore new EEG data analysis methods. However, the research community still lacks knowledge on specific discriminant features of EEG suable for biometry [18]. Up to now, the EEG power spectrum features were used to achieve relatively good classification performance [18]. Several methods, which focus on the concepts and methods adopted from the network science, such as functional connectivity [19] and network organization [20], have been proposed. Fuzzy commitment (FC) scheme [21] can be used as a theoretical background for combining cryptography and biometrics. In the FC scheme, a secret key is linked to the reference biometric template, and the difference vector is calculated in such way that the secret key may be restored using the difference vector and the query biometric template. Another approach is a fuzzy vault (FV) based on polynomial reconstruction [22]. The FC and FV schemes have been applied to biometrics before [23, 24].

Here we propose a secure EEG-based cryptographic authentication scheme based on the commitment scheme adopted from [25], provide a theoretical analysis of the security characteristics of the proposed scheme, apply the scheme to biometric systems to construct a biometric cryptosystem using EEG signals, and evaluate it using our own dataset recorded from 42 subjects. The rest of the paper is organized as follows. In Section 2 we present the state-of-the-art overview of related work in EEG biometrics. We describe the proposed method in Section 3. We state theorems regarding the security characteristics of the cryptographic system in Section 4. We describe the application of the method on EEG dataset in Section 5. We present the experimental results and their evaluation in Section 6. Finally, the conclusions are given in Section 7.

2. State of the Art

Cognitive biometrics [26] uses brain signals as the source of information for user identification (authentication). User authentication is a process that ensures and confirms a user's identity in security systems. Using EEG signals for user authentication can be effective with varying degrees of accuracy. For example, Fladby [27] used power spectral features of alpha, beta low, beta high, and theta bands from just one EEG channel of 12 subjects performing eight different tasks (from simple relaxation to counting and reading) and a custom feature based distance metric for subject discrimination, achieving an EER of 21.42%. Palaniappan [28] used gamma band of visually evoked potential (VEP) signals and the neural network (NN) classifier to identify 20 individuals with an average accuracy of 99.06%.

Liang et al. [29] extracted the AR features from 8 EEG channels and used Support Vector Machine (SVM) to achieve an accuracy of 45.52% to 54.96% for subject separation task and an accuracy of 48.41% to 56.07% for subject identification task. Marcel and Millán [30] implemented a Gaussian mixture model (GMM) with maximum a posteriori (MAP) estimation for 9 subjects, achieving a half total error rate (HTER) of 6.6%.

Hema et al. [31] adopted feed forward NN for EEG using Power Spectral Density (PSD) features from EEG beta waves and reached an average accuracy of 94.4 to 97.5% on 6 subjects. He et al. [32] used a naïve Bayes (NB) classifier with autoregressive (AR) features and achieved a HTER of 6.7% for 4 subjects.

Mu and Hu [33] used the back-propagation NN on data derived from 6 channels of 3 subjects and achieved an 80.7% to 86.7% accuracy. Brigham and Kumar [34] used linear SVM classifier with the AR features and achieved accuracy of 98.96% on 122 subjects tested. Hu [35] used the NN on seven EEG signal features and obtained an 80% to 100% true acceptance rate (TAR) and a 0 to 30% false acceptance rate (FAR), while using data received from only 3 subjects.

Zúquete et al. [36] demonstrated the stability of EEG biometrics using visual stimulus to measure visual evoked potentials (VEP) and a combination of one-class classifiers (OCCs), including k-Nearest Neighbor (kNN) and Support Vector Data Description (SVDD). Ashby et al. [37] used linear SVM with AR and spectral characteristics of EEG signals from 14 EEG channels and achieved 2.4% to 5.1% false rejection rate (FRR) and 0.7% to 1.1% FAR for 5-subject authentication. Shedeed [38] used the NN on features obtained by fast Fourier transform (FFT) and wavelet packet decomposition (WPD) from 4 channels, achieving a 66% to 93% correct classification rate (CCR) using data from 3 subjects.

Chuang et al. [39] recorded single-channel EEG signals when a subject performs a custom task (e.g., singing or moving finger). The authentication system analyses the similarity between such brain data and training data to authenticate subjects, reaching about 99% accuracy. Yeom et al. [40]

used Gaussian kernel SVM on the signal difference and time derivative features from 18 EEG channels and managed to achieve the accuracy around 86% on 10 subjects.

Dan et al. [41] used the polynomial kernel SVM based on the AR model parameters calculated on the EEG signal, recorded a single EEG channel, and obtained an accuracy of 65% to 75% on 13 subjects.

Delpozo-Banos et al. [18] used the functional connectivity patterns to represent effective features for improving EEG-based biometric systems and classification using Convolutional Neural Network (CNN) and achieved 97.5% accuracy in eyes-closed (EC) and 96.26% in eyes-open (EO) resting state conditions states when fusing PSD information from the parietooccipital (centroparietal in EO) parts of the brain of 10 subjects.

Abo-Zahhad et al. [42] achieved more than 99% authentication accuracy by using single-channel EEG signals from 10 and 15 subjects. Koike-Akino et al. [43] achieved 72% accuracy for 25-subject identification from EEG using a single 800 ms epoch and partial least-squares (PLS) dimensionality reduction method applied before quadratic discriminant analysis (QDA) classification.

Crobe et al. [44] obtained good results in the EEG gamma (EER = 0.131 and AUC = 0.943 in EO condition; EER = 0.130 and AUC = 0.933 in EC condition) and high beta (EER = 0.172 and AUC = 0.905 in EO condition; EER = 0.173 and AUC = 0.906 in EC condition) frequency bands.

Several studies presented the fusion of EEG with other modalities to get a multimodal biometric system such as in [45, 46]. Also see a survey of security and privacy challenges in BCI applications in [47]. EEG-based authentication was also considered as a part of smart driving systems to verify the driver's identity on demand [48]. However, using EEG brainwaves for authentication might result in risks for the privacy of users. For example, authors in [49] propose an authentication system that verifies an individual EEG signal when a subject performs a custom task. They also design an attack model by impersonating the thoughts of subjects to test the robustness of the authentication system. An adversary also can attack the authentication system via synthetic EEG signals, which are generated using a model based on the historical EEG data from a subject [50].

3. Description of EEG Biometry Method

First, we provide definitions required for understating of the biometric authentication method as given in [25].

Definition 1 (discrete logarithm). Let G be a finite cyclic group of order n. Let g be a generator of G and let $h \in G$. The discrete logarithm of h to the base g, $\log_g h$, is the unique integer u, $0 \le u \le n-1$, such that $h = g^u$.

Definition 2 (discrete logarithm problem (DLP)). Given a prime number p, a generator of g of z_p^*, and an element $h \in z_p^*$, find the integer u such that $h = g^u \pmod p$.

Definition 3 (block code). A block code $C(n,k)$ over an alphabet A^* of w symbols is a set of w^k n-vectors called codewords. Associated with the code is an encoder $\{0,1\}^k \to C$ which maps a message M, a k-tuple, to its associated codeword.

Definition 4 (decoding function). Let $C(n,k)$ be a block code set with $w = \{0,1\}$. A decoding function $f_d : \{0,1\}^n \to C \cup \varepsilon$ maps a message c', a n-tuple, to correct codeword c, if c' and c are sufficiently close according to appropriate metric. Otherwise, it maps it to invalid codeword ε.

Definition 5 (hamming distance). Given code set $C(n,k)$, the Hamming distance between two words c_i and c_j from the code set C is given by

$$H\left(c_i, c_j\right) = \frac{1}{n}\sum_{r=1}^{n}\left|c_i^r - c_j^r\right|. \tag{1}$$

Definition 6 (error correction threshold). Error correction threshold t_σ of the error-correcting code $C(n,k)$ is the largest number of errors that can be corrected in the corrupted codeword.

Definition 7 (statistical distance). Let X_1 and X_2 be two random variables over the same space Ψ, and let P_1 and P_2 be their discrete probability distribution functions (PDFs). Then, the statistical distance between P_1 and P_2 is as follows:

$$D\left(P_1, P_2\right) = \sum_{\psi\in\Psi}\left|\Pr\left(X_1 = \psi\right) - \Pr\left(X_2 = \psi\right)\right|. \tag{2}$$

Definition 8 (Bose-Chaudhuri-Hocquenghem (BCH) codes). Let α be a primitive element of Galois field GF(q^m). For any positive integer i, let $m_i(x)$ be the minimal polynomial of α_i over GF(q^m). The generator polynomial of the BCH code is defined as the least common multiple $P(x) = \mathrm{lcm}(m_1(x), \ldots, m_{d-1}(x))$.

The method, proposed by [25] and adopted here for EEG biometry, consists of three procedures: (1) *Setup*, which outputs a public key, (2) *Commit*, which takes as input and the message and outputs commitment to be sent and the opening value to be used for message verification, and (3) *Open*, which outputs true if verification succeeds or false otherwise. Three actors participate: the sender *Alice*, the receiver *Bob*, and the trusted third party *Trent*, who generated system parameters and publishes it to Alice and Bob parties.

Let M be the space of messages to commit to. The first stage is Setup stage (see Algorithm 1), where Trent generates and sends the keys to Alice and Bob. The second stage is Commit stage, where Alice sends Bob its commitment for a private message $m \in M$ and secretly holds an opening value. The third stage is Open stage, where Alice sends Bob the original message $m \in M$ along with the opening value, so that Bob can verify that the message committed in the first stage was indeed $m \in M$.

Definition 9 (commitment function). First we define the commitment function $F : (\{0,1\}^n \times \{0,1\}^n) \to (\{0,1\}^n \times \{0,1\}^n)$, defined as $F(c,x) = (\varphi, \delta)$; here $\varphi = F_k(m,x) = g^m h^x \pmod p$ and $\delta = x - c$ is the difference vector.

Input: Security parameter k.
(1) Generate randomly two prime numbers p and q of length k, such that $p = 1 \pmod{q}$
(2) Choose randomly $1 \leq a \leq p - 1$
(3) Compute $g = a^{(p-q)/2} \neq 1 \pmod{p}$
(4) Choose randomly $1 \leq b \leq q - 1$
(5) Compute $h = g^b \neq 1 \pmod{p}$
Output: Parameters p, q, g, h

Algorithm 1: Initialization.

Definition 10 (commitment protocol). Commitment protocol π is a scheme (for a message space M) defined by a triple (Setup, Commit, Open) such that

(a) $(p, q, g, h) \leftarrow \text{Setup}(\cdot)$ generates the public commitment key,

(b) for any $m \in M$,$(\varphi, \delta) \leftarrow \text{Commit}_{(p,q,g,h)}(m)$ is the commitment/opening pair for m,

(c) $\text{Open}_{(p,q,g,h)}(\varphi, \delta) \rightarrow m \in M \cup \{\varepsilon\}$, where ε is returned if (φ, δ) is not a valid commitment to any message.

To set the system parameters, Trent executes the following procedure.

Setup Procedure

(1) *Trent* generates two prime numbers p and q such that $p = 1 \pmod{q}$.

(2) *Trent* finds a random generator $g \in G_q \setminus \{1\}$, where $g \in G_q$ is a subgroup of the order q in Z_p^*.

(3) *Trent* computes an element $h = g^a \in Z_p^* \setminus \{1\}$, where $a \in Z_q$ that is randomly chosen (h is a generator element of G_q).

(4) *Trent* sends the system parameters (p, q, g, h) to Alice and Bob.

Commit Procedure. To commit to a message $m \in M_k \subseteq Z_q$ in the message space $M_k \subset \{0, 1\}^k$, *Alice* encodes the message into a codeword $c = g(m) \in C \subseteq \{0, 1\}^n$, chooses a random witness $x \in X_n \subseteq Z_q$ in the witness space $X_n \subset \{0, 1\}^n$, and then computes the commitment $F(c, x) = (g^c h^x, x - c) = (\varphi, \delta)$. The commitment is sent to *Bob*.

Open Procedure. To open the commitment (φ, δ), *Alice* reveals the witness x', which is in proximity to the original x using some metric distance (e.g., Hamming distance $H(x, x') \leq t_\sigma$). Using the difference vector δ the witness x' restores the codeword $f(c') = f(x' - \delta) = f((x' - x) + c)$ and then translates $x'' = \delta + f(c')$. Then *Bob* computes the commitment $\varphi' = F_k(f(c'), x'')$ and verifies $\varphi' \stackrel{?}{=} \varphi$. In case of failure, the commitment will not open using x'. Otherwise, the commitment is successfully opened and therefore the secret message is $m = m' = g^{-1}(f(c'))$.

4. Security Properties and Analysis of the Proposed Scheme

Let π = (Setup, Commit, Open) be a commitment scheme, and its security properties are (i) correctness, i.e., for every message the commitment generated is valid, (ii) hiding, where any attacker cannot learn information from the commitment c about the message m with any advantage (perfect) or with a negligible advantage, and (iii) binding, where the message m is uniquely bound to c (perfect) or finding another message with the same commitment has negligible probability of success. In further analysis, we assume that both the codeword c and the witness x are drawn randomly from the finite set $\{0, 1\}^n$.

Definition 11 (correctness). A commitment protocol π defined by the quadruplet (p, q, g, h) is correct if, for all messages $m \in M$, $\text{Open}_{(p,q,g,h)}(\text{Commit}_{(p,q,g,h)}(m)) = m$.

The hiding property of the biometrical scheme describes the resilience of the system against adversarial attempts performed by impostor *FakeBob* to crack codeword c or the witness x. We allege that impostor *FakeBob* knows F and can access the commitment (φ, δ).

The binding property represents the resistance of the system against adversarial attempts by an impostor *FakeBob** to guess a codeword c' with $H(x, x') \leq t_\sigma$, such that $F_k(c, x) = F_k(c', x') = \varphi$, for some $x, x' \in X$.

For hiding and binding, we have two different adversaries [51]:

(i) the *unhider* U, which plays the hiding game and has two abstract procedures, one to choose a pair of messages and another to guess which of the two messages corresponds to a given commitment;

(ii) the *binder* B, which plays the binding game and has only a procedure to output two different pairs (message, opening value) that bind to the same commitment.

A commitment protocol satisfies the hiding security property if no adversary exists such that the probability of winning the hiding game is (significantly) better than a blind guess [51]. If this is true, the committer is guaranteed that no information can be inferred by the commitment itself.

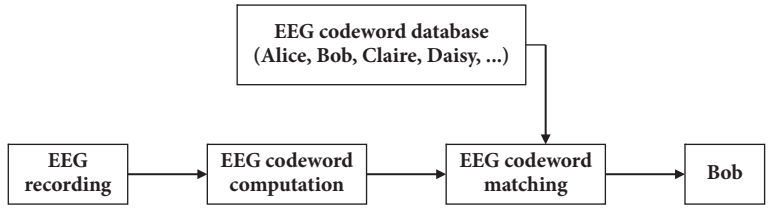

Figure 1: EEG-based user identification/authentication framework.

Definition 12 (hiding). Let $\pi = (\text{Setup}, \text{Commit}, \text{Open})$ be a commitment protocol. Then we can define the hiding properties for adversary U as $\Pr(G_\pi^H(n) = 1) = 1/2$.

Hiding Game. The hiding game G_π^H runs as follows:

(1) The adversary U is given the output of Setup procedure and asked to choose two messages.

(2) The game randomly selects one of them and calls Commit procedure to compute its commitment.

(3) The adversary U is asked to guess which one of the two messages the commitment corresponds to.

(4) The game outputs 1 if the guess of the adversary U is correct.

A commitment protocol satisfies the binding security property if no adversary exists such that the probability of winning the binding game is higher than negligible [51]. If this is true, the receiver is guaranteed that the value committed cannot be changed.

Definition 13 (binding). Let $\pi = (\text{Setup}, \text{Commit}, \text{Open})$ be a commitment protocol. Then one can define the binding properties for each adversary B as $\Pr(G_\pi^B(n) = 1) = 0$.

Binding Game. The binding game G_π^B runs as follows:

(1) The adversary B is given the output of Setup procedure and asked to bind two messages to the same commitment value.

(2) The game outputs 1 if the two messages differ and the commitment is valid for both the messages, that is, if both can be verified by calling the Open procedure.

5. Application of the Method in EEG-Based Biometric System

Here we present the biometric cryptosystem using the EEG signals. Its implementation consists of the system initialization stage, the enrolment stage, and the authentication stage as represented in Figure 1.

At the start of enrolment (see Algorithm 3), the user EEG biometrics is acquired, and feature extraction is performed using the EEG encoding algorithm, which outputs a 400-bit EEG code. We use the EEG features derived from the covariance matrix of EEG data from different EEG channels in the 10–20 international system. The covariance matrix is calculated from N channels in matrix as follows:

$$\text{cov}(X) = \frac{1}{N}\sum_{k=1}^{N}\left(X_{i,k} - X_i\right)\left(X_{j,k} - X_j\right), \tag{3}$$

where X_i holds the mean of all observations in the respective EEG channels.

Next, we compute z-scores of the values in the covariance matrix as follows:

$$z_{i,j} = \frac{\text{cov}_{i,j} - (1/N)\sum_{i=1}^{N}\text{cov}_{i,j}}{\sqrt{\sum_{i=1}^{N}\left(\text{cov}_{i,j} - (1/N)\sum_{i=1}^{N}\text{cov}_{i,j}\right)^2/(N-1)}}; \tag{4}$$

here $\text{cov}_{i,j}$ is an element of the covariance matrix.

And perform normalization of z-score values of the covariance matrix into the range $[0, 1]$ as follows:

$$Z_{\text{norm}} = \frac{Z - \min(Z)}{\max(Z) - \min(Z)}. \tag{5}$$

Finally, we perform the binarization of data using thresholding as follows:

$$Z_{\text{bit}}(i,j) = \begin{cases} 0, & \left[z_{i,j} < 0.5\right] \\ 1, & \left[z_{i,j} \geq 0.5\right]; \end{cases} \tag{6}$$

here $[\cdot]$ is the Iverson bracket operator.

The result is a matrix that contains binary codeword of 400 bit length (obtained from 20×20 covariance matrix). The procedure is summarized in Algorithm 2.

At the same time, a random cryptographic key $\kappa \in \{0,1\}^k$ is prepared using a BCH$(\ldots, k)$ error correction encoded function $\{0,1\}^k \rightarrow C$. The result is a codeword $c \in$ BCH$(\ldots, k)$, which is combined with reference EEG code (both have 400 bits of length).

Authentication phase is described in Algorithm 4. The input EEG biometric B_{EEG} is acquired from a person, resulting in a test EEG code x_{test}. The test EEG code x_{test} with "exclusive OR" denoted as $\oplus$ extracts the codeword $\bar{c} = (x_{\text{test}} \oplus x_{\text{ref}}) \oplus c$. Once it is extracted, the error correction decoded function of BCH$(\ldots, k)$ is used to compute $f(\bar{c}) = f(x_{\text{test}} \otimes \delta)$. Function $f(\bar{c})$ is used to compute $x'_{\text{test}} = \delta \otimes f(\bar{c}) = x_{\text{ref}}(c \oplus f(\bar{c}))$. Nonvalid user will receive a codeword $f(\bar{c})$, such that $H(f(\bar{c}), c) > t_\sigma$. Then $\varphi' = F_k(f(\bar{c}), x'_{\text{test}})$ is computed and matched against the stored φ. If $\varphi' = \varphi$, then the sample x_{test} is accepted and the key κ is released. Otherwise, the identity of a person is rejected.

The biometric scheme is summarized in Figure 2.

6. Experimental Results and Discussion

The implementation of the proposed scheme was made in MATLAB 8.6.0.267246 (R2015b) on an Intel (R) Core (TM)

Input: EEG channel signal values
(1) Calculate covariance matrix of EEG channels.
(2) Calculate z-scores of covariance matrix values.
(3) Normalize z-scores.
(4) Binarize z-scores into EEG code using zero value as threshold.
Output: EEG code x_{ref}

Algorithm 2: Encoding.

Input: EEG biometric B_{EEG} and cryptographic key κ.
(1) Extract EEG code x_{ref} from the EEG biometric data B_{EEG}.
(2) Prepare the cryptographic key κ using BCH codes and obtain the codeword c.
(3) Compute the difference vector $\delta = x_{\text{ref}} \oplus c$.
(4) Compute the commitment $\varphi = F_k(c, x_{\text{ref}})$.
Output: (φ, δ)

Algorithm 3: Enrolment.

Input: EEG biometric B_{EEG} and fuzzy commitment (φ, δ).
(1) Extract EEG code x_{test} from EEG biometric B_{EEG}.
(2) Compute the codeword $f(\bar{c}) = f(x_{\text{test}} \otimes \delta)$
(3) Compute $x'_{\text{test}} = \delta \otimes f(\bar{c})$
(4) Compute $\varphi' = F_k(f(\bar{c}), x'_{\text{test}})$
(5) Check $\varphi' \stackrel{?}{=} \varphi$
Output: The user is authenticated or rejected.

Algorithm 4: Authentication.

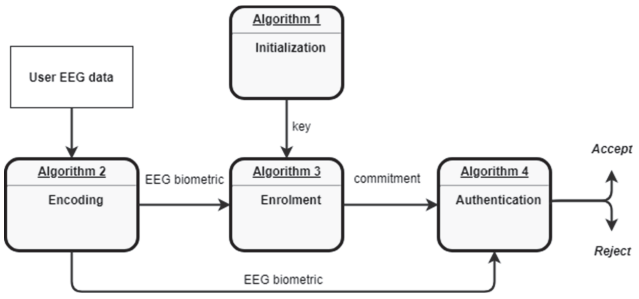

Figure 2: Summary of the proposed EEG biometric scheme.

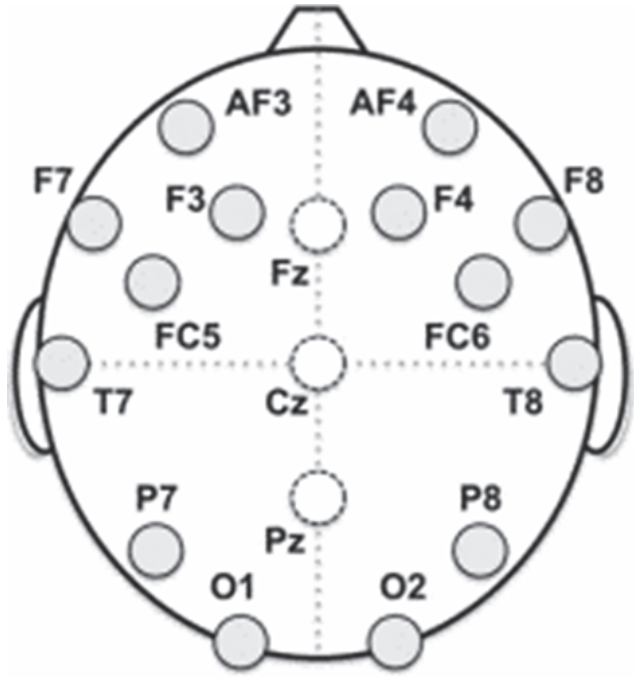

Figure 3: Electrode locations for collection of EEG data.

i5-4590 CPU (x64), running at 3.30 GHz with 12 GB of RAM in Windows 10 Enterprise ver. 1709. For the performance evaluation, we have used a dataset that consists of 65 EEG samples from 42 different subjects, where each sample consisted of 1000 signal values. The number of subjects satisfies the condition of Lazar et al. [52], who stated that studies using data collected from 20 or more participants are more convincing than those performed with a lesser number of participants. The EEG data we use in this study was collected from 42 healthy adults. During data collection, the subjects were instructed to lie still on a table and breathe normally. The data was collected using a medical-grade EEG device from the electrodes attached to subjects following the international 10–20 standard, which are depicted as circles in Figure 3. The sampling rate was 256 s^{-1}.

To perform code matching, we computed the Hamming distance between two EEG codewords A and B as follows:

$$H = \frac{1}{n}\sum_{i=1}^{n}\left(\text{code}\left(A_i\right) \oplus \text{code}\left(B_i\right)\right); \tag{7}$$

here code(A_i) and code(B_i) are the ith bit in EEG codes of persons A and B, respectively.

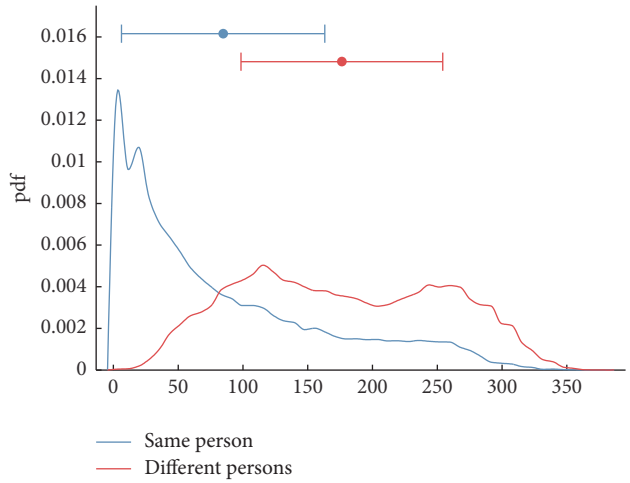

Figure 4: Probability density functions Hamming distances between the same person and the different persons.

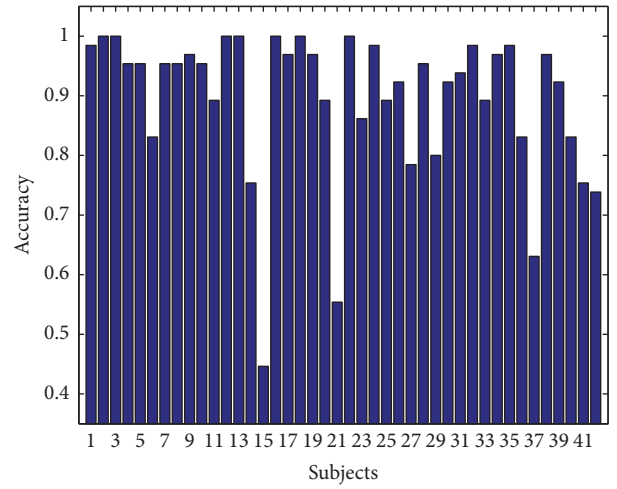

Figure 5: Subject-wise correct classification rate.

The intraperson Hamming distances have been computed using EEG samples from the same subjects, while the interperson Hamming distances were computed using samples from different subjects. We carried out 65 comparisons for the same subjects and 118,335 comparisons between different subjects. The result of the probability distribution function (pdf) of the intraperson and interperson Hamming distances is shown in Figure 4. One can see that up to 87 bits of error (intersection of both graphs) are tolerated.

We use the following scenarios as suggested by Gui et al. [53].

Scenario 1. The aim is to identify correctly each of the 42 subjects participating in the study. The training and testing datasets include data from all 42 subjects and the classification outcome belongs to one of 42 classes.

Scenario 2. The aim is to identify one subject versus all other 41 subjects. There are only two classes: positive (target subject) and negative (all other subjects). The training dataset was combined using the data from all subjects and the performing resampling so that both classes are balanced.

Evaluation. Following the suggestion of Jorgensen and Yu [54], we use False Accept Rate (FAR), False Reject Rate (FRR), and Equal Error Rate (EER) as key effectiveness metrics of the biometric system. FAR and FRR describe whether the system correctly identifies the subject. ERR specifies the error rate where the values of FAR and FRR become equal. The metrics are calculated as follows:

$$\begin{aligned} \mathrm{FRR} &= \frac{|\mathrm{FR}|}{|\mathrm{AA}|}, \\ \mathrm{FAR} &= \frac{|\mathrm{FA}|}{|\mathrm{IA}|}; \end{aligned} \tag{8}$$

here |FR| is the number of false rejections, that is, falsely rejecting a verification attempt of a valid subject, |AA| is the number of authorized attempts, |FA| is the number of false acceptances, i.e., falsely accepting the claim of an impostor as a valid user, and |IA| is the number of attempts by an impostor.

The performance is evaluated using the correct classification rate (CCR) as follows:

$$\mathrm{CCR} = \frac{|C|}{|T|}; \tag{9}$$

here |C| is the number of correct classification decisions and |T| is the number of trials.

EER is defined as a unique point where FRR is equal to FAR. A lower EER indicates a more accurate system.

$$\mathrm{EER} = \mathrm{FAR}\left(T^*\right) = \mathrm{FRR}\left(T^*\right); \tag{10}$$

here $T^* = \arg\min(|\mathrm{FAR}(T) - \mathrm{FRR}(T)|)$

This ensures that the threshold found will satisfy the equality condition between FRR and FAR as closely as possible.

We have implemented both Scenarios 1 and 2 testing, as subjected by Gui et al. [53]. In Scenario 1, CCR for each of the subjects is presented in Figure 5.

Note that while the overall accuracy is quite good (mean accuracy 0.895), for some of the subjects, it was quite low (e.g., only 0.446 for subject 15). This result may have been caused by the infamous BCI illiteracy effect [55]. Nevertheless, when inspecting the cumulative distribution plot of accuracy distribution (see Figure 6), we can see that 50% of subjects have accuracy higher than 0.93, while only 10% of subjects have accuracy lower than 73%.

As accuracy data is not normally distributed, the Fisher Z-transformation was applied to calculate population mean and standard deviation, yielding the mean accuracy of 0.892 with standard deviation of 0.135.

The subject-wise confusion matrix is presented in Figures 7 and 8. As the number of subjects is too high for meaningful visualization, the confusion matrix was sorted according to its diagonal value (correct hits), and the values for only 10

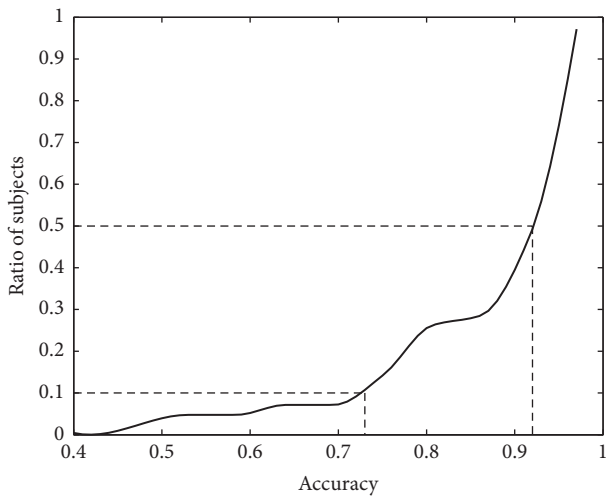

Figure 6: Cumulative distribution plot of accuracy distribution in subject classification.

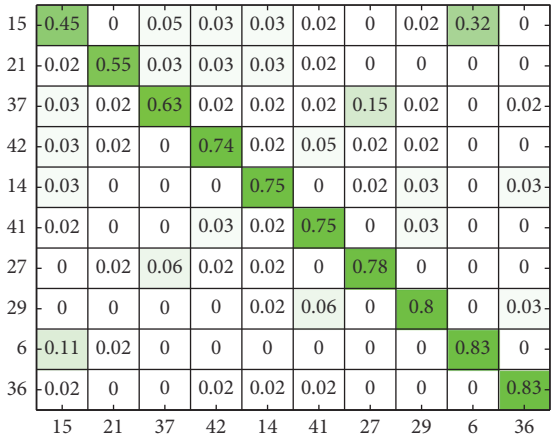

Figure 7: Subject-wise confusion matrix of classification results in Scenario 1: 10 worst performing subjects.

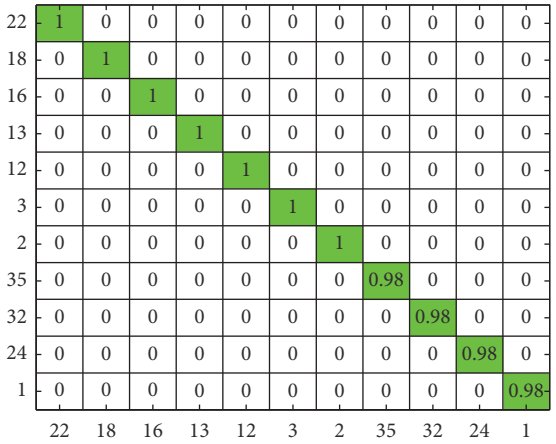

Figure 8: Subject-wise confusion matrix of classification results in Scenario 1: 10 best performing subjects.

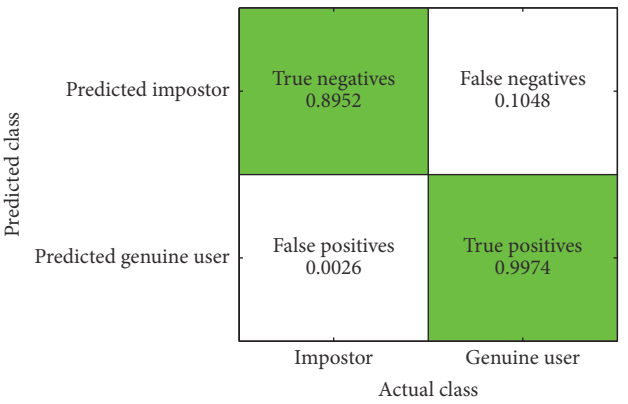

Figure 9: Confusion matrix of classification results in Scenario 2.

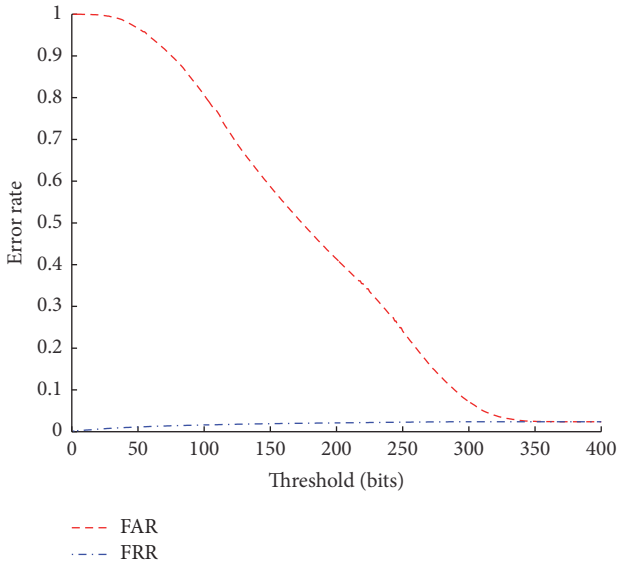

Figure 10: FAR and FRR of the proposed EEG biometric system.

worst performing subjects (Figure 7) and 10 best performing subjects (Figure 8) are shown.

For Scenario 2, the confusion matrix is presented in Figure 9. We can see that True Positive Rate (TPR) is 0.9974. We have evaluated the confusion matrix statistically using the McNemar test. Critical value at 95% significance level is 3.8415. McNemar chi-square with Yates correction is 0.001, while $p = 0.966$. Therefore, the results are significant at alpha = 0.05 level.

The values for FAR, FRR, and ERR are represented in Figure 10.

The Area Under Curve (AUC) is calculated as the area under the Receiver Operating Characteristic (ROC) [56] curve and represents discrimination, that is, the ability of the classifier to discriminate between a positive example and a negative example.

We have achieved the following results, which are summarized in Table 1.

Table 1: Summary of classification results.

TAR	FRR	ERR	AUC	TPR
0.8952	0.026	0.024	0.9271	0.9974

Table 2: Comparison of the proposed method with the Fladby's method [27].

EER (proposed method + our dataset)	EER (Fladby method + Fladby dataset)	EER (Fladby method + our dataset)
0.024	0.2142	0.3059 (mean, all channels) 0.2945 (Fp1) 0.2283 (best, P4)

Comparison. In Table 2 and Figure 11, we compare our results with those of Fladby [27]. Note that Fladby used a simple EEG reading device (Neurosky ThinkGear) with only one channel of EEG data (Fp1), which may be affected by eye artefacts. Sampling frequency was only 128 Hz, and 20 seconds of signal samples for each of eight different tasks was used for authentication, which is unpractical for many applications. Nevertheless, the method of Fladby [27], which employs widely used power spectral features of EEG bands, can be considered as a baseline, against which our method could be compared. We have thoroughly replicated the conditions of the experiment by Fladby on our dataset, using the same number of samples (2560) for each snippet of subject EGG data and a feature based distance metric to discriminate between genuine and fraudulent authentication results, and calculated the EER value. Note that our method uses all 20 EEG channels of the 10–20 international system, while Fladby used only one EEG channel. Nevertheless, we have replicated the calculations of the Fladby's method on each EEG channel to make a fair comparison. The results are presented in Table 2 as well as in Figure 11. Fladby's method achieved mean ERR of 0.3059, while the Fp1 channel originally used by Fladby achieved an ERR of 0.2945, and best ERR was achieved using the P4 channel (0.2283). Note that we could not apply our method on Fladby's data, because it is not available.

Based on the presented comparison, we can claim that the proposed method achieved better results for subject authentication than the Fladby [27] method.

7. Conclusion

This paper presents a secure cryptographic authentication scheme for EEG-based biometrics based on the fuzzy commitment scheme and the error-correcting Bose-Chaudhuri-Hocquenghem (BCH) codes. The EEG features are derived from the covariance matrix of EEG data from different EEG channels in the 10–20 international system. The biometric system was evaluated using the EEG dataset obtained from 42 subjects. The experimental results show that the system can generate up to 400 bits of cryptographic key from the EEG codes, while tolerating up to 87 bits of error. The performance of the biometric cryptosystem is an Equal Error Rate (EER) of 0.024, True Positive Rate (TPR) of 0.9974, and Area Under Curve (AUC) of 0.927.

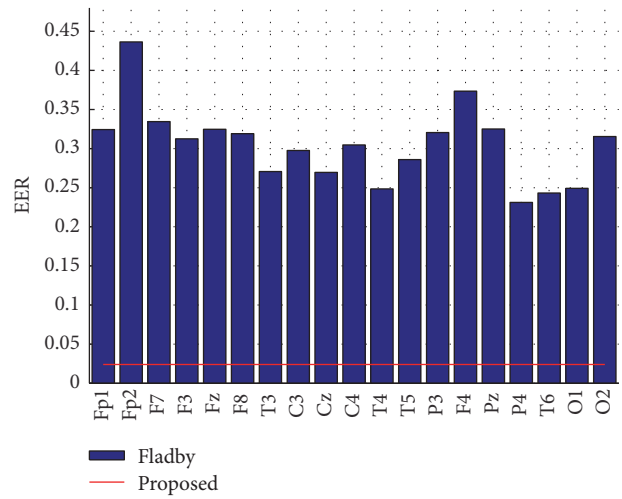

Figure 11: Comparison of EER of our method and Fladby's method [27] for each EEG channel.

Conflicts of Interest

The authors declare that there are no conflicts of interest regarding the publication of this paper.

Acknowledgments

The authors would like to acknowledge the support from the Rector pro-quality Grant no. 09/010/RGJ18/0034 at the Silesian University of Technology. The authors would also like to thank professor A. Vainoras of Lithuanian University of Health Sciences for kindly provided EEG dataset.

References

[1] T. M. Vaughan, W. J. Heetderks, L. J. Trejo et al., *Brain-Computer Interface Technology: A Review of The Second International Meeting*, 2003.

[2] C. G. Lim, T. S. Lee, C. Guan et al., "A brain-computer interface based attention training program for treating attention deficit hyperactivity disorder," *PLoS ONE*, vol. 7, no. 10, Article ID e46692, 2012.

[3] M. Ahn, M. Lee, J. Choi, and S. C. Jun, "A review of brain-computer interface games and an opinion survey from researchers, developers and users," *Sensors*, vol. 14, no. 8, pp. 14601–14633, 2014.

[4] I. Martišius and R. Damaševičius, "A prototype SSVEP based real time BCI gaming system," *Computational Intelligence & Neuroscience*, vol. 2016, Article ID 3861425, 15 pages, 2016.

[5] Y. Iidal, D. Tsutsumi, S. Saeki, Y. Ootsuka, T. Hashimoto, and R. Horie, "The effect of immersive head mounted display on a brain computer interface game," *Advances in Intelligent Systems and Computing*, vol. 483, pp. 211–219, 2017.

[6] J. D. Woodward, N. M. Orlans, and P. T. Higgins, *Biometrics*, McGraw-Hill, Berkeley, Calif, USA, 1953.

[7] A. S. Danko and G. C. Fernández, "My brain is my passport. Verify me," in *Proceedings of the 2016 IEEE International Conference on Consumer Electronics (ICCE)*, pp. 19–22, Las Vegas, NV, USA, 2002.

[8] C.-C. Hsu and P.-T. Shih, "A novel sleep apnea detection system in electroencephalogram using frequency variation," *Expert Systems with Applications*, vol. 38, no. 5, pp. 6014–6024, 2011.

[9] M. Taghavi, R. Boostani, M. Sabeti, and S. M. A. Taghavi, "Usefulness of approximate entropy in the diagnosis of schizophrenia," *Iranian Journal of Psychiatry and Behavioral Sciences*, vol. 5, no. 2, pp. 62–70, 2011.

[10] M. Li, W. Chen, and T. Zhang, "Classification of epilepsy EEG signals using DWT-based envelope analysis and neural network ensemble," *Biomedical Signal Processing and Control*, vol. 31, pp. 357–365, 2017.

[11] U. A. Qidwai and M. Shakir, "Fuzzy classification-based control of wheelchair using EEG data to assist people with disabilities," in *Proceedings of the 19th International Conference on Neural Information Processing, ICONIP 2012*, vol. 7666 of *Springer Lecture Notes in Computer Science 7666*, pp. 458–467, Doha, Qatar, 2012.

[12] R. N. Khushaba, C. Wise, S. Kodagoda, J. Louviere, B. E. Kahn, and C. Townsend, "Consumer neuroscience: Assessing the brain response to marketing stimuli using electroencephalogram (EEG) and eye tracking," *Expert Systems with Applications*, vol. 40, no. 9, pp. 3803–3812, 2013.

[13] Researchbeam, "Global EEG and ECG Biometrics Market 2016-2020," 2016.

[14] S. Z. Li and A. K. Jain, "EEG biometrics," *Encyclopedia of Biometrics*, pp. 389–396, 2015.

[15] H. Van Dis, M. Corner, R. Dapper, G. Hanewald, and H. Kok, "Individual differences in the human electroencephalogram during quiet wakefulness," *Electroencephalography and Clinical Neurophysiology*, vol. 47, no. 1, pp. 87–94, 1979.

[16] C. E. M. Van Beijsterveldt and G. C. M. Van Baal, "Twin and family studies of the human electroencephalogram: A review and a meta-analysis," *Biological Psychology*, vol. 61, no. 1-2, pp. 111–138, 2002.

[17] E. Maiorana, D. La Rocca, and P. Campisi, "On the permanence of EEG signals for biometric recognition," *IEEE Transactions on Information Forensics and Security*, vol. 11, no. 1, pp. 163–175, 2016.

[18] M. Delpozo-Banos, C. M. Travieso, C. T. Weidemann, and J. B. Alonso, "EEG biometric identification: A thorough exploration of the time-frequency domain," *Journal of Neural Engineering*, vol. 12, no. 5, Article ID 056019, 2015.

[19] D. L. Rocca, P. Campisi, B. Vegso et al., "Human brain distinctiveness based on EEG spectral coherence connectivity," *IEEE Transactions on Biomedical Engineering*, vol. 61, no. 9, pp. 2406–2412, 2014.

[20] M. Fraschini, A. Hillebrand, M. Demuru, L. Didaci, and G. L. Marcialis, "An EEG-based biometric system using eigenvector centrality in resting state brain networks," *IEEE Signal Processing Letters*, vol. 22, no. 6, pp. 666–670, 2015.

[21] A. Juels and M. Wattenberg, "A fuzzy commitment scheme," in *Proceedings of the 1999 6th ACM Conference on Computer and Communications Security (ACM CCS)*, pp. 28–36, November 1999.

[22] A. Juels and M. Sudan, "A fuzzy vault scheme," *Designs, Codes and Cryptography. An International Journal*, vol. 38, no. 2, pp. 237–257, 2006.

[23] F. Hao, R. Anderson, and J. Daugman, "Combining crypto with biometrics effectively," *IEEE Transactions on Computers*, vol. 55, no. 9, pp. 1081–1088, 2006.

[24] C. Rathgeb and A. Uhl, "A survey on biometric cryptosystems and cancelable biometrics," *EURASIP Journal on Information Security*, vol. 2011, article no. 3, pp. 1–25, 2011.

[25] A. A. Al-Saggaf, "Secure method for combining cryptography with iris biometrics," *Journal of Universal Computer Science*, 2018, Special Issue on Advances in Security and Privacy of Multimodal Interfaces.

[26] K. Revett, F. Deravi, and K. Sirlantzis, "Biosignals for user authentication - towards cognitive biometrics?" in *Proceedings of the 2010 International Conference on Emerging Security Technologies, EST 2010, Robots and Security, ROBOSEC 2010, Learning and Adaptive Behavior in Robotic Systems, LAB-RS 2010*, pp. 71–76, Canterbury, UK, September 2010.

[27] K. Fladby, *Brain Wave Based Authentication*, Gjøvik University College, 2008.

[28] R. Palaniappan, "Method of identifying individuals using VEP signals and neural network," *IEE Proceedings Science, Measurement and Technology*, vol. 151, no. 1, pp. 16–20, 2004.

[29] N. Liang, P. Saratchandran, G. Huang, and N. Sundararajan, "Classification of mental tasks from EEG signals using extreme learning machine," *International Journal of Neural Systems*, vol. 16, no. 1, pp. 29–38, 2006.

[30] S. Marcel and J. D. R. Millán, "Person authentication using brainwaves (EEG) and maximum a posteriori model adaptation," *IEEE Transactions on Pattern Analysis and Machine Intelligence*, vol. 29, no. 4, pp. 743–752, 2007.

[31] C. R. Hema, M. P. Paulraj, and H. Kaur, "Brain signatures: a modality for biometric authentication," in *Proceedings of the International Conference on Electronic Design (ICED '08)*, pp. 1–3, Penang, Malaysia, December 2008.

[32] C. He, X. Lv, and Z. J. Wang, "Hashing the mAR coefficients from EEG data for person authentication," in *Proceedings of the IEEE International Conference on Acoustics, Speech, and Signal Processing (ICASSP '09)*, pp. 1445–1448, Taipei, Taiwan, April 2009.

[33] Z. Mu and J. Hu, "Research of EEG identification computing based on AR model," in *Proceedings of the 2009 International Conference on Future BioMedical Information Engineering, FBIE 2009*, pp. 366–368, Sanya, China, December 2009.

[34] K. Brigham and B. V. K. V. Kumar, "Subject identification from Electroencephalogram (EEG) signals during imagined speech," in *Proceedings of the 4th IEEE International Conference on Biometrics: Theory, Applications and Systems, BTAS 2010*, pp. 1–8, September 2010.

[35] J.-F. Hu, "Biometric system based on EEG signals by feature combination," in *Proceedings of the 2010 International Conference on Measuring Technology and Mechatronics Automation (ICMTMA 2010)*, pp. 752–755, Changsha City, China, March 2010.

[36] A. Zúquete, B. Quintela, J. Cunha, and A. Zúquete, "Biometric authentication with electroencephalograms: evaluation of its suitability using visual evoked potentials," in *Biomedical Engineering Systems and Technologies*, A. Fred, J. Filipe, and H. Gamboa, Eds., vol. 127, pp. 290–306, Springer, Heidelberg, Berlin, Germany, 2011.

[37] C. Ashby, A. Bhatia, F. Tenore, and J. Vogelstein, "Low-cost electroencephalogram (EEG) based authentication," in *Proceedings of the 2011 5th International IEEE/EMBS Conference on Neural Engineering, NER 2011*, pp. 442–445, Cancun, Mexico, May 2011.

[38] H. A. Shedeed, "A new method for person identification in a biometric security system based on brain EEG signal processing," in *Proceedings of the 2011 World Congress on Information and Communication Technologies, WICT 2011*, pp. 1205–1210, Mumbai, India, December 2011.

[39] J. Chuang, H. Nguyen, C. Wang, and B. Johnson, "I think therefore I am: Usability and security of authentication using brainwaves," in *Financial Cryptography and Data Security*, vol. 7862 of *Lecture Notes in Computer Science*, pp. 1–16, Springer, Heidelberg, Berlin, Germany, 2013.

[40] S.-K. Yeom, H.-I. Suk, and S.-W. Lee, "Person authentication from neural activity of face-specific visual self-representation," *Pattern Recognition*, vol. 46, no. 4, pp. 1159–1169, 2013.

[41] Z. Dan, Z. Xifeng, and G. Qiangang, "An Identification System Based on Portable EEG Acquisition Equipment," in *Proceedings of the 2013 Third International Conference on Intelligent System Design and Engineering Applications (ISDEA)*, pp. 281–284, Hong Kong, China, January 2013.

[42] M. Abo-Zahhad, S. M. Ahmed, and S. N. Abbas, "A new EEG acquisition protocol for biometric identification using eye blinking signals," *Intelligent Systems and Applications*, vol. 7, no. 6, pp. 48–54, 2015.

[43] T. Koike-Akino, R. Mahajan, T. K. Marks et al., "High-accuracy user identification using EEG biometrics," in *Proceedings of the 38th Annual International Conference of the IEEE Engineering in Medicine and Biology Society, EMBC 2016*, pp. 854–858, USA, August 2016.

[44] A. Crobe, M. Demuru, L. Didaci, G. L. Marcialis, and M. Fraschini, "Minimum spanning tree and k-core decomposition as measure of subject-specific EEG traits," *Biomedical Physics and Engineering Express*, vol. 2, no. 1, 2016.

[45] S. Barra, A. Casanova, M. Fraschini, and M. Nappi, "Fusion of physiological measures for multimodal biometric systems," *Multimedia Tools and Applications*, vol. 76, no. 4, pp. 4835–4847, 2017.

[46] M. Garau, M. Fraschini, L. Didaci, and G. L. Marcialis, "Experimental results on multi-modal fusion of EEG-based personal verification algorithms," in *Proceedings of the 9th IAPR International Conference on Biometrics, ICB 2016*, pp. 1–6, Halmstad, Sweden, June 2016.

[47] Q. Q. Li, D. Ding, and M. Conti, "Brain-Computer Interface applications: Security and privacy challenges," in *Proceedings of the 2015 IEEE Conference on Communications and Network Security (CNS)*, pp. 663–666, Florence, Italy, September 2015.

[48] I. Nakanishi, K. Ozaki, and S. Li, "Evaluation of the brain wave as biometrics in a simulated driving environment," in *Proceedings of the 2012 International Conference of the Biometrics Special Interest Group, BIOSIG 2012*, pp. 1–5, Darmstadt, Germany, September 2012.

[49] B. Johnson, T. Maillart, and J. Chuang, "My thoughts are not your thoughts," in *Proceedings of the 2014 ACM International Joint Conference on Pervasive and Ubiquitous Computing, UbiComp 2014*, pp. 1329–1338, USA, September 2014.

[50] S. T. Archer and B. D. Pless, *Stimulation Signal Generator for an Implantable Device*, US Patent 6690974, 2004.

[51] R. Metere and C. Dong, "Automated cryptographic analysis of the pedersen commitment scheme," in *Proceedings of the International Conference on Mathematical Methods, Models, and Architectures for Computer Network Security, MMM-ACNS 2017*, vol. 10446 of *Lecture Notes in Computer Science 10446*, pp. 275–287, Springer, Warsaw, Poland, 2017.

[52] J. Lazar, J. H. Feng, and H. Hochheiser, *Research Methods in Human-Computer Interaction*, Wiley, New York, NY, USA, 2010.

[53] Q. Gui, Z. Jin, and W. Xu, "Exploring EEG-based biometrics for user identification and authentication," in *Proceedings of the 2014 IEEE Signal Processing in Medicine and Biology Symposium (SPMB)*, pp. 1–6, Philadelphia, PA, USA, December 2014.

[54] Z. Jorgensen and T. Yu, "On mouse dynamics as a behavioral biometric for authentication," in *Proceedings of the 6th International Symposium on Information, Computer and Communications Security, ASIACCS 2011*, pp. 476–482, China, March 2011.

[55] C. Vidaurre and B. Blankertz, "Towards a cure for BCI illiteracy," *Brain Topography*, vol. 23, no. 2, pp. 194–198, 2010.

[56] H. V. Poor, *An Introduction to Signal Detection and Estimation*, chapter 4, Springer, New York, NY, USA, 1985.

Hindawi
Computational Intelligence and Neuroscience
Volume 2018, Article ID 9672871, 8 pages
https://doi.org/10.1155/2018/9672871

Research Article

Single-Trial Evoked Potential Estimating Based on Sparse Coding under Impulsive Noise Environment

Nannan Yu,[1] Ying Chen,[1] Lingling Wu,[1] and Hanbing Lu [2]

[1] *School of Electrical Engineering and Automation, Jiangsu Normal University, Xuzhou 221116, China*
[2] *Department of Internal Neurology, Xuzhou Central Hospital, Xuzhou 221116, China*

Correspondence should be addressed to Hanbing Lu; luhanbing111@126.com

Received 24 October 2017; Accepted 11 February 2018; Published 22 March 2018

Academic Editor: Plácido R. Pinheiro

Estimating single-trial evoked potentials (EPs) corrupted by the spontaneous electroencephalogram (EEG) can be regarded as signal denoising problem. Sparse coding has significant success in signal denoising and EPs have been proven to have strong sparsity over an appropriate dictionary. In sparse coding, the noise generally is considered to be a Gaussian random process. However, some studies have shown that the background noise in EPs may present an impulsive characteristic which is far from Gaussian but suitable to be modeled by the α-stable distribution ($1 < \alpha \leq 2$). Consequently, the performances of general sparse coding will degrade or even fail. In view of this, we present a new sparse coding algorithm using p-norm optimization in single-trial EPs estimating. The algorithm can track the underlying EPs corrupted by α-stable distribution noise, trial-by-trial, without the need to estimate the α value. Simulations and experiments on human visual evoked potentials and event-related potentials are carried out to examine the performance of the proposed approach. Experimental results show that the proposed method is effective in estimating single-trial EPs under impulsive noise environment.

1. Introduction

Evoked potentials (EPs) are time-locked biological signals recorded from the scalp in response to a variety of well-defined external stimuli [1]. Depending on the modality of stimulation, EPs are categorized into auditory (AEPs), visual (VEPs), somatosensory (SEPs), and motor (MEPs) evoked potentials. EPs contain several components that can be distinguished according to their respective latencies and amplitudes [2]. The latency variations of specific components can objectively reflect changes in the underlying state of the neural pathways, which is very meaningful in cognitive science research and clinical applications, such as brain-computer interface, the diagnosis of possible brain injury, and the intraoperative monitoring [3, 4]. Many single-trial EP extracting methods have been proposed in order to enhance the ability to track latency variations [5].

EP signals have time-locked (quasi-periodic) characteristics and are always accompanied by nonstationary ongoing electroencephalogram (EEG) signals. Moreover, the signal-to-noise ratio (SNR) of EP records is usually low (0 to −30 dB). Estimating single-trial EPs corrupted by EEG can be regarded as signal denoising problem. Sparse coding is a powerful tool for the analysis of nonstationary signals [6, 7]; it has achieved significant success in signal denoising and separation. Huang et al. [8] proposed the mixed overcomplete dictionary-based sparse component decomposition method (MOSCA), which decomposes the EP and EEG signals in the wavelet dictionary (WA) and discrete cosine transform (DCT) dictionary, respectively. However, the WA and DCT dictionaries cannot meet completely the characteristics of EPs and EEG. Their partial components are represented by the wrong dictionaries and their corresponding coefficients. Therefore, MOSCA cannot separate the EP and EEG signals sufficiently. To solve this problem, we proposed a dictionary construction method for the EP signal and a double-trial estimation method based on joint sparse representation [9].

Traditionally, for mathematical convenience, the noise in EP signals is considered to be a Gaussian random process. However, some studies have shown that the background noise in clinical EP signals is often impulsive non-Gaussian distributed [10]. Consequently, the EP estimation algorithms developed under a Gaussian background noise assumption may fail or be not optimal. That is, the impulsive feature in

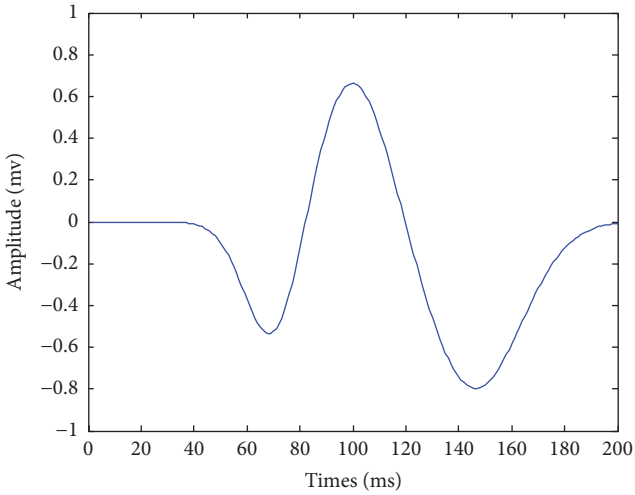

Figure 1: Stimulated EP.

the noise may cause the performance of algorithms based on the second-order moment (SOM) to degrade or even fail. The α-stable distribution is a widely used class of statistical distributions for impulsive non-Gaussian random processes [11]. In comparison with a Gaussian process, an α-stable process often has many more sharp spikes in its realization and a probability density function (PDF) with a heavy tail [12, 13]. It has been shown that an α-stable ($1 < \alpha \leq 2$) process is more suitable for modeling the background noise in EP observations than is a Gaussian process because the noise is often impulsive and its PDF has a heavy tail. This will degrade the performance of the sparse coding algorithm.

In this paper, we present a novel approach to solving the EP estimating problem under impulsive noise environment based on sparse coding using least mean p-norm (SC-LMP) optimization. It has been proven that least mean p-norm algorithm always works if p is set to 1 when $1 < \alpha \leq 2$ [14]. So in SC-LMP, in order to facilitate solving the sparse coefficients, the 1-norm is used in place of the p-norm. We then formulate the minimization of the cost function into a linear programming (LP) problem. The EPs can be reconstructed by the sparse coefficients and the dictionary. Experimental results show that the SC-LMP algorithm can work well when the α value dynamically changes. It can track latency variations even in situations of extremely low SNR. The rest of this paper is organized as follows. Section 2 gives a detailed description of our single-trial estimation algorithm. Section 3 contains our experimental results obtained by using the SC-LMP method and a comparison with traditional sparse coding methods with least-mean-square (LMS) optimization and MOSCA. Section 4 presents our conclusions.

2. Single-Trial Evoked Potential Estimation with SC-LMP

Numerous studies have shown that in EPs the background noise is found to be non-Gaussian and suitable to be modeled by the α-stable distribution. The main parts of our method consist of removing the noise $e(t)$ from the measurement $y(t)$ and then reconstructing the single-trial EP $s(t)$. The measurement $y(t)$ is

$$y(t) = s(t) + e(t), \tag{1}$$

where $s(t)$ is a time-locked signal and $e(t)$ is a zero-mean α-stable distribution process. A fractional lower-order α-stable (FLOA) distribution is obtained if $0 < \alpha < 2$ for an α-stable distribution. One distinct feature of an FLOA process is that there are more samples far away from the mean or the median than those of a Gaussian process. Thus, the wave forms of FLOA observations have many more impulsive spikes.

2.1. 1-Norm Cost Function. Estimating single-trial evoked potentials (EPs) corrupted by the spontaneous electroencephalogram (EEG) can be regarded as signal denoising problem. A least square (2-norm) approach is commonly used. However, it has been shown that the background noise in EPs may present an impulsive characteristic which is far from Gaussian but suitable to be modeled by the α-stable distribution ($0 < \alpha < 2$). Compared with L_2-norm, L_P-norm is a better option.

Sparse coding is a powerful tool in analysing nonstationary signals, and it has shown significant success in signal denoising and separation. And in our previous papers [9], we have proved that EPs have strong sparsity over an appropriate dictionary. The EPs can be represented as

$$s(t) = D\theta, \tag{2}$$

where $D \in R^{M\times N}$ is the dictionary and $\theta \in R^{N\times 1}$ is the sparse coefficient.

The EP estimating problem can be solved using sparse coding with least mean p-norm (SC-LMP) optimization. The cost function is

$$E(\theta) = \left\| y(t) - D\theta \right\|_p + \lambda \left\| \theta \right\|_1. \tag{3}$$

It has been proven that the least mean p-norm algorithm always works if p is set to 1 when $1 < \alpha < 2$. So in SC-LMP, in order to facilitate solving the sparse coefficients, the L_1-norm is used in place of the p-norm. So the function can be rewritten as

$$E(\theta) = \left\| y(t) - D\theta \right\|_1 + \lambda \left\| \theta \right\|_1. \tag{4}$$

The problem for the estimation of θ by minimizing (4) could be formulated into

$$\min_{\theta} \quad \|P\theta - Y\|_1 \qquad \text{where } P = \begin{bmatrix} D \\ \lambda I^{N\times N} \end{bmatrix},\ Y = \begin{bmatrix} y(t) \\ 0^{N\times 1} \end{bmatrix}, \tag{5}$$

where 0 denotes the vector of all zeros with appropriate size.

2.2. Optimization. In order to solve the optimization problem in (5), we formulate the problem as a LP problem as follows. Let $x = P\theta - Y$, $x^+ = \max(x, 0)$, and $x^- = \max(-x, 0)$. Then x can be expressed as $x^+ - x^-$. The minimization problem can now be rewritten as

$$\begin{aligned} \min_{\theta, x^+, x^-} \quad & 1^T x^+ + 1^T x^- \\ \text{s.t.} \quad & P\theta - Y = x^+ - x^- \\ & x^+, x^- \geq 0, \end{aligned} \tag{6}$$

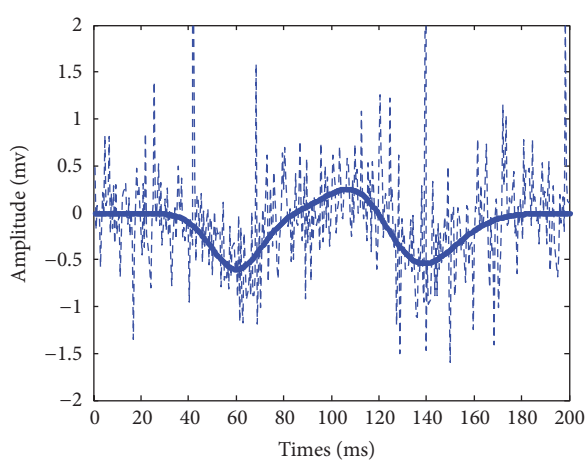

(a1)

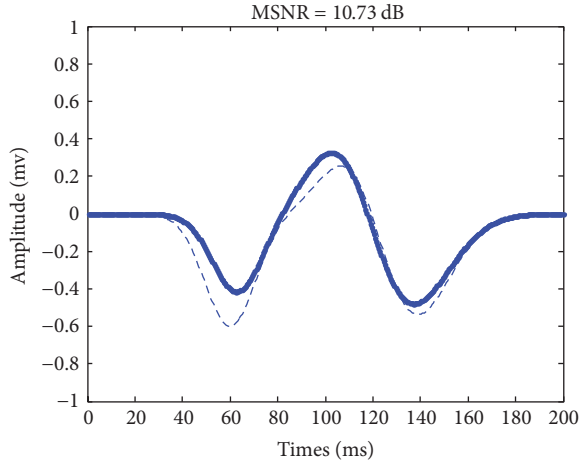

(b1)

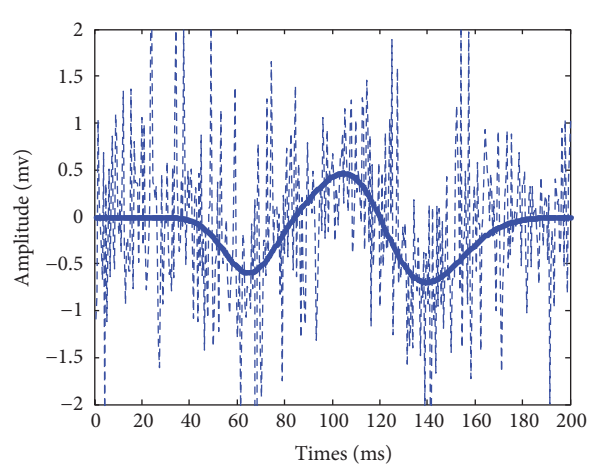

(a2)

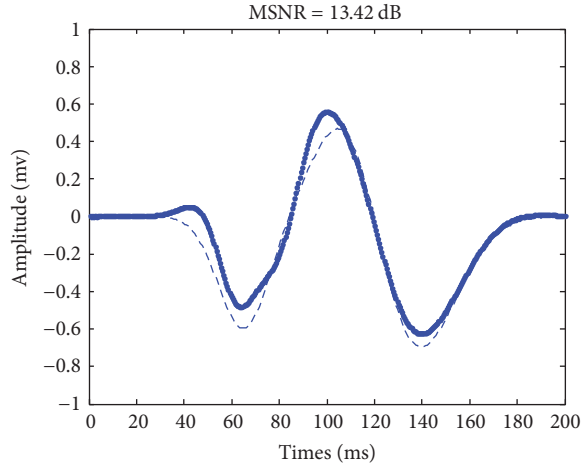

(b2)

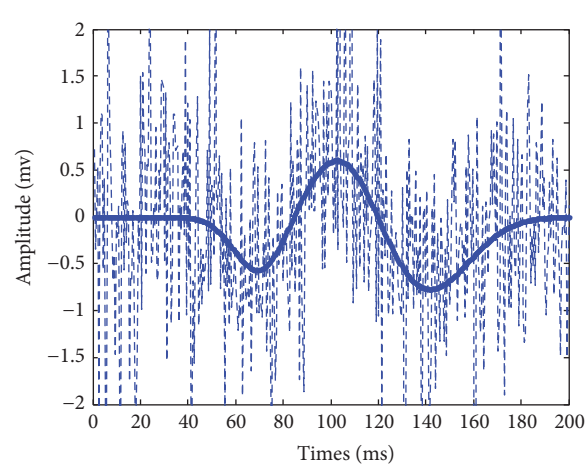

(a3)

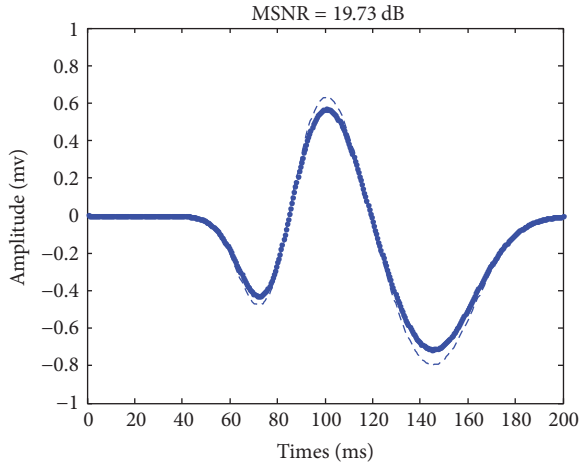

(b3)

Figure 2: Continued.

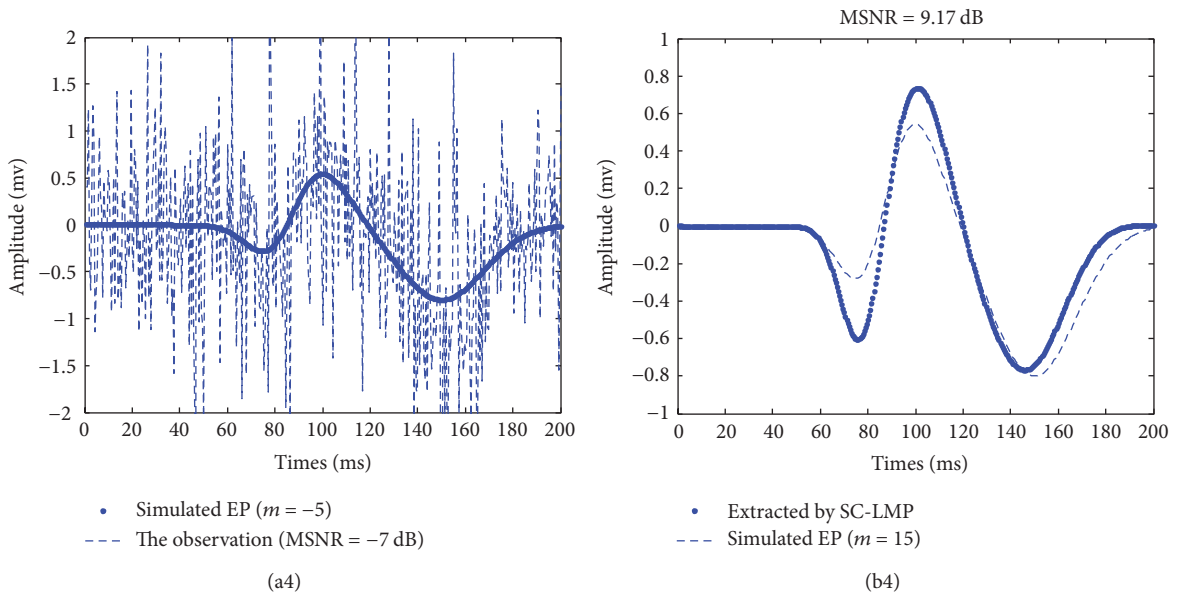

FIGURE 2: Single-trial EPs $s(t, m = 15, 10, 5, -5)$ with MSNR = −7 dB estimated using our method.

where 1 denotes the vector of all ones with appropriate size. The equation above can be written as a LP problem in a standard form as follows:

$$\begin{aligned} \min_{x} \quad & q^T x \\ \text{s.t.} \quad & Ax = Y \\ & \text{where } q = \begin{bmatrix} 0 \\ 1 \\ 1 \end{bmatrix}, \; x = \begin{bmatrix} \theta \\ x^+ \\ x^- \end{bmatrix}, \; A = \begin{bmatrix} P & -I & I \end{bmatrix}. \end{aligned} \tag{7}$$

Then we can solve the LP problem using linear interior point solver (LIPSOL), which is based on a primal-dual interior point method.

$$q = \begin{bmatrix} 0 \\ 1 \\ 1 \end{bmatrix}, \quad x = \begin{bmatrix} \theta \\ x^+ \\ x^- \end{bmatrix}, \quad A = \begin{bmatrix} P & -I & I \end{bmatrix}. \tag{8}$$

2.3. Reconstructing. After solving (7), we can use the solution x to reconstruct the single-trial EP $\hat{s}(t)$ as follows:

$$\hat{s}(t) = D\hat{\theta}. \tag{9}$$

3. Experiment Results

Computer simulation was conducted to verify the performance of the SC-LMP algorithm for EP signal estimation under FLOA noise environments. The simulated EP data is constructed by superimposing three Gauss distribution functions [15] and the waveform is shown in Figure 1; thus,

$$\begin{aligned} s(t, m) = & -0.6 \exp\left(-\frac{(t - (75 - m))^2}{15^2}\right) \\ & + 0.7 \exp\left(-\frac{(t - (100 + m))^2}{20^2}\right) \\ & - 0.8 \exp\left(-\frac{(t - (145 - m))^2}{25^2}\right). \end{aligned} \tag{10}$$

FLOA noise with various α values was generated to simulate background noise. The observations were additive mixtures of the noise-free signals and the simulated FLOA background noise. The mixed signal-to-noise ratio (MSNR) is defined as follows:

$$\text{MSNR} = 10 \lg\left(\frac{\sigma_s^2}{\gamma_v}\right), \tag{11}$$

where σ_s^2 and γ_v are the variance of the noise-free signal and the dispersion of the FLOA background noise, respectively. Two estimation algorithms, namely, LMS-RBFNN [16] and ARX [17], were compared in the following simulations. In ARX, the $s(t, 0)$ is used as the exogenous input to the estimated ARMA (autoregressive-moving-average) model; the model order is estimated by FPE [18] and the parameters are calculated by LMS [19]. To measure the performance of the algorithms, the correlation coefficient ρ is defined as

$$\rho = \frac{\sum_{t=0}^{M-1} (s(t, m) - \bar{s})\left(\hat{s}(t, m) - \bar{\hat{s}}\right)}{\sqrt{\sum_{t=0}^{M-1} (s(t, m) - \bar{s})^2} \sqrt{\sum_{t=0}^{M-1} \left(\hat{s}(t, m) - \bar{\hat{s}}\right)^2}}, \tag{12}$$

where $\bar{s}$ and $\bar{\hat{s}}$ are the time mean values with M samples of $s(t, m)$ and $\hat{s}(t, m)$.

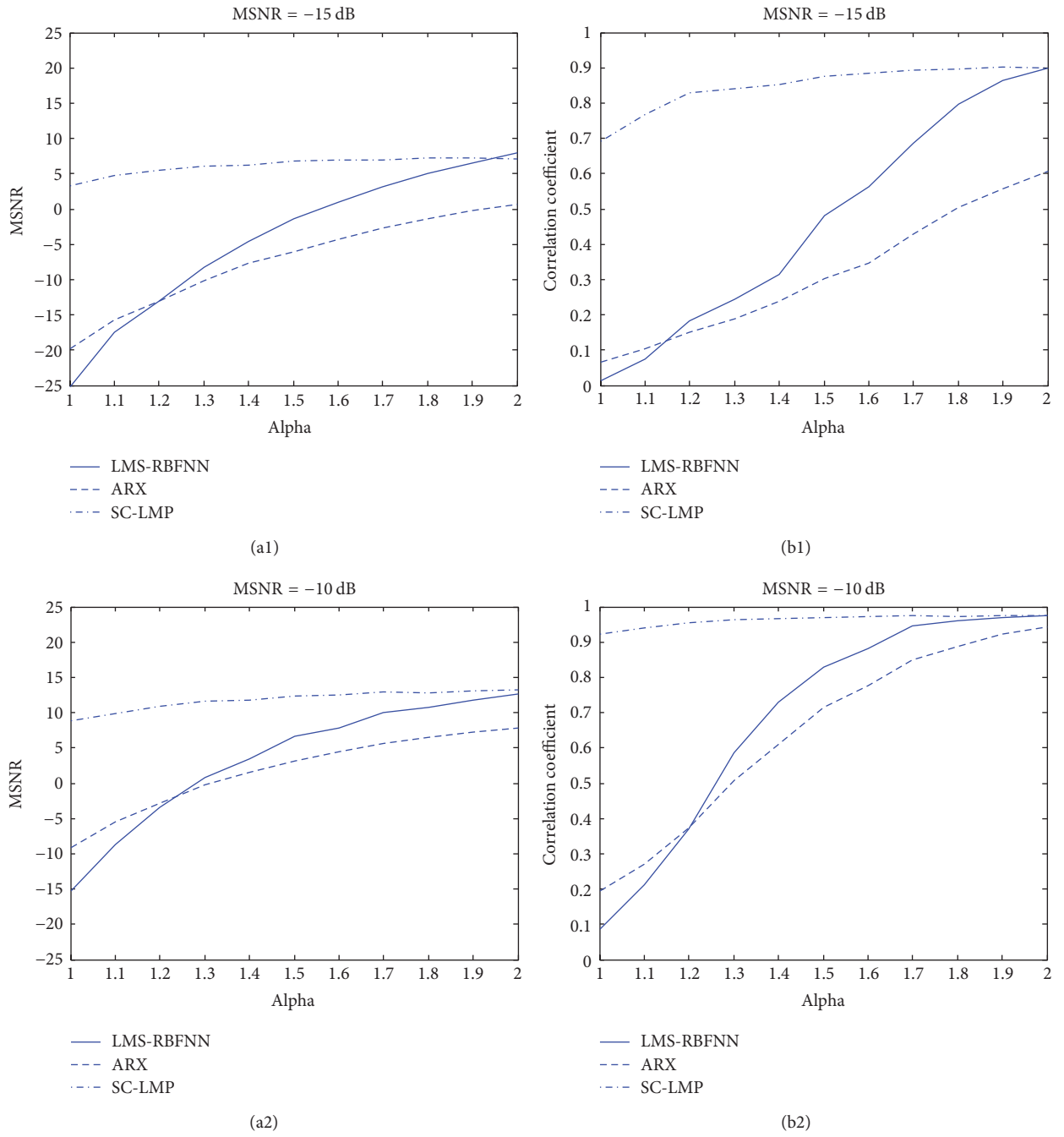

Figure 3: Comparison of three methods in different alpha values.

3.1. Simulation Experiment. In this section, the proposed method is compared with two other methods, namely, ARX and LMS-RBFNN. ARX and LMS-RBFNN are one of the commonly used methods to extract EP signal. ARX modeling for single-trial EP estimation was proposed by Cerutti et al. [20]. This method can estimate single-trial EPs even when the SNR is very low and has been applied to the monitoring of the depth of anesthesia during surgery. RBENN is a kind of supervised feedforward neural network based on function approximation theory. Fung et al. [21] proposed LMS-RBFNN method according to the strong approximation ability and fast training speed of RBENN. Figure 2 shows 4 graphs of the estimated single-trial EP signals based on our method. Figures 2(a1)–2(a4) include stimulated EP in various latencies ($m = 15, 10, 5, -5$) which are indicated by dotted line and the accordingly observed signals are mixed by MSNR = −7 dB which are indicated by dashed-dotted line. Figures 2(a1)–2(a4) show the accordingly estimated results by SC-LMP. From Figure 2, we can see that, with the increase of the value of the MSNR, our method has better dynamic estimation ability of latency and amplitude in different m value.

As shown in Figure 3, we changed α value from 1 to 2 and calculated the improvement of MSNR and the correlation

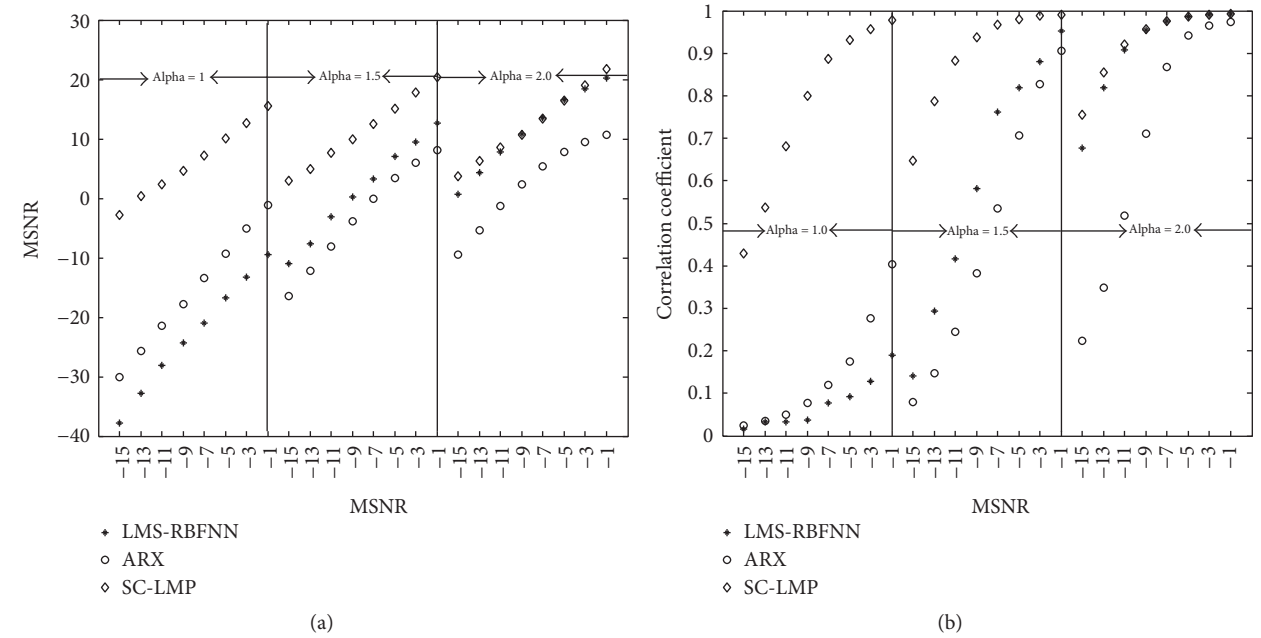

Figure 4: Comparison of three methods in different MSNR values.

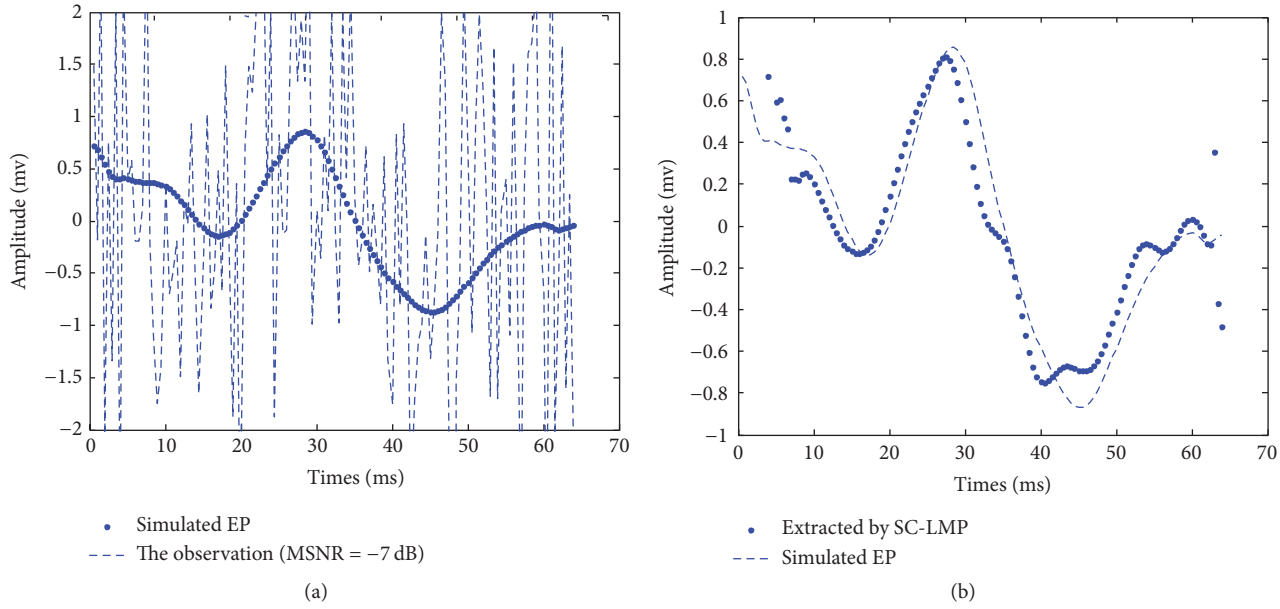

Figure 5: The extracted result by using real data.

coefficient in the corresponding MSNR value (MSNR = −15, −10 dB) obtained with our method, ARX and LMS-RBFNN. Compared with ARX and LMS-RBFNN, our method exhibits better performance, with slight decreasing of MSNR when alpha varies from 2 to 1.

The improvement of MSNR and the correlation coefficient of our method, ARX and LMS-RBFNN in three alpha values (alpha = 1, 1.5, and 2), are shown in Figure 4. From Figure 4, with the decrease of the value of MSNR, the estimated value of MSNR and the correlation coefficient of three methods decline. However, compared with the other 2 methods, our method has better performance.

3.2. Real Data. For further evaluation of the performance of our method, real VEPs were used by [22]. We chose a small piece of data for trial. The data was then rereferenced to the average of channels O1, Oz, and O2, low-pass filtered between 0 and 9 Hz with a 7th-order Butterworth filter, and downsampled to 128 Hz.

Figure 5(a) shows the stimulated EP and the accordingly observed signals which are the mixture of the stimulated EP and α-stable distribution noise by MSNR = −7 dB. We extract the EP with SC-LMP, and results are shown in Figure 5(b). Clearly, the signal estimated using our method

better resembles the stimulated EP. The component P300 of VEPs extracts with our method is distinct.

4. Conclusion

To sum up, we proposed a novel single-trial EP estimated method based on SC-LMP. This method uses sparse coding to represent EPs and utilize a zero-mean α-stable distribution process to express spontaneous EEG according to the characteristics of background signal. In order to facilitate solving the sparse coefficients, the p-norm is used in place of the $L2$-norm. We conducted a series of experiments on simulated and real data, and the results were evaluated using waveform extractions and other metrics. As the experimental results show, our method has better estimated capacity and performance than other existing algorithms. Future works will focus on improving the stability and practicability of the new proposed method to obtain a better real-time monitoring of the components. This could lead to the development of more advanced applications for real-world signals.

Conflicts of Interest

The authors declare that they have no financial and personal relationships with other people or organizations that can inappropriately influence their work; there are no professional or other personal interests of any nature or kind in any product, service, and/or company that could be construed as influencing the position presented in, or the review of, this manuscript. And the funding in "Acknowledgments" would not lead to any conflicts of interest regarding the publication of this manuscript.

Acknowledgments

This work was supported by the Nature Science Foundation of China (Grant no. 61401181) and Xuzhou Municipal Science and Technology Project (Grant no. KC16SY160)

References

[1] Q. Wang, Y. Wu, W. Liu, and L. Gao, "Dominant eye and visual evoked potential of patients with myopic anisometropia," *BioMed Research International*, vol. 2016, Article ID 5064892, 6 pages, 2016.

[2] A. S. Gevins, "Analysis of the electromagnetic signals of the human brain: milestones, obstacles, and goals," *IEEE Transactions on Biomedical Engineering*, vol. 31, no. 12, pp. 833–850, 1984.

[3] M. H. Costa, "Estimation of the noise autocorrelation function in auditory evoked potential applications," *Biomedical Signal Processing and Control*, vol. 7, no. 5, pp. 542–548, 2012.

[4] C. Reynolds, B. A. Osuagwu, and A. Vuckovic, "Influence of motor imagination on cortical activation during functional electrical stimulation," *Clinical Neurophysiology*, vol. 126, no. 7, pp. 1360–1369, 2015.

[5] N. Yu, L. Wu, D. Zou, Y. Chen, and H. Lu, "A MISO-ARX-Based Method for Single-Trial Evoked Potential Extraction," *BioMed Research International*, vol. 2017, Article ID 7395385, 10 pages, 2017.

[6] N. Yu, Q. Ding, and H. Lu, "Single-Trial Estimation of Evoked Potential Signals via ARX Model and Sparse Coding," *Journal of Medical Biological Engineering*, vol. 37, no. 2, p. 11, 2017.

[7] P. Xu and D. Yao, "Development and evaluation of the sparse decomposition method with mixed over-complete dictionary for evoked potential estimation," *Computers in Biology and Medicine*, vol. 37, no. 12, pp. 1731–1740, 2007.

[8] Y. Huang, Z. You, X. Gao, L. Wong, and L. Wang, "Using weighted sparse representation model combined with discrete cosine transformation to predict protein-protein interactions from protein sequence," *BioMed Research International*, vol. 2015, Article ID 902198, 10 pages, 2015.

[9] N. N. Yu, H. K. Liu, X. Y. Wang, and H. Lu, "A joint sparse representation-based method for double-trial evoked potentials estimation," *Computers in Biology and Medicine*, vol. 43, no. 12, pp. 2071–2078, 2013.

[10] X. Kong and T. Qiu, "Adaptive estimation of latency change in evoked potentials by direct least mean p-norm time-delay estimation," *IEEE Transactions on Biomedical Engineering*, vol. 46, no. 8, pp. 994–1003, 1999.

[11] F. Bi, T. Qiu, and N. Yu, "Robust adaptive estimator for evoked potentials based on non-linear transform under impulsive noise environments," *Journal of Medical & Biological Engineering*, vol. 32, no. 6, pp. 443–452, 2012.

[12] M. Shao and C. L. Nikias, "Signal processing with fractional lower order moments: stable processes and their applications," *Proceedings of the IEEE*, vol. 81, no. 7, pp. 986–1010, 1993.

[13] X. Kong and T. Oiu, "Latency change estimation for evoked potentials: A comparison of algorithms," *Medical & Biological Engineering & Computing*, vol. 39, no. 2, pp. 208–224, 2001.

[14] K.-H. Yap, Y. He, Y. Tian, and L.-P. Chau, "A Nonlinear L1-Norm Approach for Joint Image Registration and Super-Resolution," *IEEE Signal Processing Letters*, vol. 16, no. 11, pp. 981–984, 2009.

[15] N. Yu, F. Hu, D. Zou, Q. Ding, and H. Lu, "Single-trial sparse representation-based approach for VEP extraction," *BioMed Research International*, vol. 2016, Article ID 8569129, 9 pages, 2016.

[16] J. Park and I. W. Sandberg, "Universal approximation using radial basis function networks," *Neural Computation*, vol. 3, no. 2, pp. 246–257, 1991.

[17] D. H. Lange, H. Pratt, and G. F. Inbar, "Modeling and estimation of single evoked brain potential components," *IEEE Transactions on Biomedical Engineering*, vol. 44, no. 9, pp. 791–799, 1997.

[18] C. Corbier and J.-C. Carmona, "Robust final prediction error criterion for control oriented models validation using L2-L1 norm," in *Proceedings of the 2nd International Conference on Communications Computing and Control Applications, CCCA 2012*, France, December 2012.

[19] I. Song, G. P. Park, and R. W. Newcomb, "A Normalized Least Mean Squares Algorithm With a Step-Size Scaler Against Impulsive Measurement Noise," *IEEE Transactions on Circuits & Systems II Analog & Digital Signal Processing*, vol. 60, no. 7, pp. 442–445, 2013.

[20] S. Cerutti, G. Baselli, D. Liberati, and G. Pavesi, "Single sweep analysis of visual evoked potentials through a model of parametric identification," *Biological Cybernetics*, vol. 56, no. 2-3, pp. 111–120, 1987.

[21] K. S. Fung, F. H. Chan, and F. K. Lam, "A tracing evoked potential estimator," *Medical & Biological Engineering & Computing*, vol. 37, no. 2, pp. 218–227, 1999.

[22] U. Hoffmann, G. Garcia, J.-M. Vesin, K. Diserenst, and T. Ebrahimi, "A boosting approach to P300 detection with application to brain-computer interfaces," in *Proceedings of the 2nd International IEEE EMBS Conference on Neural Engineering*, pp. 97–100, March 2005.

Hindawi
Computational Intelligence and Neuroscience
Volume 2018, Article ID 5623165, 7 pages
https://doi.org/10.1155/2018/5623165

Research Article

The EEG Activity during Binocular Depth Perception of 2D Images

Marsel Fazlyyyakhmatov, Nataly Zwezdochkina, and Vladimir Antipov

Kazan Federal University, 18 Kremlyovskaya Street, Kazan 420008, Russia

Correspondence should be addressed to Marsel Fazlyyyakhmatov; mfazlyjy@kpfu.ru

Received 26 October 2017; Accepted 1 January 2018; Published 30 January 2018

Academic Editor: Victor Hugo C. De Albuquerque

The central brain functions underlying a stereoscopic vision were a subject of numerous studies investigating the cortical activity during binocular perception of depth. However, the stereo vision is less explored as a function promoting the cognitive processes of the brain. In this work, we investigated a cortical activity during the cognitive task consisting of binocular viewing of a false image which is observed when the eyes are refocused out of the random-dot stereogram plane (3D phenomenon). The power of cortical activity before and after the onset of the false image perception was assessed using the scull EEG recording. We found that during stereo perception of the false image the power of alpha-band activity decreased in the left parietal area and bilaterally in frontal areas of the cortex, while activity in beta-1, beta-2, and delta frequency bands remained to be unchanged. We assume that this suppression of alpha rhythm is presumably associated with increased attention necessary for refocusing the eyes at the plane of the false image.

1. Introduction

The central brain functions underlying a stereoscopic vision were a subject of numerous studies focusing on the assessment of cortical activity during binocular perception of depth [1, 2]. The BA7 area of parietal cortex and BA19 area of occipital cortex were demonstrated to play a key role in the binocular stereo vision [3]. The perception of depth was also shown to be associated with bilateral activation of BA37 and BA39 areas of temporal cortex, and the dorsal regions of occipital-temporal cortex were found to be sensitive to the power of depth perception [3–5]. All these works focused on the process of binocular vision itself and used the stereoscope or other approaches to promote the perception of depth in the observed scenes. In our study, we explored the cortical activity during the execution of cognitive task consisted of viewing a false image in front of the plane of random-dot stereogram without a stereoscope or any other aids to binocular fusion, which requires a high concentration of attention. With this aim, we assessed the power of cortical rhythms using the scull EEG recording before and after the onset of the false image perception.

The 3D phenomenon [6] is a new and insufficiently investigated process of visual perception. For the first time, the information about novel abilities of vision was published in the auxiliary materials of our invention (patent number 226499 RU).

Our goal in the present study was the EEG activity measurement during viewing of plane images that create the depth perception and volume. To detect the depth and volume on the images, a binocular eye tracker was used. Eye tracker provides registration of eye movement. The article presents the results of measuring the alpha rhythm of nine volunteers. In the second part of this article the results of EEG activity of one subject are presented. Alpha, high-frequency beta, low-frequency beta, theta, and delta rhythms were analyzed. We found that during stereo perception of the false image the power of alpha-band activity decreased in the left parietal area and bilaterally in frontal areas of the cortex, while activity in beta-1, beta-2, and delta frequency bands remained to be unchanged.

2. Methods

Stereoscopic vision of a human (or stereopsis) is two eyes and two points of view. Stereopsis forms on the retinal photoreceptors two slightly displaced images (or horizontal disparity) of objects located at different distances from the eyes. The

fusion of information in the visual centers of the brain from two mesh images creates a sense of the volume and the spatial location of objects in the visual field. When a planar image enters in the visual field, all images on it are located at the same distance from the observation points. Consequently, there is no disparity as a necessary condition for structuring the stereoscopic spatial perception of the images.

The third author of this work developed the educational technology of developing the ability to perceive the depth, volume, and spatial perspective on planar images, that is, 3D phenomenon, in other words, the transfer of three-dimensional perception from the objects of the habitat to the planar images, which are the results of human thinking. It is assumed that the 3D phenomenon develops as a result of training to observe the stereoscopic depth on the stereoscopic projections, stereograms, and 3D raster images. It is possible to assume that the ability to perceive the depth and volume on the planar images refers to the evolutional mechanisms of the visual system in the modern conditions of the technogenic habitat.

The binocular eye tracker with the function of determining the X-coordinates of the right and left eye is used to study the 3D phenomenon. In the first experiments on the study of the 3D phenomenon, eye movements were recorded using the SMI HiSpeed eye tracker in the binocular mode (recording frequency 500 Hz). The images were displayed on a 19″ CRT monitor ViewSonic 90Gf, located at a distance $h = 58$ cm from the observer's eyes (resolution 1280×1024 pixels, 38 pixels/cm). Exposure time was from 15 to 150 sec. The software allows determining the X-coordinate of the direction of the right (X^{R}) and left (X^{L}) eyes in the numerical scale of the monitor. The difference $\Delta X = X^{\mathrm{L}} - X^{\mathrm{R}}$, which determines the position of the plane of the perceived image, was calculated from the coordinates. Perceived image plane is the plane on which the direction of the right and left eye concentrates on the point. If $\Delta X = 0$, then it coincides with the plane of the image location, that is, with the monitor plane. Under the condition $\Delta X \neq 0$, it is either closer to or further from the monitor screen.

The binocular eye tracker allows obtaining the perception of the depth and volume of a planar image. In the conditions of three-dimensional perception of the image, perceived image plane is located behind it at a distance of 8–58 cm [6].

Formation of the 3D phenomenon elements is shown on the all planar images demonstrated to the participants in the experiment.

We believe that the 3D phenomenon correlates with the neurophysiological mechanisms of creative activity. The right hemisphere dominates with the synchronization of the biopotentials of alpha-activity, especially in the frontal cortical areas [7, 8]. On the other hand, the opposite activation effects of EEG activity of creative thinking were shown in [9, 10].

Some researchers have shown that when solving creative problems, the activity of the brain depends on the background state associated with the level of creativity [11]. Also, recent studies show that the perception of three-dimensional attributes depends on the background state of the subject. It is possible that the study of EEG activity under conditions of the three-dimensional perception of planar images will reveal correlates of divergent thinking, as was done in the study of EEG activity with simultaneous analysis of the level of intelligence and divergent thinking [7]. Data on the positive relationship between the effectiveness of divergent thinking and the level of intelligence previously were obtained [12, 13]. The great importance of right hemisphere activity when changing the effectiveness of divergent thinking was shown [8].

The above literature sources show that the functional activity of intelligence and divergent thinking in a wide range are represented in alpha, low-frequency delta, and high-frequency beta ranges of EEG activity. In addition to the experimental models of creativity are the individual characteristics of the subjects.

Although human perceptual responses to binocular disparity have been studied extensively [14], there have been relatively few studies of how human cortical activity is related to stereo depth perception. In these few studies [15–17], the authors relied on measurements of visually evoked potentials, a method that has a limited spatial resolution. Methods of EEG activity in the study of creativity was shown in [18]. Here, we explore the 3D phenomenon using EEG recording of cortical activity.

Nine female voluntaries of 20 years old participated in the study. They all have previously passed a semester cycle of training the spatial perception skills at the three-dimensional images. The scull EEG was recorded using 8-channel digital EEG system Neuron-Spectrum-1 (Neurosoft, Russia). The EEG electrode placement was organized by standard 10–20 system with a reference electrode placed unilaterally at the ear. The bipolar longitudinal row montage included eight recording electrodes: Fp1, Fp2, C3, C4, T3, T4, O1, and O2. After visual inspection of the EEG recordings using Neuron-Spectrum.NET software (Neurosoft, Russia) the data were processed and analyzed using custom-written routines in MATLAB environment (MathWorks, USA). The independent component analysis was used for removing the artifacts from the EEG recordings. Statistical analysis was performed using the MATLAB Statistics toolbox. The two-side Wilcoxon rank sum test was performed to assess the significance of differences between groups of data with the level of significance kept at $p < 0.05$.

3. Results and Discussion

The EEG activity was recorded under three conditions: (1) with closed eyes, (2) during focusing at the plane of stereogram, and (3) during perception of the false image in front of the stereogram plane. When the eyes were closed, the alpha rhythm was recorded in both right and left occipital areas (T3O1, C3O1, T4O2, and C4 O2 channels) with average frequency of 9.9 ± 1.6 Hz ($n = 9$). After opening of the eyes and focusing at the stereogram plane the alpha rhythm was depressed bilaterally to the same extent. The test was signalized about the onset of the false image perception by raising up the pencil, and a suppression of activity in alpha-band was recorded after the onset of stereo perception was revealed in the frontal areas (Fp1C3, Fp2C4) and in the left

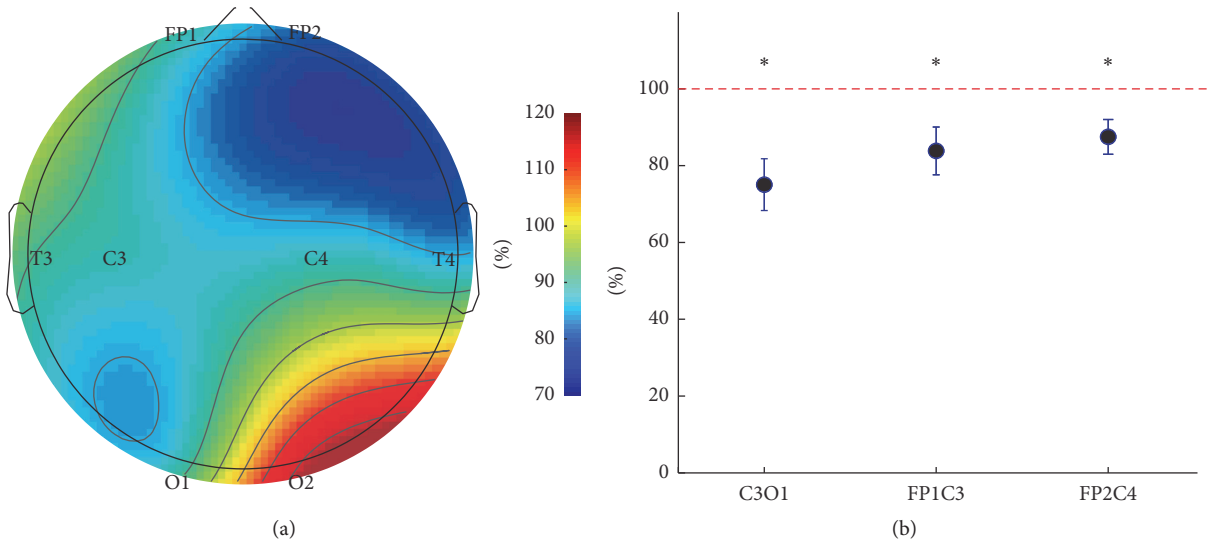

Figure 1: The dynamic of EEG activity in alpha frequency band during perception of depth with false objects appearing to be in front of the flat plane of random-dot stereogram without using a stereoscope: (a) the topo map of alpha-activity represented as a ratio of alpha oscillation power after/before the onset of the false image perception built for individual EEG recording; (b) averaged alpha oscillation power at C3O1, FP1C3, and FP2C4 recording sites, mean ± SE; ∗ corresponds to $p < 0.05$.

parietal area (C3O1) of the cortex. Thus, the average power of alpha rhythm before and after the onset of false image perception was, respectively, 0.867 ± 0.143 μV2/Hz and 0.599 ± 0.088 μV2/Hz at C3O1 channel, 0.567 ± 0.121 μV2/Hz and 0.457 ± 0.096 μV2/Hz at Fp1C3, and 0.613 ± 0.114 μV2/Hz and 0.515 ± 0.089 μV2/Hz at Fp2C4 channel ($n = 9$; $p < 0.05$; Figure 1(b)).

There were not any significant changes in alpha-band activity power at other recording channels, and no changes of EEG activity in beta-1, beta-2, and delta frequency bands were detected. The changes in alpha-band cortical activity are considered to be promoted by nonspecific factors like attention, arousal state, emotions, and so on [19–21]. Thereby, we assume that suppression of alpha rhythm during the false image perception is caused by desynchronization of cortical activity associated with an increased attention, which is necessary for the viewer to refocus and fix the eyes at the plane of the false image.

In addition to the results presented above, the following data were obtained. (1) The power spectra of the EEG activity were recorded. During perception of the 3D phenomenon in comparison with the planar perception in the entire range of EEG rhythms (eighth leads), a decreasing of power was observed. The change in power depends on the color palette of the planar image. (2) Extraction of the biorhythm index for beta, alpha, theta, and delta band components does not have a unique influence on them of various types of planar images. (3) Processing of the spectrograms of rhythms shows that, under conditions of three-dimensional perception of planar images, the total coherence amplitude over all leads and components of EEG rhythms is 1.8 and more times higher in comparison with the perception of the white paper sheet (Figure 2). (4) In the process of planar and three-dimensional perception of planar images creating effects of perception

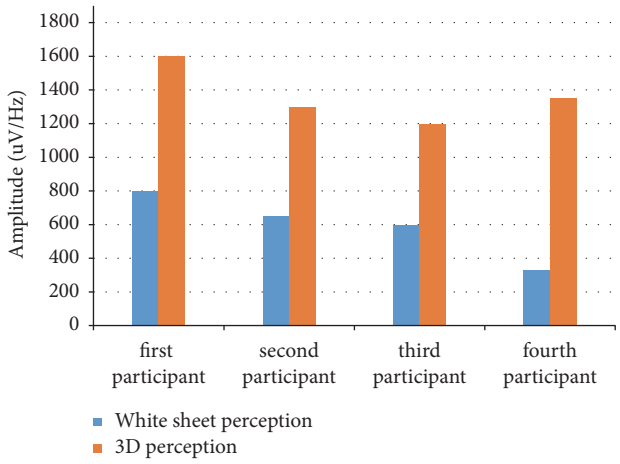

Figure 2: The total coherence amplitude over all leads and components of the EEG rhythms.

of depth and volume, the following is shown: firstly, the excess of theta rhythms power over alpha rhythms, secondly, that the theta and alpha rhythms power are exceeded in the right hemisphere in comparison with the left one, and thirdly, the detection of the increase in power in conditions of three-dimensional perception in comparison with the planar (Figure 3).

We also presented the EEG activity of the participant, who passed the first study on the binocular eye tracker [6]. When the first plane image (FPI) was perceived, the power of the spectrum of the right hemisphere in the frontal compartment was greater than for the left one 1.5 times in all leads, with a range of changes from 1.3 to 2 times. Under conditions of three-dimensional perception (i.e., the 3D phenomenon),

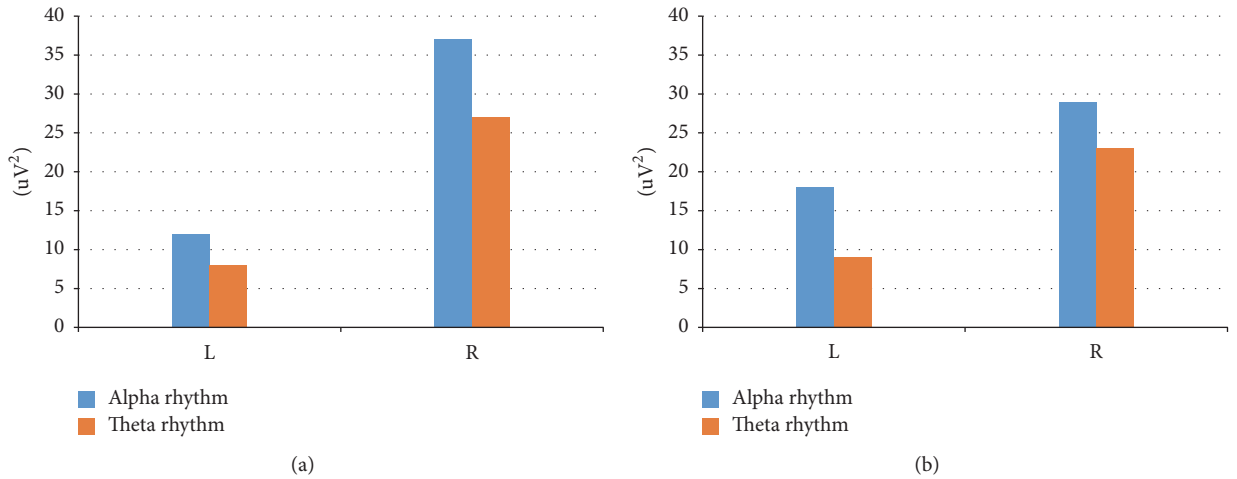

Figure 3: EEG power on left (L) and right (R) hemisphere; blue bar: theta rhythm; brown bar: alpha rhythm: (a) 2D perception and (b) 3D perception.

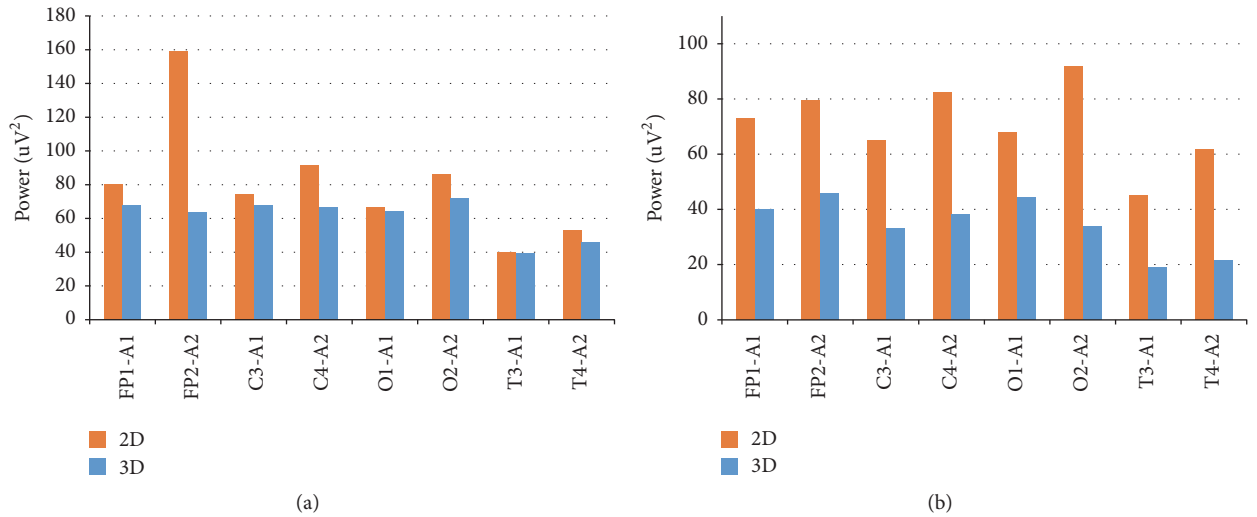

Figure 4: Full spectral power (all diapason): (a) first visual stimulus and (b) second visual stimulus.

the ratio of the spectrum power of the leads in the right hemisphere actually aligned with the left one. The average value of the ratio is 1.1; the interval is from 0.9 to 1.2. The total average ratio for all leads of the right and left hemispheres under conditions of three-dimensional perception to two-dimensional perception is 0.8 with a change interval from 0.4 to 1.0. In all leads with a planar perception of the second planar image (SPI), values for the right hemisphere are greater than for the left. The average value of the ratio is 1.3; the interval is from 1.1 to 1.4. Under conditions of three-dimensional perception, the average value of the analogous ratio is 1.1 with the variation interval from 0.75 to 1.2. For all leads, the power of the spectrum under conditions of three-dimensional perception is less than for a planar. The average value of the ratio is 0.5; the interval is from 0.4 to 0.7.

Thus, under conditions of a three-dimensional perception of the presented planar images, a decrease in power spectra in comparison with planar perception and less pronounced interhemispheric asymmetry is observed (Figure 4).

Horizontally, we have frontal (FP), central (C), occipital (O), and temporal (T) leads. Odd numbers refer to the left, and even numbers to the right hemisphere. Vertically, we have power values. Brown bar represents two-dimensional (2D) and blue bar represents three-dimensional (3D) perception.

Figure 5 shows the graphs of the EEG rhythm index: high-frequency beta (HF) and low-frequency beta (LF), alpha, theta, and delta rhythms.

The index of high-frequency beta rhythm for both images in planar and three-dimensional perception is higher in all leads in the right hemisphere. The range of the index with a plane perception in comparison with the three-dimensional is from 10 to 21%, with the exception of the frontal lead, which is lower, about 9%. With three-dimensional perception, the index is in the range of 6–16%. It is known that high-frequency

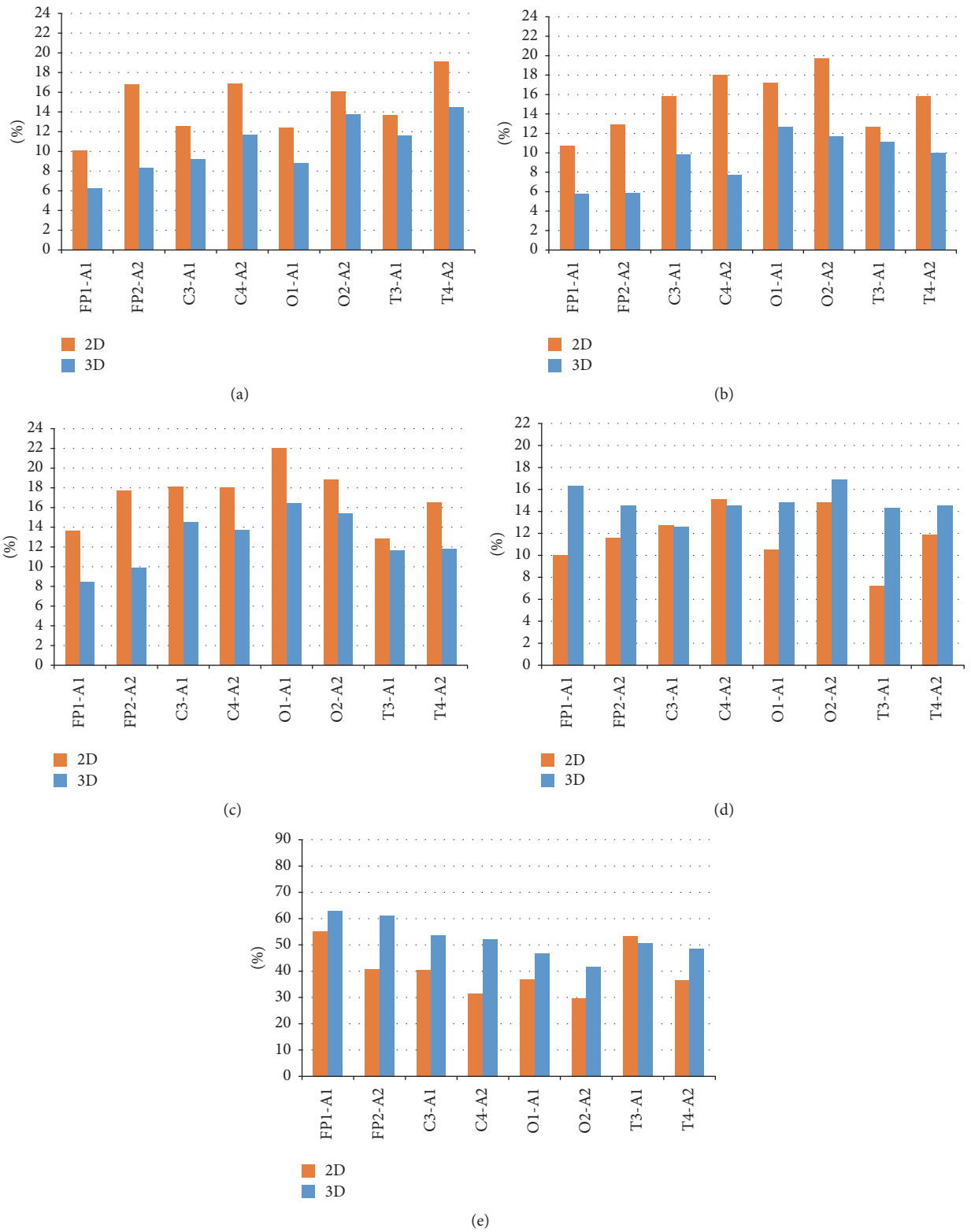

Figure 5: The EEG rhythm index: (a) high-frequency beta (HF); (b) low-frequency beta (LF); (c) alpha; (d) theta; (e) delta rhythms.

beta rhythm has a special functional significance for the integration of various signs of complex stimuli, both figurative and verbal nature. It can be assumed that this integration is reflected in the intensification of interaction between the anterior and posterior parts of the left hemisphere, which is especially pronounced in the presence of both intellectual and creative abilities.

The index of low-frequency beta rhythm with FPI perception is in the range from 5 to 16%. There is an asymmetry of the index value on the left in the frontal and occipital leads. In terms of three-dimensional perception, rhythm indices are in the range from 13 to 16%. Left-sided asymmetry is observed in the occipital-temporal leads. With a planar perception of SPI in all leads, the indices are in the range of 10 to 20%. In all leads, the value of this index in the right hemisphere is higher than in the left hemisphere. The indices of this rhythm under conditions of three-dimensional perception are significantly lower (5–12% range).

The alpha rhythm index with a planar perception of the FPI image is generally lower than in the case of three-dimensional perception. In the temporal and central leads, the right and left hemispheres have a rhythm index of one level, about 12%. In the occipital lead, values for the right hemisphere are twice as high as for the left hemisphere and in the frontal leads above the value on the left. The change interval is within 5–12%. The transition to a three-dimensional perception increases the rhythm index. It is in the range from 13 to 22%. In the temporal leads, the right and left hemispheres have approximately the same indices in the range 15-16%. It can be noted that, under the conditions of three-dimensional perception, the alpha rhythm is almost twice as high as for planar perception of FPI image in all leads with left-hemispheric asymmetry. Gradual increase in the power of the alpha rhythm with open eyes is a sign of the inhibitory condition of the oculomotor system. On the other hand, the increase in the power of the alpha rhythm may indicate a decrease in visual attention caused by the monotony of the FPI image.

With a plane perception of the SPI image, the value of the alpha rhythm index is higher than for the three-dimensional one. In the frontal and temporal leads, the alpha rhythm index is higher on the right; in the occipital lead the alpha rhythm index is higher on the left. The value of the index varies between 13 and 22%. With three-dimensional perception, the alpha rhythm index is 8–16% without a clearly expressed asymmetry.

That is, when looking at FPI image, the index of the alpha rhythm with three-dimensional perception increases; with the SPI image, it decreases almost half.

In low-frequency bands, the dynamics of the rhythm index in the case of a planar and three-dimensional perception of the images are ambiguous. However, in general, the theta rhythm index is higher for a three-dimensional than for a two-dimensional perception, especially in the right hemisphere. With a two-dimensional perception, the theta rhythm index variates in the range of 4–14%, while the three-dimensional index is 9–19%.

The change in the delta rhythm index is in the range of 40–80%. When looking at FPI image in a plane perception, the delta rhythm index is higher than in the case of three-dimensional perception (40–76%), for the SPI image is lower (38–57%). In the right hemisphere, the value of the index is clearly reduced in case of plane perception. The severity of asymmetry in three-dimensional perception is insignificant in both cases.

4. Conclusions

We show that during stereo perception of false image appearing in front of the stereogram plane the power of alpha-band activity decreases in the left parietal area and frontal areas of the cortex, and this suppression of alpha rhythm is presumably associated with increased attention necessary for refocusing the eyes at the plane of the false image.

The use of coherent analysis of EEG activity allows obtaining an objective evaluation of the ability of three-dimensional perception of planar images, to expand the psychophysiological features of the ability to perceive plane images with depth and volume effects.

In the future studies, it would be interesting to determine the reason underlying bilateral asymmetry in the suppression of alpha-band activity power in parietal cortical areas observed during stereo perception.

In the future, we plan to conduct experiments on recording EEG activity in the 3D phenomenon and compare them with known methods of analyzing intelligence and divergent thinking. For this, it is necessary to jointly measure EEG factors and eye movements.

Conflicts of Interest

The authors declare no conflicts of interest related to the material presented in this paper.

Acknowledgments

This work is performed according to the Russian Government Program of Competitive Growth of Kazan Federal University. E. Zaitceva and A. Nasretdinov are acknowledged for technical support and valuable assistance with data analysis.

References

[1] W. Skrandies and A. Jedynak, "Learning to see 3-D: Psychophysics and brain electrical activity," *NeuroReport*, vol. 10, no. 2, pp. 249–253, 1999.

[2] T. Naganuma, I. Nose, K. Inoue, A. Takemoto, N. Katsuyama, and M. Taira, "Information processing of geometrical features of a surface based on binocular disparity cues: An fMRI study," *Neuroscience Research*, vol. 51, no. 2, pp. 147–155, 2005.

[3] F. P. S. Fischmeister and H. Bauer, "Neural correlates of monocular and binocular depth cues based on natural images: A LORETA analysis," *Vision Research*, vol. 46, no. 20, pp. 3373–3380, 2006.

[4] B. T. Backus, D. J. Fleet, A. J. Parker, and D. J. Heeger, "Human cortical activity correlates with stereoscopic depth perception," *Journal of Neurophysiology*, vol. 86, no. 4, pp. 2054–2068, 2001.

[5] R. M. Rutschmann and M. W. Greenlee, "BOLD response in dorsal areas varies with relative disparity level," *NeuroReport*, vol. 15, no. 4, pp. 615–619, 2004.

[6] V. N. Antipov and A. V. Zhegallo, "Three-dimensional perception of flat images in computerized environment," *Experimental Psychology*, vol. 7, no. 3, pp. 97–111, 2014.

[7] A. Fink and M. Benedek, "EEG alpha power and creative ideation," *Neuroscience & Biobehavioral Reviews*, vol. 44, pp. 111–123, 2014.

[8] K. M. Mihov, M. Denzler, and J. Förster, "Hemispheric specialization and creative thinking: A meta-analytic review of lateralization of creativity," *Brain and Cognition*, vol. 72, no. 3, pp. 442–448, 2010.

[9] D. Bendetowicz, M. Urbanski, C. Aichelburg, R. Levy, and E. Volle, "Brain morphometry predicts individual creative potential and the ability to combine remote ideas," *Cortex*, vol. 86, pp. 216–229, 2017.

[10] A. Dietrich, "The cognitive neuroscience of creativity," *Psychonomic Bulletin & Review*, vol. 11, no. 6, pp. 1011–1026, 2004.

[11] R. E. Beaty, M. Benedek, R. W. Wilkins et al., "Creativity and the default network: A functional connectivity analysis of the creative brain at rest," *Neuropsychologia*, vol. 64, pp. 92–98, 2014.

[12] M. Batey and A. Furnham, "Creativity, intelligence, and personality: A critical review of the scattered literature," *Genetic, Social, and General Psychology Monographs*, vol. 132, no. 4, pp. 355–429, 2006.

[13] E. Jauk, M. Benedek, B. Dunst, and A. C. Neubauer, "The relationship between intelligence and creativity: New support for the threshold hypothesis by means of empirical breakpoint detection," *Intelligence*, vol. 41, no. 4, pp. 212–221, 2013.

[14] I. P. Howard and B. J. Rogers, *Binocular Vision and Stereopsis*, Oxford University Press, Oxford, UK, 1995.

[15] O. J. Braddick and J. Atkinson, "Some recent findings on the development of human binocularity: A review," *Behavioural Brain Research*, vol. 10, no. 1, pp. 141–150, 1983.

[16] A. M. Norcia and C. W. Tyler, "Temporal frequency limits for stereoscopic apparent motion processes," *Vision Research*, vol. 24, no. 5, pp. 395–401, 1984.

[17] A. M. Norcia, E. E. Suiter, and C. W. Tyler, "Electrophysiological evidence for the existence of coarse and fine disparity mechanisms in human," *Vision Research*, vol. 25, no. 11, pp. 1603–1611, 1985.

[18] N. Srinivasan, "Cognitive neuroscience of creativity: EEG based approaches," *Methods*, vol. 42, no. 1, pp. 109–116, 2007.

[19] A. A. Morozov, Yu. V. Obukhov, T. A. Stroganova, M. M. Tsetlin, and A. O. Prokofiev, "The search of the regularity in the spatio-temporal dynamics of the brain oscillations," *Iskusstvennyi Intellect [Artificial Intelligence]*, vol. 3, pp. 499–509, 2004.

[20] W. Klimesch, P. Sauseng, and S. Hanslmayr, "EEG alpha oscillations: the inhibition-timing hypothesis," *Brain Research Reviews*, vol. 53, no. 1, pp. 63–88, 2007.

[21] S. Makeig, M. Westerfield, T.-P. Jung et al., "Dynamic brain sources of visual evoked responses," *Science*, vol. 295, no. 5555, pp. 690–694, 2002.

Hindawi
Computational Intelligence and Neuroscience
Volume 2018, Article ID 4613740, 11 pages
https://doi.org/10.1155/2018/4613740

Research Article

n-Iterative Exponential Forgetting Factor for EEG Signals Parameter Estimation

Karen Alicia Aguilar Cruz,[1] **María Teresa Zagaceta Álvarez**,[2] **Rosaura Palma Orozco**,[3] **and José de Jesús Medel Juárez**[1]

[1]*Centro de Investigación en Computación, Instituto Politécnico Nacional (CIC-IPN), Avenida Juan de Dios Bátiz, Esq. Miguel Othón de Mendizábal, Col. Nueva Industrial Vallejo, Delegación Gustavo A. Madero, 07738 Ciudad de México, Mexico*
[2]*Escuela Superior de Ingeniería Mecánica y Eléctrica, Unidad Azcapotzalco, Instituto Politécnico Nacional, Avenida de las Granjas, No. 682, Col. Santa Catarina, Delegación Azcapotzalco, 02250 Ciudad de México, Mexico*
[3]*Escuela Superior de Cómputo, Instituto Politécnico Nacional, Avenida Juan de Dios Bátiz, Esq. Miguel Othón de Mendizábal, Col. Lindavista, Delegación Gustavo A. Madero, 07738 Ciudad de México, Mexico*

Correspondence should be addressed to José de Jesús Medel Juárez; jjmedelj@gmail.com

Received 26 October 2017; Accepted 6 December 2017; Published 15 January 2018

Academic Editor: Plácido R. Pinheiro

Electroencephalograms (EEG) signals are of interest because of their relationship with physiological activities, allowing a description of motion, speaking, or thinking. Important research has been developed to take advantage of EEG using classification or predictor algorithms based on parameters that help to describe the signal behavior. Thus, great importance should be taken to feature extraction which is complicated for the Parameter Estimation (PE)–System Identification (SI) process. When based on an average approximation, nonstationary characteristics are presented. For PE the comparison of three forms of iterative-recursive uses of the Exponential Forgetting Factor (EFF) combined with a linear function to identify a synthetic stochastic signal is presented. The one with best results seen through the functional error is applied to approximate an EEG signal for a simple classification example, showing the effectiveness of our proposal.

1. Introduction

Electroencephalogram (EEG) is a technique to obtain information related to brain activity, extracting information measuring electric fields from the brain, allowing obtaining information related to the intention for different mental activities, like motor imagery, motor planning, imagined speech or subject identification [1]. When information from EEG is obtained their features should be processed and used in classification algorithms.

According to [2], neural signal oscillations are the most important EEG characteristics to study because the relationship among specific patterns, perceptual, motor, and emotional processes, is described by these changes. Because of EEG stochastic characteristics, an adaptive description is needed within the time analysis especially when changes are neither smooth nor slow [3, 4].

Nevertheless, their neural nature makes them difficult to analyze without using an adequate descriptor. Hence, new EEG signal modelling techniques allow selecting specific information helping neuropathology clinical studies [5] to obtain the parameters to be used in, for example, classification algorithms [6] such as Fuzzy Logic Classifier (FLC), Artificial Neural Networks (ANN), Particle Swarm Optimization, and Sliding Modes, [1, 7–10].

In [11] the use of Time-Frequency Distributions (TFD), Fast Fourier Transform (FFT), eigenvector methods (EM), Wavelet Transform (WT), and Auto-Regressive Method (ARM) is discussed, for EEG feature extraction in time and frequency domain. Results from this comparison indicate frequency methods may be not adequate for EEG signals while time-frequency do not give detailed information; now the election of one method will depend on the application objective [4, 5, 12].

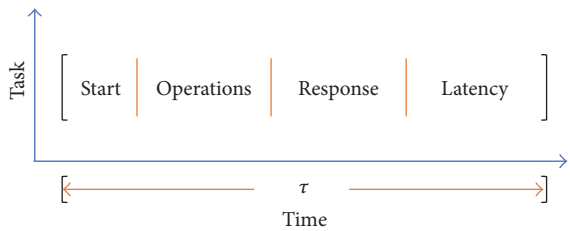

Figure 1: Representation of the processes for the corresponding time τ.

The sampled neural signal in a mathematical sense corresponds to a stochastic, time variant, and nonlinear description with a specific bounded distribution function for each clinical case. From this, the neuron is represented by a Black Box (BB) system with only its excitation (input) and answer (output) available without knowing what happens inside.

Variations of Adaptive Auto-Regressive (AR) models have been proved to be adequate to model systems, where the number of parameters to determine depends on the model order. Other methods include Recursive Least Squares (RLS), Least Mean Squares (LMS), and Kalman Filter (KF) and their variations [9, 12–15]. In general algorithms by themselves are not adequate when abrupt changes are presented, giving rise to hybrid or correction forms such as Forgetting Factor (FF) [16]. The great importance of the identifier lies in describing the internal time system evolution and observing its stability and stationary properties [3, 9, 17].

Considering computational operation latencies shown in Figure 1, the time interval between two consecutive output system steps makes the estimation-identification process achievable and feasible to add a second stage in the same interval, obtaining a recursive version using the Exponential Forgetting Factor (EFF) to modify the first identification.

A previous EFF analysis using (1) from [18] about the identification experiment was developed in [19], showing its effectiveness when using the sign function to give a correction factor, decreasing the identification error when implemented in nondeterministic signals:

$$\mathrm{EFF}_t = \mathrm{sign}\left(\widehat{A}_t\right) e^{\mathrm{sign}(\widehat{A}_t)\widehat{e}_t}, \tag{1}$$

where $\widehat{A}_t$ is the parameter estimated on average [20].

Equation (1) has been proved only for point to point corrections, integrating a second stage operation after the first developed on average, as shown in Figure 2.

Searching for a better identification, three different implementation cases of additional correction stages inside the second correction indicated in Figure 2 (dashed line) are compared. To accomplish this task, expression (1) is modified to create a recursive description for y_t, based on stochastic input w_t, interacting in (2) and leading to the identification error $\widehat{e}_t$ (3). Applying modifications in (1) the new parameter (4) is described and used instead of $\widehat{A}_t$ in (2), obtaining a new identification and identified error.

$$\widehat{y}_t = \widehat{A}_t w_t \tag{2}$$

$$\widehat{e}_t = y_t - \widehat{y}_t \tag{3}$$

$$\widehat{\widehat{A}}_t = \widehat{A}_t + \mathrm{EFF}_t - \mathrm{sign}\left(\widehat{A}_t\right). \tag{4}$$

The obtained algorithms are proved using in the first-place sinusoidal signals and, then, the one with better results is applied to a synthetic amplitude and frequency variation.

2. Recursive Exponential Forgetting Factor (REFF) Comparison

For the following algorithms, their effectiveness is analyzed by comparing their corresponding recursive EFF parameters estimation and identifications with respect to the reference in Figure 3, whose sinusoidal shape (Figure 3(b)) is given by the parameters viewed in polar representation (Figure 3(a)).

The purpose of describing the parameters in a polar graph is to determine if they lead to instability problems due to their values. The identification is considered unstable and nonadequate when the estimation parameters go out of the unitary circle giving an overpass to the reference boundaries.

2.1. Recursion through the Previous Estimated Parameter. The first approach is by considering an instant t and the previous corrected estimated parameter $\widehat{\widehat{A}}_{t-1}$ based on the estimated parameter $\widehat{A}_t$. For the second identification stage in (4) the estimation is described as $\widehat{\widehat{A}}_t$ in the iteration t as in (5). Results are shown in Figure 4.

$$\widehat{\widehat{A}}_t = \widehat{\widehat{A}}_{t-1} + \mathrm{EFF}_t - \mathrm{sign}\left(\widehat{\widehat{A}}_{t-1}\right). \tag{5}$$

2.2. Recursion through the Mean between the Previous and Actual Estimated Parameter. Continuing with (4) as the base, now the average estimated parameter for instant t and the delayed $t-1$ corrected estimation as in (6) is considered. Results are shown in Figure 4.

$$\widehat{\widehat{A}}_t = \frac{\widehat{\widehat{A}}_{t-1} + \widehat{A}_t}{2} + \mathrm{EFF}_t - \mathrm{sign}\left(\frac{\widehat{\widehat{A}}_{t-1} + \widehat{A}_t}{2}\right). \tag{6}$$

Notice in cases (a) and (b) a third stage is added to the process, having first the simple average approximation; secondly the EFF_t correction and the second parameters correction are made.

From Figure 4, it is possible to see that the identification using cases (a) and (b) is not adequate because every time the reference changes its concavity converging, it becomes more difficult, leading to undesirable peaks [15].

2.3. Iterative EFF-Estimation. In Figure 2 the dashed lines represent the first EFF correction; the same stage at the end of the process (7) is iteratively added, valid for $n \geq 2$, having $a_{t,1} = \widehat{A}_t$ and $\mathrm{EFF}_{t,1} = \mathrm{sign}(\widehat{A}_t)e^{\mathrm{sign}(\widehat{A}_t)\widehat{e}_t}$ as the initial conditions, where n is the number of iterations made for the signal instant t, being $n = 1$ the average stage.

$$\mathrm{EFF}_{t,n} = \mathrm{sign}\left(a_{t,n}\right) e^{\mathrm{sign}(a_{t,n})e_{t,n}}, \tag{7}$$

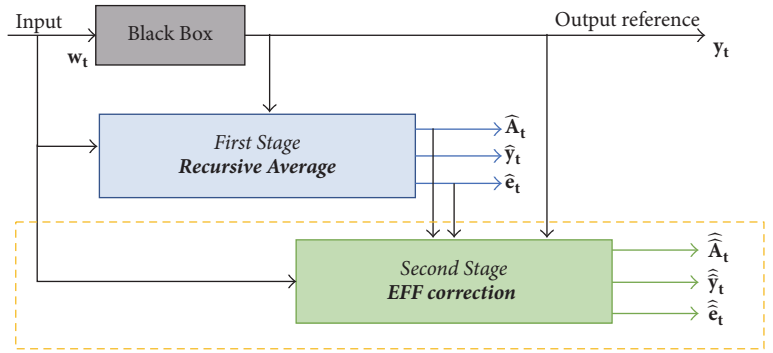

FIGURE 2: Block diagram for two stages into the estimation-identification process using a recursive average method (first) and the EFF (second, dashed line).

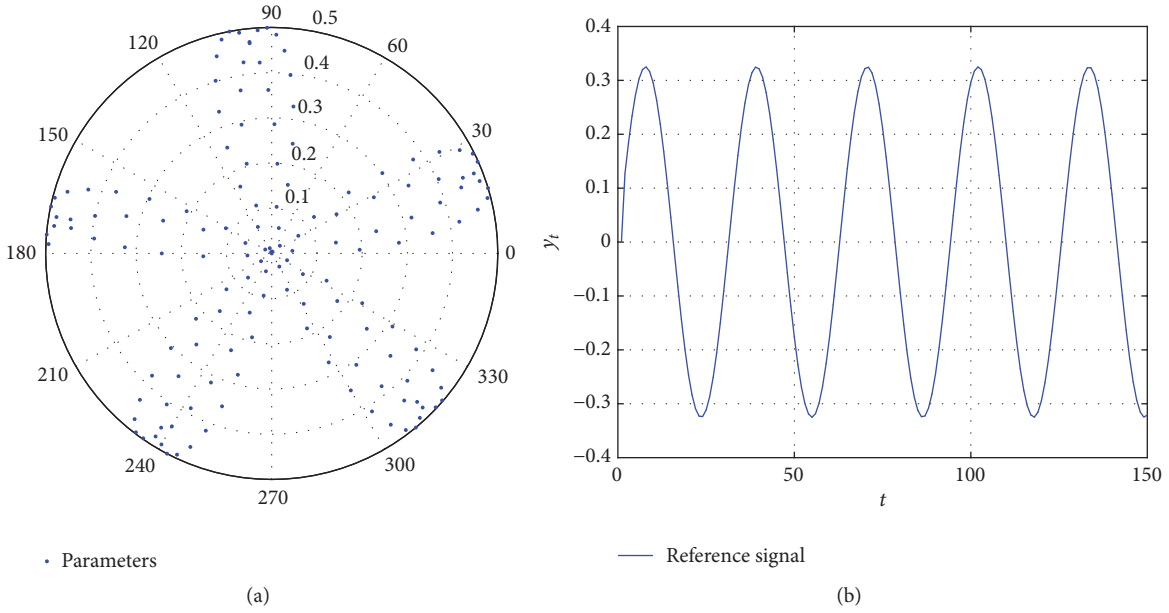

FIGURE 3: Reference parameters (a) and the output signal (b) to be identified.

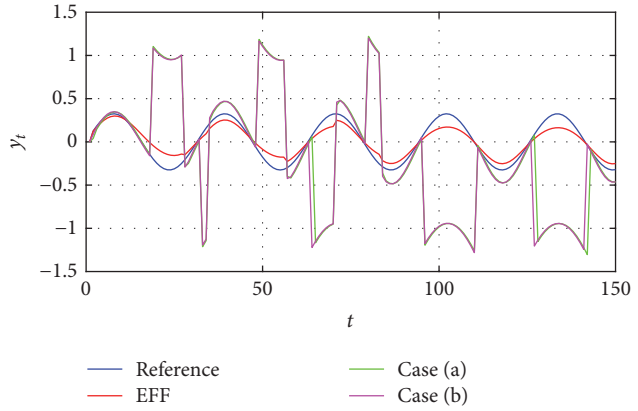

FIGURE 4: Identification using the estimation from case (a).

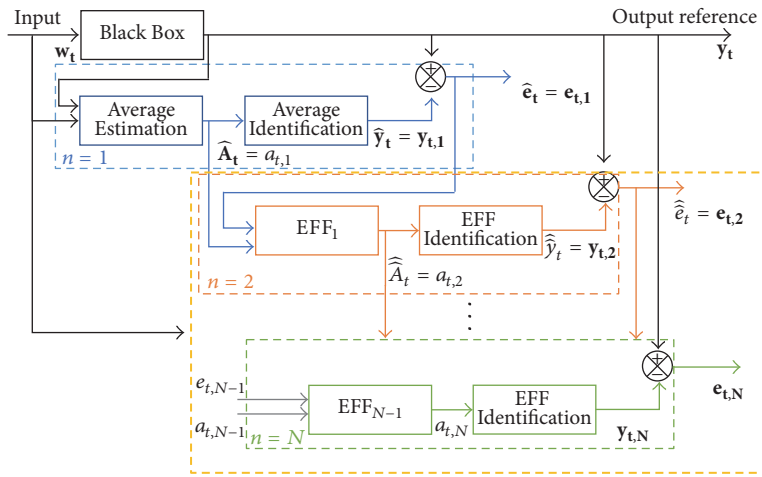

FIGURE 5: Block diagram for the estimation-identification process, case (c), with n-iterations of the EFF correction.

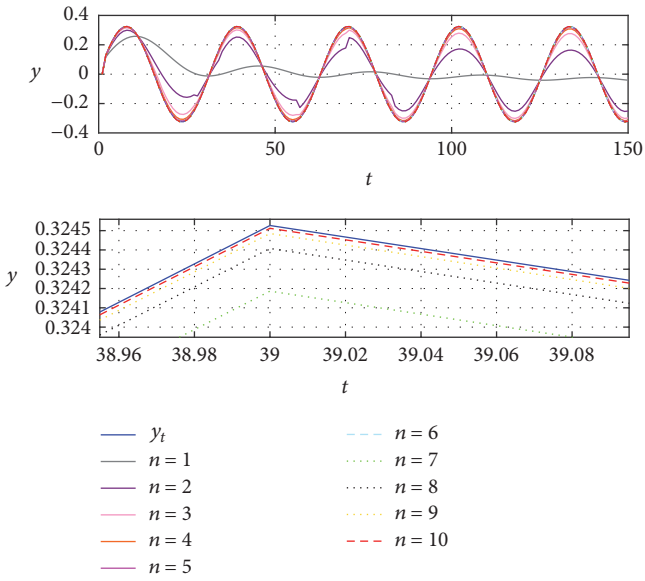

FIGURE 6: Identified signal applying case (c) for $n = 10$, from 2 to 10.

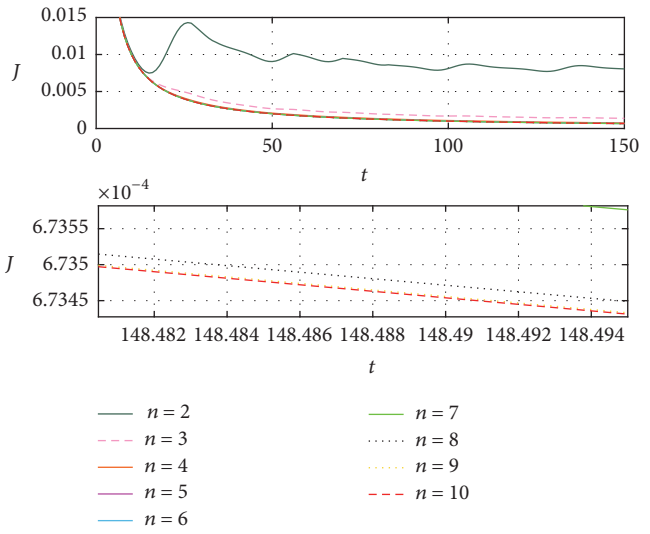

FIGURE 7: Comparison of the functional error J_t obtained from the identified signals from Figure 6.

where $a_{t,n}$ and $e_{t,n}$ are defined as (8) and (9), respectively.

$$a_{t,n} = a_{t,n-1} + \mathrm{EFF}_{t,n-1} - \mathrm{sign}\left(a_{t,n-1}\right) \tag{8}$$

$$e_{t,n} = y_t - y_{t,n}. \tag{9}$$

Considering $y_{t,n}$ as the identified signal after n iterations of the EFF and y_t as the output reference signal with input w_t, then (9) could be defined as

$$\begin{aligned} e_{t,n} &= y_t - a_{t,n} w_t \\ &= y_t - \left[a_{t,n-1} + \mathrm{EFF}_{t,n-1} - \mathrm{sign}\left(a_{t,n-1}\right)\right] w_t. \end{aligned} \tag{10}$$

Unlike cases (a) and (b), this last one changes in estimating not only the parameter, but also the EFF, correcting n times the parameters to improve the identification signal convergence, as seen in the block diagram for case (c) shown in Figure 5.

The question now lies in how many iterations would be necessary to obtain an adequate convergence rate without having redundancies in data. The answer could vary according to what is most important from one application to another; thus, the reduction of the error is one of the main objectives in identification tasks.

Thus, to verify the effectiveness of correction through the EFF, first the identified signals for $n = 2$ to $n = 10$ were obtained and ten simulations as shown in Figure 6.

Figure 6 shows that when increasing the n iterations, the identification is closer to the reference. Here is where the decision to increment the iterations depends on the desired accuracy level. To better appreciate the approximation errors, Figure 7 includes the functional error J_t, in agreement with

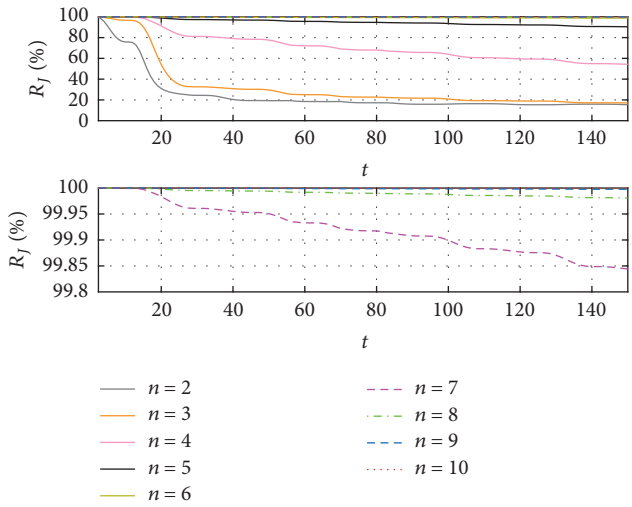

Figure 8: Resemblance errors and functionals, from consecutive EFF iterations.

[21], with respect to previous closer identifications, as viewed in Figure 7.

The second process identifies a better convergence, as shown in Figure 7, where the error between the first and second iteration is remarkably reduced, as between the second and third, and so on. To have a better visualization from the differences between the results obtained in every iteration, Figure 8 shows the relation (11), expressed in percentage, which indicates how similar the results are in each iteration based on the functional error.

$$R_{J_n/J_{n-1}} = \frac{J_{t,n}}{J_{t,n-1}} \times 100\%. \tag{11}$$

From iteration 7, the resemblance between it and the previous is above 99.8%, meaning the difference would be insignificant depending on the application. On the other hand, considering the magnitude errors obtained from this same iteration, they are less than 3% with respect to the original signal.

3. Parameter Estimation Example

Our proposed example task is to approximate an EEG reference with changes in concavity and frequency with added noise, as those illustrated in [5, 22]. The reference signal is described as follows in (12), where t is the time evolution in seconds with sample frequency of 100 Hz, $f_\theta = 7$, $f_\beta = 25$, $f_\alpha = 15$, and $f_\gamma = 40$, as shown in Figure 9.

$$y_t = \begin{cases} 2t^{0.5} \sin\left(2\pi f_\theta t\right) & t \in [0, 2) \\ t^{0.5} \sin\left(2\pi f_\beta t\right) & t \in [0, 4) \\ 2t^{0.25} \sin\left(2\pi f_\alpha t\right) & t \in [0, 6) \\ 3t^{0.25} \cos\left(2\pi f_\gamma t\right) & t \in [0, 8) \\ 0 & \text{otherwise.} \end{cases} \tag{12}$$

The estimation process generates the adequate parameters described symbolically as $\widehat{A}_t$ in each sampled point for time t,

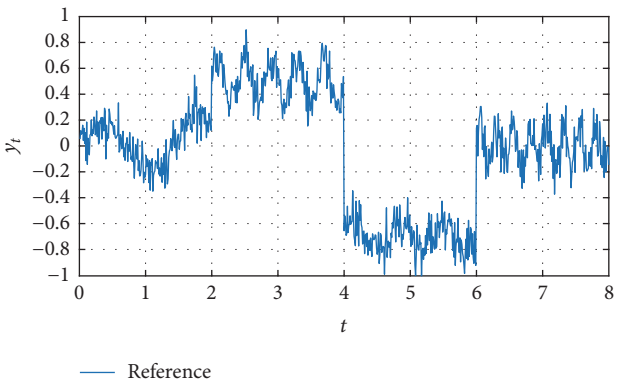

Figure 9: Reference signal described in (10), with evolution time t and sample frequency 100 Hz.

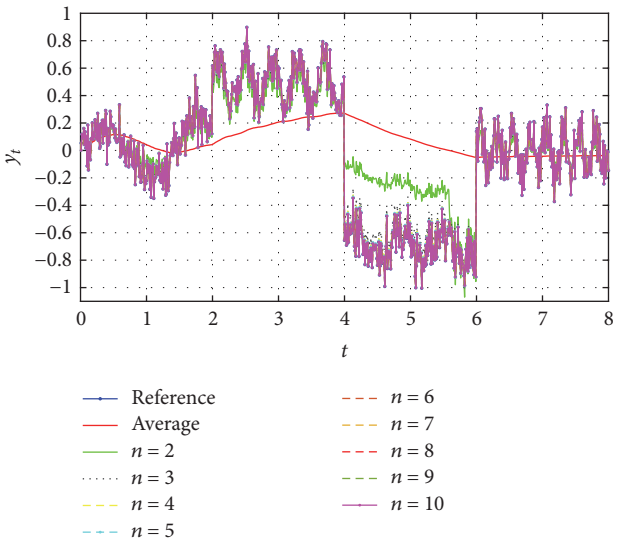

Figure 10: Identifications of the reference signal from Figure 9 applying an average identification and 10 iterations using recursive EFF.

approximating a linear variant function (2) to (12), which has stochastic properties, having variations in amplitude and frequency. The identification is composed of various iterations and the results are presented comparing the identifications with the proposed reference signal shown in Figures 10 and 11, observing the functional errors evolution.

In a Black Box (BB) system the relationship between the internal and external parameters cannot be made directly because the internal evolution is unknown, as would happen with real signals. Nevertheless, the parameters are important because they could be analyzed to obtain special features from EEG signals which are difficult to obtain for nonlinear signals. In fact, the obtainment of those parameters is the objective of the proposed technique. Figure 12 presents the parameters obtained using the estimation, for the simple EFF and its iterative description considering $n = 5$, 8, and 11 iterations, which are representative when adding more than one correction step.

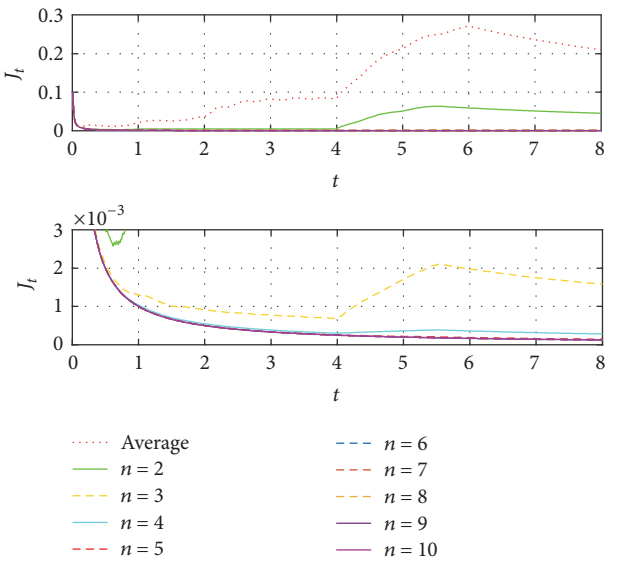

Figure 11: Functionals error obtained from the identification processes from Figure 10.

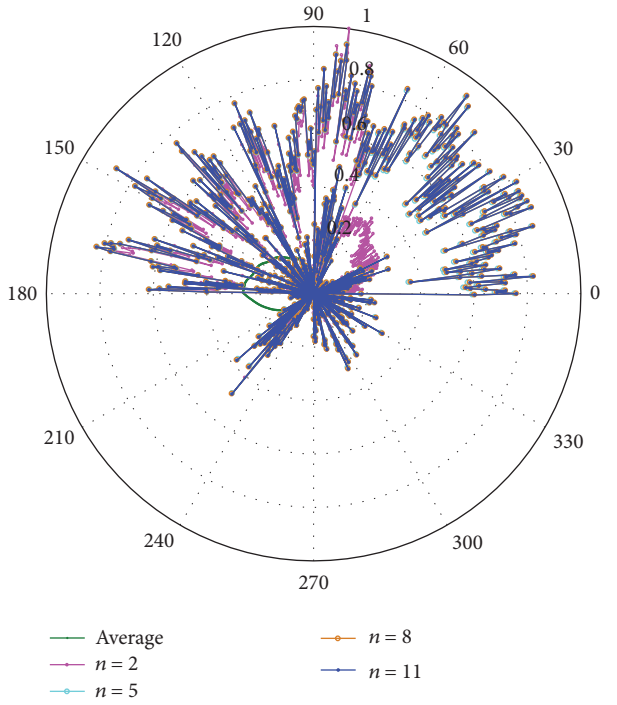

Figure 12: Parameters obtained using an average estimator (average), the simple EFF ($n = 2$), and 5, 8, and 11 iterations of the recursive description of the EFF.

From Figure 12, it is determined that the parameters have variable characteristics for each sampled point. The variation between the average estimation and the simple EFF ($n = 2$) estimation is noticeably as in size and in direction. On the other hand, between the simple EFF and the other iterations the estimated parameters are similar in direction, presenting

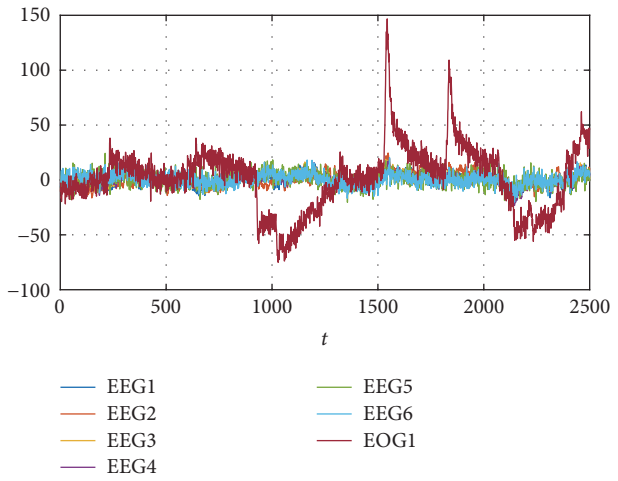

Figure 13: Sampled signals for Counting tasks, taken from [8, 9], for subject 1, considering 6 EEG channel and 1 EOG.

changes with the characteristic of never being able to leave the reference, maintaining the stability identification.

3.1. Estimation of EEG Signals. As a second part of the test, the estimation-identification process is applied to sampled signals taken from [7, 23], which are for subject 1 from 6 Electroencephalogram (EEG) and one Electrooculogram (EOG) channels for different activities. The objective is to apply the EFF iterative description from case (c) to obtain the parameters that allow the approximation by using (2). The reference data as in Figure 13 have 10 seconds of recording with a sampling frequency of 250 Hz, obtaining in total 2500 samples representing instants t. The results of applying the average description and 5 and 10 iterations of the EFF are shown in Figure 14.

In Figure 14, signals from Figure 13 are separated to improve the convergence to each. These are different from one another. Having different signals is useful to determine the fact that the identification using the EFF is adequate for chaotic nonstationary cases, such as the EEG or EOG, presented in this work. To conclude, the measured error is viewed as the functional errors average from the seven signals for each estimation as shown in (13), where n is the number of iterations. Results are given in a polar graph in Figure 15, observing functionals errors that tend to zero in all corrected approximations, having a better performance when more iterations are applied.

$$J_{Tn} = \frac{J_{\mathrm{EEG1}_n} + J_{\mathrm{EEG2}_n} + \cdots + J_{\mathrm{EEG6}_n} + J_{\mathrm{EOG1}_n}}{7}. \quad (13)$$

3.2. Classification of EEG Signals. In the previous section, the EEG signals parameter estimation was possible. Then we present the application of the estimated parameters into the classification of EEG signals viewed in our case as a stochastic system with multioutput EEG responses. For different instances, we consider the same database used in

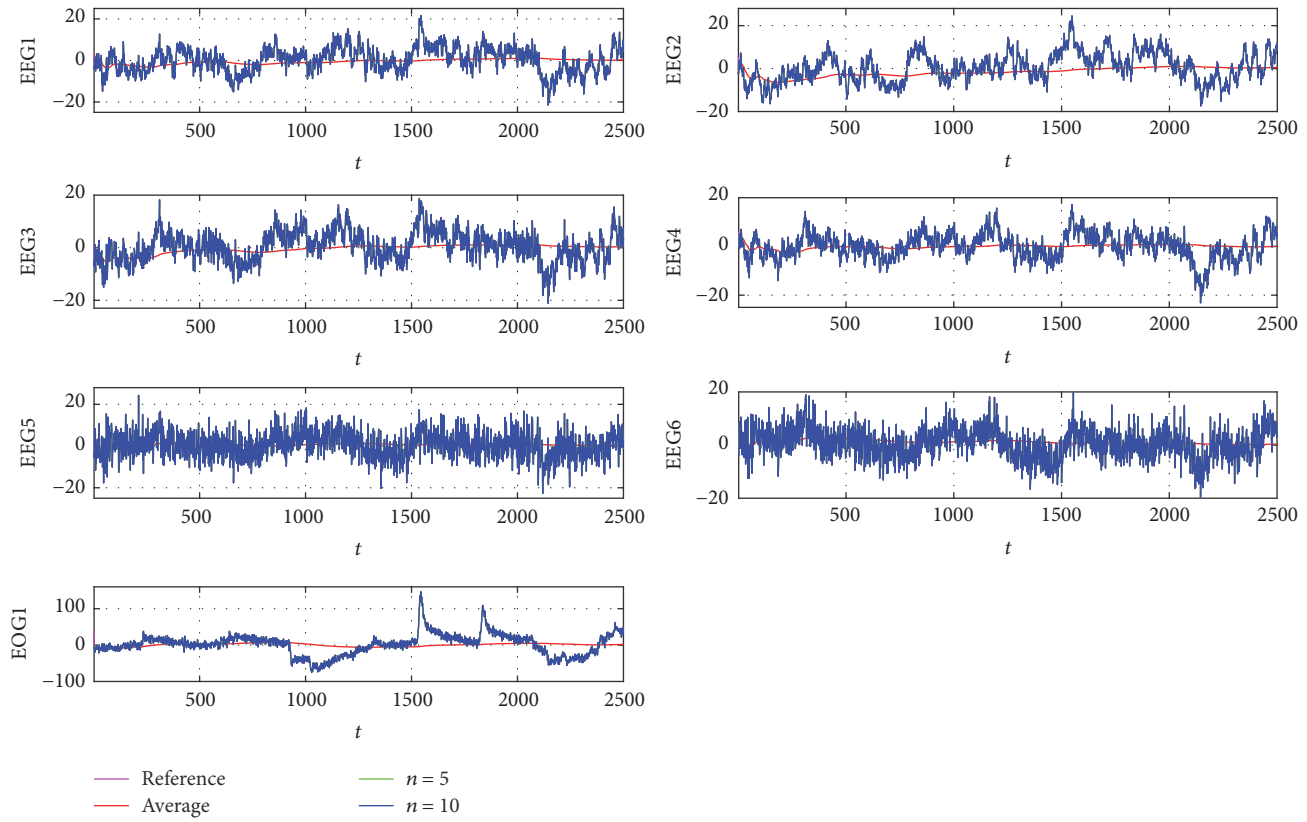

Figure 14: Identification for signals from Figure 13, comparing the sampled signal, the average approximation, and the identification by using 5 and 10 iterations with EFF.

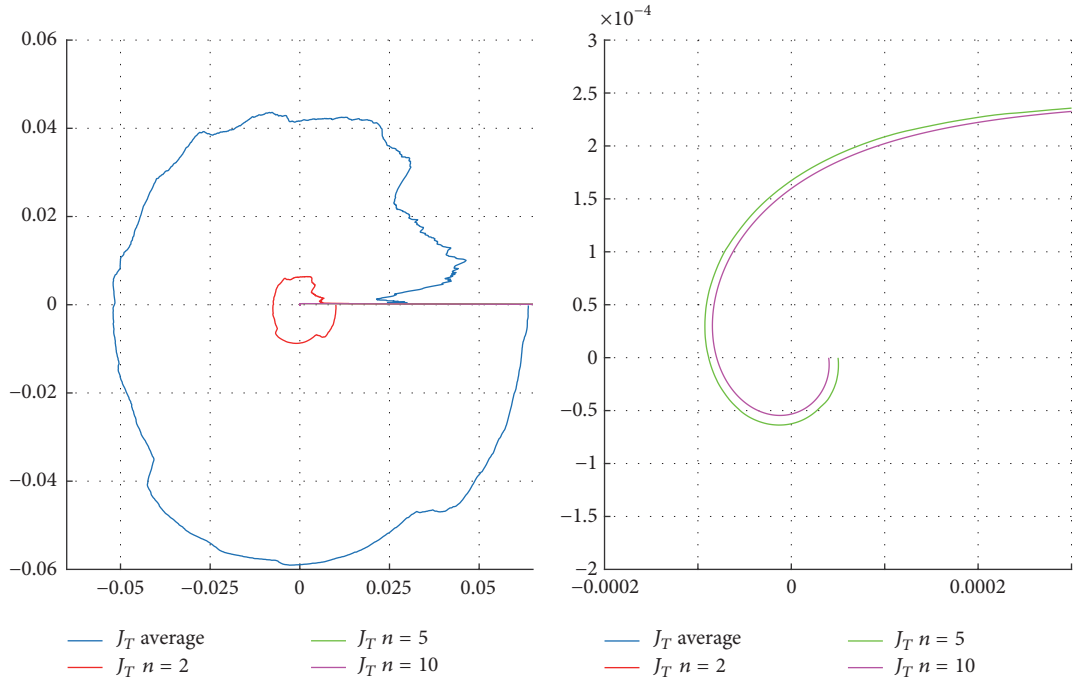

Figure 15: Polar representation of the combination of error functionals obtained by identifying the signal from Figure 14.

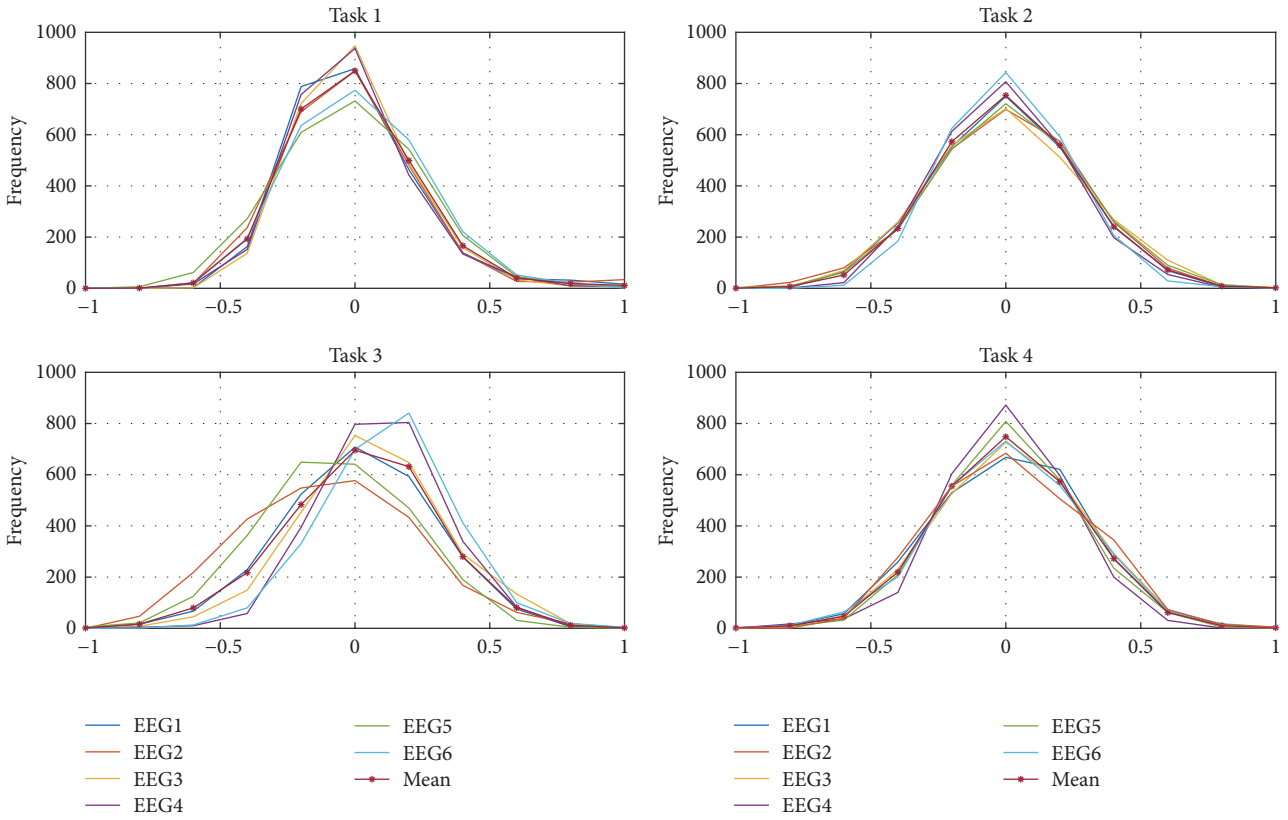

Figure 16: Four tasks defined by six EEG signals distributions with their representative mean distributions.

Section 3.1 [7, 23] and the estimation-identification process with iterative EFF iterating 10 times.

The regarded four tasks are multiplication (Task 1), letter (Task 2), rotation (Task 3). and counting (Task 4). For each task, six EEG channels (1 to 6) are considered having specific distributions as seen in Figure 16, which presents the normalized signals distributions divided into ten principal intervals between $[-1, 1]$, for a better appreciation. The average of the six distributions signals for every task was obtained and presented also in Figure 16. The mean distribution is the representative one to be used as the base for the stochastic EEG classification.

For a specific task, when identifying its six signals, their corresponding distributions could be obtained as well as the mean identified representative distribution. The classification is made by comparing the four base distributions from Figure 16 to the mean identified and determining the convergence error between them. The assignment is then for the task where the minimum error is found. Figure 17 presents four different instances.

In Figure 17 the similarities between the identification of different tasks are seen. For example, within instance 1, the identified distribution is closer to Task 1 than to the others, so that it is possible to say that the identification corresponds to it. To quantify how close they are, the recursive error functional [21] based on the second probability moment considering the errors from the distribution comparison is calculated and presented in Figure 18 for each instance.

From Figure 18, the minimum cumulative error corresponds to the correct assigned classification. On the other hand, Table 1 represents a decision chart based on the errors for the four instances, summarizing the classification process to minimum error identification, obtaining good results in all considered instances.

4. Conclusion

The results obtained for cases (a) and (b) are obvious because the changes are made considering the past, and the EFF description is for actual information. Therefore, the use of previous parameters would break the convergence after using the parameter obtained with the EFF leading to a poorer convergence.

For case (c) it could be said that special care must be taken when the time is important to obtain the identification because having more iterations, and in consequence less error, implies more execution time. However, the latency is big enough to allow a considerable number of iterations, modifying the EFF, and then the parameter as in case (c), from iteration 7 (as shown in Figures 7 and 8), results in better correction than that obtained by modifying only the parameters.

The estimation-identification process is adequate for nonlinear signals, such as those obtained from EEG. The importance of describing these signals lies in the description

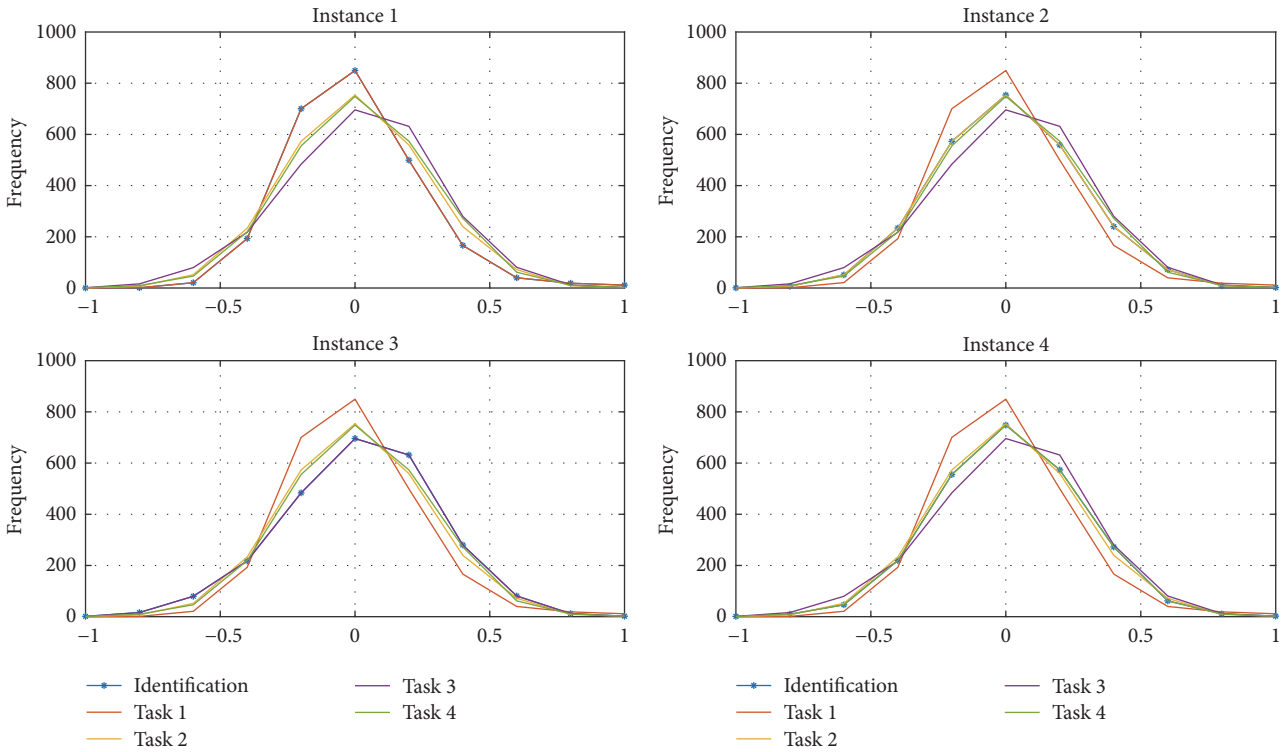

Figure 17: Comparison between the base EEG signal distributions and four identified signals instances.

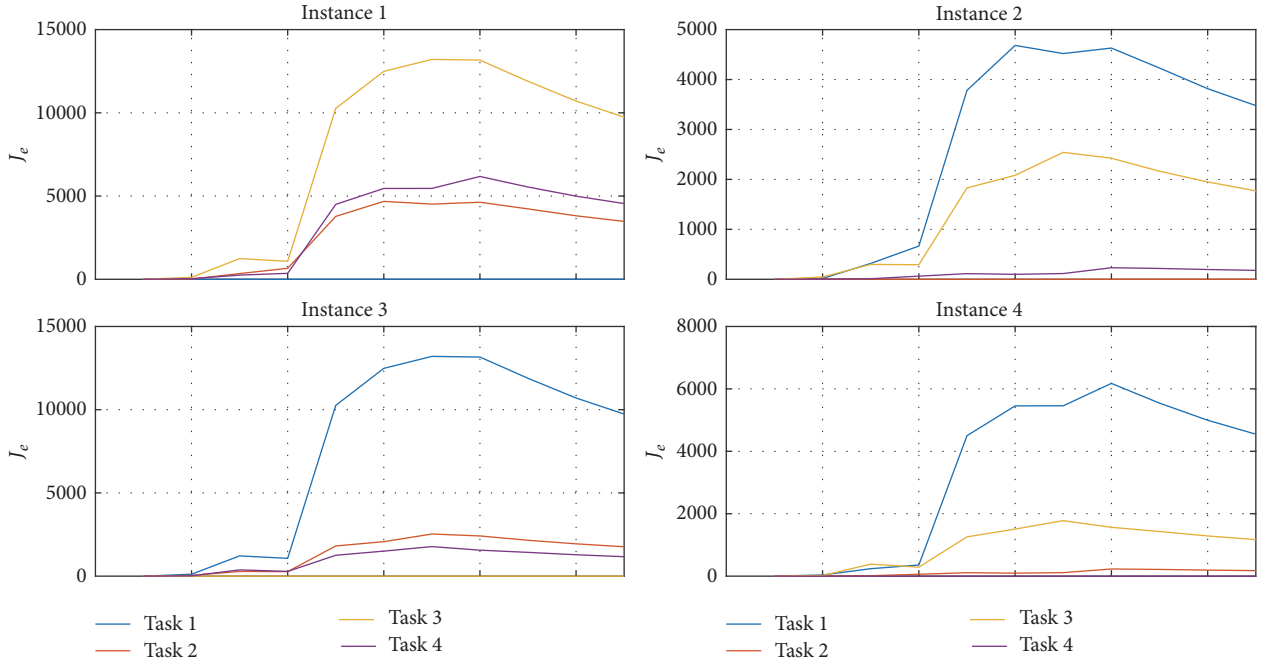

Figure 18: Functional errors comparing the EEG base and identified distributions from Figure 17.

of possible missing information when drastic changes in concavity and frequency are given. Even when in this paper only time-variant analysis is shown, the reconstruction of chaotic signals gave good results in comparison with a simple average approach, as seen in Figure 14.

Even when the main objective of this work is the parameter estimation, a simple classification test has been performed to demonstrate one possible use of the parameters obtained by using our technique, achieving good results is the four presented instances (Table 1).

Table 1: Classification of different instances of EEG signals considering the minimum error viewed as a decision chart from the cumulative errors.

Instance	Task 1	Task 2	Task 3	Task 4	Minimum error	Classification
1	**001.10**	485.26	772.26	525.93	001.10	Task 1
2	485.26	**001.43**	326.76	105.10	001.43	Task 2
3	772.26	325.10	**0.4333**	252.10	0.4333	Task 3
4	525.93	105.10	252.76	**0.4333**	0.4333	Task 4

As future work, comparisons using more real signals should be performed, and finally, the obtained parameters could be helpful to create a database and obtain more characteristics to create useful synthetic signals and prove the effectiveness of new methods or techniques.

Conflicts of Interest

The authors declare that there are no conflicts of interest regarding the publication of this article.

Acknowledgments

The authors would like to thank the Instituto Politécnico Nacional (IPN) and the Consejo Nacional de Ciencia y Tecnología (CONACYT) for their support while carrying out the research work through projects SIP-20171418, SIP-20170018, and SIP-20171694.

References

[1] K. A. Aguilar Cruz, *Filtro digital para la estimación de parámetros variantes usando el factor de olvido exponencial*, 2016.

[2] K. A. Aguilar Cruz, J. J. Medel Juárez, and R. Urbieta Parrazales, "Exponential function argument variation to obtain a Directional Forgetting Factor," in *Proceedings of the XVI Congreso Nacional de Ingeniería Electromecánica y de Sistemas (CNIES 2017)*, México, 2017.

[3] G. Box, G. Jenkins, G. Reinsel, and G. Ljung, *Time series analysis: forecasting and control*, John Wiley & Sons, 2015.

[4] J. J. Medel Juárez, R. Urbieta Parrazales, and R. Palma Orozco, "Estimador estocástico para un sistema tipo caja negra," *Revista Mexicana de Física*, vol. 57, no. 3, pp. 204–210, 2011.

[5] M. X. Cohen, "Where does EEG come from and what does it mean?" *Trends in Neurosciences*, vol. 40, no. 4, pp. 208–218, 2017.

[6] Y. Li, M.-L. Luo, and K. Li, "A multiwavelet-based time-varying model identification approach for time-frequency analysis of EEG signals," *Neurocomputing*, vol. 193, pp. 106–114, 2016.

[7] A. Schlögl, S. J. Roberts, and G. Pfurtscheller, "A criterion for adaptive autoregressive models," *Proceedings of the 22nd Annual International Conference of the IEEE Engineering in Medicine and Biology Society*, vol. 2, pp. 1581-1582, 2000.

[8] H. Nai-Jen and R. Palaniappan, "Classification of mental tasks using fixed and adaptive autoregressive models of EEG signals," in *26th Annual International Conference of the IEEE Engineering in Medicine and Biology Society, IEMBS'04*, vol. 1, pp. 507–510, San Francisco, CA, USA, 2004.

[9] C. Anderson, "1989 Keirn and Aunon," Brain-Computer-Interfaces Laboratory, 2017, http://www.cs.colostate.edu/~anderson.

[10] A. Schloegl, K. Lugger, and G. Pfurtscheller, "Using adaptive autoregressive parameters for a brain-computer-interface experiment," in *Proceedings of the 1997 19th Annual International Conference of the IEEE Engineering in Medicine and Biology Society*, pp. 1533–1535, November 1997.

[11] K. Brigham and B. V. K. V. Kumar, "Subject identification from Electroencephalogram (EEG) signals during imagined speech," in *Proceedings of the 4th IEEE International Conference on Biometrics: Theory, Applications and Systems, BTAS 2010*, pp. 1–8, September 2010.

[12] A. S. Al-Fahoum and A. A. Al-Fraihat, "Methods of EEG signal features extraction using linear analysis in frequency and time-frequency domains," *ISRN Neuroscience*, vol. 2014, Article ID 730218, 7 pages, 2014.

[13] A. Adam, M. I. Shapiai, M. Z. M. Tumari, M. S. Mohamad, and M. Mubin, "Feature selection and classifier parameters estimation for EEG signals peak detection using particle swarm optimization," *The Scientific World Journal*, vol. 2014, Article ID 973063, 13 pages, 2014.

[14] Y. Li, H.-L. Wei, S. A. Billings, and P. G. Sarrigiannis, "Identification of nonlinear time-varying systems using an online sliding-window and common model structure selection (CMSS) approach with applications to EEG," *International Journal of Systems Science*, vol. 47, no. 11, pp. 2671–2681, 2016.

[15] Y. Guo, L. Z. Guo, S. A. Billings, and H.-L. Wei, "Identification of continuous-time models for nonlinear dynamic systems from discrete data," *International Journal of Systems Science*, vol. 47, no. 12, pp. 3044–3054, 2016.

[16] K. A. Aguilar Cruz, J. D. J. Medel Juárez, and R. Urbieta Parrazales, "Equivalent neural network optimal coefficients using forgetting factor with sliding modes," *Computational Intelligence and Neuroscience*, vol. 2016, Article ID 4642052, 6 pages, 2016.

[17] M. L. Padmanabh, R. K. Shastri, and D. Biradar, "EEG signal processing techniques for mental task classification," *International Journal of Advanced Computing and Electronics Technology*, vol. 2, pp. 66–73, 2015.

[18] J. Zhang and S. Yang, "An incremental-PID-controlled particle swarm optimization algorithm for EEG-data-based estimation of operator functional state," *Biomedical Signal Processing and Control*, vol. 14, pp. 272–284, 2014.

[19] İ. Güler, M. K. Kiymik, M. Akin, and A. Alkan, "AR spectral analysis of EEG signals by using maximum likelihood estimation," *Computers in Biology and Medicine*, vol. 31, no. 6, pp. 441–450, 2001.

[20] J. Lerga, N. Saulig, and V. Mozetič, "Algorithm based on the short-term Rényi entropy and IF estimation for noisy EEG signals analysis," *Computers in Biology and Medicine*, vol. 80, pp. 1–13, 2017.

[21] P. Li, X. Wang, F. Li et al., "Autoregressive model in the Lp norm space for EEG analysis," *Journal of Neuroscience Methods*, vol. 240, pp. 170–178, 2015.

[22] S. Motamedi-Fakhr, M. Moshrefi-Torbati, M. Hill, C. M. Hill, and P. R. White, "Signal processing techniques applied to human sleep EEG signals—a review," *Biomedical Signal Processing and Control*, vol. 10, no. 1, pp. 21–33, 2014.

[23] Y. Li, Q. Liu, S.-R. Tan, and R. H. M. Chan, "High-resolution time-frequency analysis of EEG signals using multiscale radial basis functions," *Neurocomputing*, vol. 195, pp. 96–103, 2016.

Hindawi
Computational Intelligence and Neuroscience
Volume 2017, Article ID 2721846, 10 pages
https://doi.org/10.1155/2017/2721846

Research Article

Reducing the Schizophrenia Stigma: A New Approach Based on Augmented Reality

Rafael D. de C. Silva,[1] Saulo G. C. Albuquerque,[2,3] Artur de V. Muniz,[2] Pedro P. Rebouças Filho,[4] Sidarta Ribeiro,[5] Plácido Rogerio Pinheiro,[1] and Victor Hugo C. Albuquerque[1]

[1] *Programa de Pós-Graduação em Informática Aplicada, Laboratório de Bioinformática, Universidade de Fortaleza, Fortaleza, CE, Brazil*
[2] *Hospital de Saúde Mental de Messejana, Fortaleza, CE, Brazil*
[3] *Internato em Saúde Coletiva e Mental, Universidade de Fortaleza, Fortaleza, CE, Brazil*
[4] *Laboratório de Processamento de Imagens e Simulação Computacional, Instituto Federal de Educação, Ciência e Tecnologia do Ceará, Maracanaú, CE, Brazil*
[5] *Instituto do Cérebro, Universidade Federal do Rio Grande do Norte, Natal, RN, Brazil*

Correspondence should be addressed to Victor Hugo C. Albuquerque; victor.albuquerque@unifor.br

Received 20 July 2017; Revised 1 November 2017; Accepted 5 November 2017; Published 29 November 2017

Academic Editor: Saeid Sanei

Schizophrenia is a chronic mental disease that usually manifests psychotic symptoms and affects an individual's functionality. The stigma related to this disease is a serious obstacle for an adequate approach to its treatment. Stigma can, for example, delay the start of treatment, and it creates difficulties in interpersonal and professional relationships. This work proposes a new tool based on augmented reality to reduce the stigma related to schizophrenia. The tool is capable of simulating the psychotic symptoms typical of schizophrenia and simulates sense perception changes in order to create an immersive experience capable of generating pathological experiences of a patient with schizophrenia. The integration into the proposed environment occurs through immersion glasses and an embedded camera. Audio and visual effects can also be applied in real time. To validate the proposed environment, medical students experienced the virtual environment and then answered three questionnaires to assess (i) stigmas related to schizophrenia, (ii) the efficiency and effectiveness of the tool, and, finally (iii) stigma after simulation. The analysis of the questionnaires showed that the proposed model is a robust tool and quite realistic and, thus, very promising in reducing stigma associated with schizophrenia by instilling in the observer a greater comprehension of any person during an schizophrenic outbreak, whether a patient or a family member.

1. Introduction

The World Health Organization (WHO) describes schizophrenia as one of the most serious and challenging psychiatric diseases nowadays, which still demands strong efforts in order to acquire a more solid knowledge on the pathology. It is a complex disease categorized by distortions of thought, self-perception, and external reality, as well as inadequacy and dullness of affection [1]. Schizophrenia affects more than 21 million people worldwide, and one in every two schizophrenia-afflicted subjects does not receive care for the disease [2], despite the fact that there are effective schizophrenia symptom-mitigation treatments and affected people can lead a productive life and be inserted into society [3].

Amongst the main schizophrenia manifestations the positive symptoms stand out, ordinarily termed psychotic symptoms, which include hallucinations and delusions, typifying the loss of the patient's contact with reality. Negative symptoms (mostly impairment of motivation, reduction of spontaneous speech, and social isolation) and cognitive impairment are also considered key features of this illness [4].

Hallucinations can be defined as the perception of an object, such as voice, noise, or image, without it being present,

that is, without the respective sensorial stimulus [5]. They are experiences comparable to perception that occur without an external stimulus; it means that the patient experiences the behavior as not being under voluntary control [6]. In schizophrenia, hallucinations concerning visual, somatic, tactile, and olfactory modalities may take place, but the auditory ones are the most frequent indicators [7].

Over the past years, a greater access to technology has allowed the use of tools such as virtual reality (VR) in medicine. VR is an instrument capable of inserting the user into an interactive three-dimensional virtual world, using a computer that can generate images and a display that presents sensory information. Over the last few decades, the use of VR in psychotic disorders, such as schizophrenia, has been a promising candidate, for example, for a clearer understanding of symptoms, for training of instrumental and social skills, and for the treatment of the disease, as an adjuvant technique [8, 9]. With reference to the stigma, VR has been shown to be useful for diminishing negative stereotypes [10] and as a supporting device to increase empathy and positive impressions towards schizophrenic people [11] amongst other applications [12–24].

In addition to the severe symptoms of the disease, patients afflicted with schizophrenia face another key trouble: the stigma. Discrimination against these patients can be perceived when they try to make or maintain friendships, look for a job, or maintain intimate or sexual relations. Moreover, discrimination often comes from members of their own family [25]. In a study conducted in the United Kingdom, it was observed that more than 70% of the general public classified schizophrenia-afflicted people as dangerous or unpredictable [26].

One aspect to fight the stigma is intervention in specific groups of the population, such as police authorities and health providers. There are studies showing that training of police forces to recognize mental disorders could decrease the number of arrests and unnecessary force used against people with mental illnesses, as well as increase the adequate referral to psychiatric institutions [27].

Even though the effects of the stigma on the evolution of schizophrenia are still scarcely addressed by patients families and health practitioners, they have been observed in a number of studies. In recent times, it has been demonstrated, for instance, that stress instigated by stigma may be related to the transition to schizophrenia in young people at risk of psychosis [28]. Habitually, the patient feels downgraded. The disorder itself often leads to a condition of hypobulia and decreased motivation, which culminates with impaired physical conditioning. Environment-generated stimuli maybe cannot induce severe side effects, as there are no literary reports of serious symptoms generation (e.g., convulsive crisis) [29].

A number of approaches have been developed aiming at reducing the public stigma of mental illness and the damage it causes to the patient's life. For example, virtual environments to educate patients with schizophrenia of the hallucinations they suffer [30]. Amongst these approaches, social protest or activism, education of the public, and contact with mentally handicapped people stand out, while the latter two show positive results in the stigma reduction. Educational strategies comprise public messages, books, pamphlets, films, videos, web pages, virtual reality, and other audiovisual tools [31].

A healthy sample of the population submitted to the demonstration of the proposed environment can reduce interrelated obstacles, for example, to the delay in the beginning of the treatment and difficulties in interpersonal and professional relationships to have a proper approach to the conditions of people afflicted this serious mental illness.

The development of a VR-based tool capable of reducing the stigma related to schizophrenia is of utmost importance to treat this disease. To fill this gap, we propose a new augmented-reality-based tool capable of simulating the typical psychotic symptoms of schizophrenia and analyzing its effectiveness, the influence of the tool on stigmas reduction, emotional impact on users, and its validation by specialists and students of the medicine course by use and application of a questionnaire. The proposed system can interact, in real time, with a healthy sample of the population, medical students, simulating the psychotic symptoms typical of schizophrenia. The environment was developed with the support of a psychiatry specialist team.

Appraisal of the tool effectiveness is performed by Mental Health specialists through three questionnaires: schizophrenia-related stigma evaluation, environment simulation evaluation, and stigma evaluation after augmented-reality simulation. In the questionnaire assessing the schizophrenia-related stigma, volunteers' personal data, family experience in cases of schizophrenia-diagnosed persons, and a fictional history of a schizophrenia-afflicted individual were made. For the simulation evaluation, inquiries related to the performance of the AR environment were made. In the last questionnaire, the reassessment was made after an environment simulation of how the volunteer turned out to perceive the person from the fictional story about schizophrenia.

Environment-generated stimuli should not be able to trigger serious side effects, as there are no literature reports about serious symptoms induction (e.g., convulsive crises). Simulations can be applied in educational environments (school groups, colleges, and technical training) in professional settings such as hospitals and clinics, and in training and awareness-raising groups that may interact with psychosis-afflicted people, such as police officers, municipal guards, and family members of disease carriers.

By applying such virtual systems, connected with clinical purposes, they can play an important role in the healthcare area, as they are easily handled by the specialist as well as by the patient, being such a reassuring feature for the treatment continuousness [32]. For example, [9] presented a pilot study to investigate the feasibility and potential negative side effects of exposure to different virtual social risk environments in patients with first episode psychosis and in healthy controls.

2. Development of the Proposed Virtual Environment

Virtual and augmented reality are technological tools that use virtual elements that can be inserted in realistic scenarios,

becoming an alternative and complementary approach to the treatments and diagnoses, being a very promising method to be adopted definitively in the health area [33].

Virtual reality is an advanced interface for computational applications in which users can navigate and interact with a three-dimensional computer-generated environment through multisensory devices. This technology establishes the relationship between the user and the created environment, allowing real-time integration with controlled virtual objects, and can simulate touch-screen monitors, mount-head goggles, mouse, and data glove and explore virtually freely, without real constraints like gravity, according to the immersion scenario and controls in which the user is interacting. In it, the individual has the sensation, in real time, of interacting with the virtual world manipulating objects around it [34].

Augmented reality is a type of advanced virtual reality interface that allows the user to experience sensations through stimuli to see, hear, feel, and interact with information and virtual elements inserted in the real environment [35].

In this work, the voices and figures were generated from the narrative of three schizophrenic patients treated at the NUEsq Schizophrenia outpatient clinic of Frota Pinto Mental Hospital in Fortaleza, Ceará. The data collection was qualitatively focused, based on the patients' verbal description of their psychotic experiences focusing on sensory perception alterations (auditory hallucinations and visual pseudohallucinations). The evaluation was led by a psychiatrist heading the clinical follow-up of the patients under discussion.

The tool consists of a software that reproduces some schizophrenia typical psychotic symptoms in an augmented-reality environment so that healthy people can undergo a simulation and thus provides a reality immersion for a patient carrying such ailment. In the environment, a 3-minute duration simulation was set, as it could become tiring over an extended period of time.

At the beginning, in the tool created in the Unity 3D program, a software that is used to create games and animations, an environment that could simulate what would be the reality was produced; namely, it was able to produce an immersion to the user as close to the reality as possible. To achieve this, a GameObject, named Cubo1 was designed, aimed at conveying with its texture a camera, so that when the operator used the environment he/she could visualize the real scenario in which he/she was inserted.

After the creation of the object that would use the camera to visualize the real-time environment, pictures that would make the process of simulation of the appearances of figures (common visual pseudohallucinations, referred by carriers) were inserted, with 2D sprites being used as scene GameObject, which could have their humanoid or geometric shapes a little rounded, and in them a blur effect was applied (blurred feature). The human-shaped figure has its animation modeled with fade-in and fade-out effects, causing it to appear or disappear at a particular point in time according to its program design, while its total four-second appearance is the most common. The geometric figure generally features the same outline when its animation is programmed similarly to the humanoid version, but in some cases the animation suffers the spawn effect (when the GameObject undergoes a transformation on the x-axis from one particular point to another), causing the GameObject to move from side to side, with a speed script being added. Additionally, the problem of the GameObject being "spawned" though never disappearing became evident, causing a future memory error. In consequence, a script was inserted so that it destroyed itself at a given time.

In the facial detection phase, a Unity plugin called OpenCV for Unity, which is a plugin that makes Unity recognize OpenCV scripts used in facial detection, was used. In the development of the facial modification a sprite (2D animated image) of a blurred spot was used to cause a somber effect in the interviewees' gaze. The effect of the facial modification lasted about 1 second, running twice during the three minutes.

The voices heard in the simulation via headphones were digitally recorded by two actors from a script prepared by the psychiatrist who piloted the interview with the volunteer patients. The audio plays a generic content, usually heard by patients with auditory hallucinations: whispers, threatening and commanding speech, laughter, and offending content phrases. Two voices were chosen, one male and one female, based on recurrent schizophrenia hallucinatory phenomena involving voices of different characteristics that often talk to each other. The choice of actors and nonrobotic voices was aimed at promoting authenticity and naturalness, which are distinctive of true hallucinations.

All students gave their informed consent to the procedure, which was approved by the Ethics Committee of Escola de Saúde Pública do Ceará, Ceará, Brazil (permit 1.569.510, June 1, 2016).

2.1. System Architecture. The implementation of the proposed system is based on the use of Unity as an engine of the augmented-reality environment, being used as 2D sprites scene objects produced in an image editing software. The HMZ-T2, Sony Glasses, responsible for transmitting the image processor, coupled with a LifeCam Studio Microsoft is placed in the user's head with a Panasonic RP-BTGS10 phone shown in Figure 1, which uses the bone to convey sound vibrations to the nervous system, transporting the sound of the environment and not interfering in the interviewer's voice. Figure 2 shows the integration of the devices in the system.

2.2. Environment Integration with the Equipment. As the purpose of this paper was to convey the psychotic symptoms to a healthy sample of the population, it demanded a good interaction of the tool with the equipment employed. The tool consists of software that can be installed on any computer that has Windows operating system with versions from Win 7. It already has a simple interface that was created by the graphic engine Unity 3D itself, being easily accessible to any user.

2.3. Modeling and Animation

2.3.1. Modeling and Audio Animation. Sound hallucinations were created by means of sound editing software and

Figure 1: Panasonic phone RP-BTGS10.

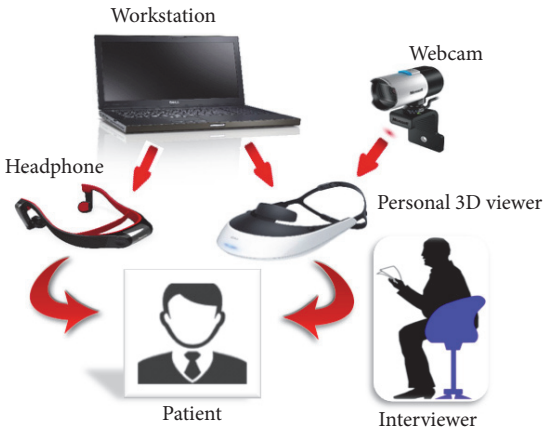

Figure 2: Device integration.

recorded with a microphone that was emitted by a headset. In creating the audio hallucinatory phrases noises, whispers and provocations, like "you aren't worth a thing" type were implemented. Some order phrases with "he will kill you" or "get out of here" were used in the environment audio. While developing the audio some pauses were made. In order to give more immersion as if a person were whispering in the ear, the procedure was applied in each and every phrase or any sound emitted by the environment, by using a sound channel coming out separately on each side of the headset. In the environment, the user of the glasses should listen to the voice of the interviewer who would make questions to the user while he/she listened to the sound effects.

2.3.2. Modeling and Figure Animation. The figure, modeled on an imaging software and animated in Unity, plays a major role in the augmented-reality environment, because it simulates one of the typical schizophrenia psychotic symptoms. This is the case when a patient has hallucinations in his/her vision that cause a perception of something nonexistent, but that is a subjective impression that it is something real without external stimulus. Consistent with reports from patients the figure may have a human appearance or a blur. To develop the figure images of a man silhouette and a flattened circumference were used, and then the blur effect was applied so that the image provided an impression of an image with twisted visual focus. Figure 3 shows model types made of figures for the environment with man silhouette, where there are more blur in Figure 3(a), less blur in Figure 3(b), and medium blur Figure 3(c). Figure 4 illustrates the model of a circumference flattened by the sides. The animations were constructed so that there was some relation with what was being heard with the audio mentioned. The figure underwent a transformation of position on the x-axis corresponding to the camera and appeared in parts demarcated by the studies. The other figures, which are the man silhouette, appeared in the extreme part of the camera view, while the fade effect was applied by varying the fade-in and fade-out time according to the sound effects.

2.3.3. Modeling and Animation of Facial Transformation Effect. In facial modification, the OpenCV plugin for Unity available in the Unity Asset Store was used. Plugins function to include the use of OpenCV in Unity. As this package is an OpenCV Java clone, we can use the same API with OpenCV Java 3.1.0. It works with Unity free and pro with iOS, Android, Windows Store Apps 8.1 support, Windows Phone 8.1, Windows 10 UWP support (beta), Support Win, Mac, and Linux Standalone Support for Editor viewing. Its image processing is in real time using the Drive WebCamTexture capabilities (real-time face detection works flawlessly on iPhone 5). Version 1.9.0 of the plugin was used. With this plugin, we can proceed with the facial recognition and thus apply deformation and facial modification effects. In this work, to perform the facial modification, a dark circumference, see Figure 4, was placed over the eyes, accompanying the movements of the user's face through a 2D sprite provided by Unity Technologies for use in prototyping of games.

The process is aimed at simulating psychopathological changes experienced by the schizophrenia-afflicted individuals during their psychotic symptoms. Some patients report illusions involving the face of interlocutors, who may appear to patients as gloomy or even monstrous. As such, the simulated effect causes discomfort and estrangement feelings, rendering the experience more threatening.

3. Results

As a result of this work, a simulator was developed in an augmented-reality environment called "Schizophrenia Simulator" originally designed as the proposal in this work, so that the environment could be evaluated as to the possibility of being used as a tool to help reducing the stigma with reference to schizophrenia.

In this work, the analysis was made through observations and analysis of the questionnaire based on multiple comparison to evaluate the significance of the changes in the observed parameters.

3.1. Screenshots of the Developed Environment and Testing Used. Figure 5(a) shows the use of an environment simulation tool by a medical student, analyzing his behavior during his interaction with the augmented-reality environment through virtual reality glasses, as well as the usability

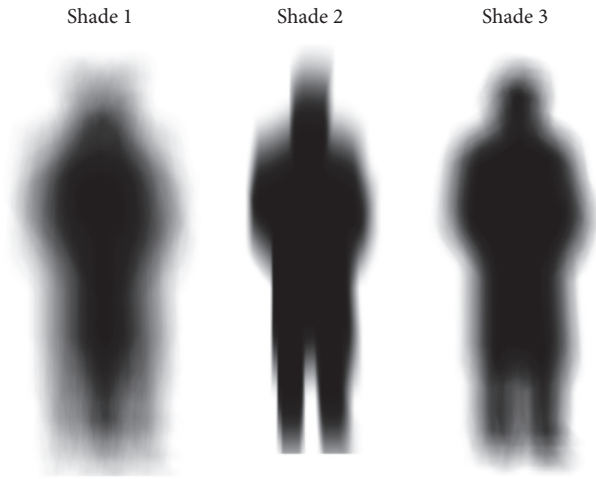

Figure 3: Models of figures with man silhouette: (a) more blur; (b) less blur; (c) middle blur.

Figure 4: Flat circumference figure model.

of the tool for possible adjustments for difficulties presented by users. From this test, it was acknowledged that initially the user had difficulties adjusting the glasses on his head, because in some cases the device did not fit properly because of its size. The infrastructure used for this test was a doctor's office of Frota Pinto Mental Hospital. A medical consultation was performed using a simulator, in which the volunteer (medical student) would answer some questions in a personal, professional, and logical reasoning scheme at a time when the schizophrenia psychotic-symptom simulating environment was running. Figure 5(b) shows how the medical student (patient) sees the visual-effect simulating figures of a schizophrenia psychotic symptom. Figure 5(c) shows the facial modification effect applied in the environment visualized by the medical student (patient) in real time.

3.2. Evaluation of the Virtual Environment. In order to validate the augmented-reality environment, medical students at Mental Hospital Frota Pinto were invited to take part in a simulation of augmented-reality environment using virtual reality glasses. They had the opportunity to use it to explore their possibilities and to analyze the feasibility of this augmented-reality environment as an alternative to help in decreasing the schizophrenia-related stigma. Twenty-one students from three universities in the state of Ceará were present for the environment trial. After using the augmented-reality environment, the medical students were submitted to three questionnaires: evaluation of the schizophrenia-related stigma, evaluation of the environment simulation, and evaluation of stigma after an augmented-reality simulation. According to Pfleeger (1994) and Wohlin et al. (2000), a questionnaire should be applied to analyze quantitative data before and/or after application of an approach.

The aim of the questionnaires was to be used as a prestudy in order to certify that important issues related to the study were anticipated, as well as to depict expectations, perceptions, and opportunities related to the possibility of the actual use of an augmented-reality environment in users as a complementary tool for understanding, stigma reduction, and prejudice. The questionnaire to assess the schizophrenia-related stigma consisted of 9 questions; the last one was related to José's story, a fictitious schizophrenic patient, in his first contact with the user, and the other 8 questions have a personal nature and asked whether there are cases of family members diagnosed with schizophrenia. The other questionnaires (Table 1 to Table 4) correspond to the evaluation of the proposed virtual environment on stigma reduction related to schizophrenia. In the last questionnaire evaluating the stigma after an augmented-reality simulation, questions related to José's story with a postsimulation feature were made.

Analyzing the results of the questionnaires application, see Table 1, it was found that in the questionnaire related to the environment simulation evaluation, on a 1–5 scale, of not at all to extremely, 42.85% of medical students chose the value 5, 42.85% of the students considered 4, and 14.30% chose 3,

Table 1: Questions and analysis of the medical students' responses on the proposed augmented-reality environment.

Objective questions made	Extremely [%]				Little [%]
	5	4	3	2	1
(1) Does the proposed environment ensure realism in the execution of its sound effects?	42.85	42.85	14.30	—	—
(2) Does the proposed environment ensure realism in the execution of its visual effects?	23.80	47.60	14.20	14.20	—
(3) Does the proposed environment create a sensation of immersion in reality (feeling of belonging to reality)?	9.50	57.15	28.60	4.75	—
(4) Was the simulation educational about schizophrenia symptoms?	80.95	19.05	—	—	—
(5) Should simulation make users more empathetic towards people with schizophrenia?	71.40	19.05	4.75	4.75	—

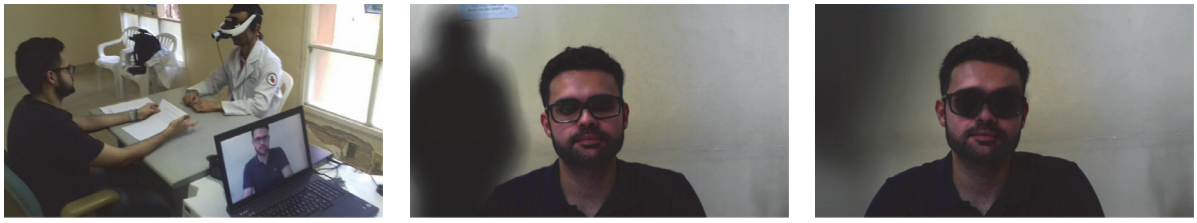

(a) (b) (c)

Figure 5: (a) Environment simulation with the medical student; (b) visualization in the simulation; (c) visualization of the facial modification in the simulation.

regarding the realism of the proposed environment in the execution of its sound effects; 23.80% of the medical students considered on a 1–5 scale, of not at all to extremely, value 5 and 47.60% considered 4, 14.20% of the medical students chose 3, and the same value chose 2, regarding the realism of the proposed environment in the execution of its visual effects. With regard to the augmented-reality environment proposed, there is the sensation of reality immersion (feeling of belonging to reality): 9.50% of the medical students considered on a 1–5 scale, of not at all to extremely, the value 5, while 57.15% considered 4 and 28.60% of the medical students chose 3 and 4.75% chose 2. On the other hand, 80.95% and 19.05% of the medical students, on a 1–5 scale, of not at all to extremely, chose 5 and 4, respectively, if the simulation was educational concerning the schizophrenia symptoms. Regarding whether the simulation should make users more empathetic towards schizophrenia-afflicted individuals, on a 1–5 scale, of not at all to extremely, 71.40% considered the value 5, 19.05% considered 4, 4.75% indicated 3, and the same value, 4.75%, chose 2. Table 1 shows the results quantitatively found with the objective questions of the questionnaire.

Questions on the environment simulation evaluation questionnaire related to the symptoms experienced during or shortly after the simulation reported that 19.05% of the medical students had a general malady (a general sensation of discomfort and uneasiness), fatigue, and "heavy headache" (due to the equipment weight); 4.76% said that they had problems with headache, dizziness with open eyes, and abdominal discomfort (stomachache). On the other hand, 38.10% reported they had a tired eye and blurred vision. It was found that 71.40% of the medical students had difficulty maintaining focus and concentration (seeing clearly and getting confused with the voices of the environment). 9.52% of the users reported sweating problems (perspiration or sweating) and nausea (an uncomfortable stomach feeling) and 14.30% reported dizziness with open eyes. Table 2 shows the analysis of the medical students' answers about the symptoms felt during or shortly after the simulation.

Table 2: Analysis of medical students' answers about the symptoms felt during or shortly after the simulation.

Questions related to symptoms	Reports [%]
(1) General malady	19.05
(2) Weariness	19.05
(3) Headache	4.76
(4) Eyestrain	38.10
(5) Difficulty to maintain focus	71.40
(6) Increased salivation	—
(7) Sweating	9.52
(8) Nausea	9.52
(9) Difficulty to concentrate	71.40
(10) "Heavy head"	19.05
(11) Blurry vision	38.10
(12) Dizziness with open eyes	14.30
(13) Dizziness with closed eyes	4.76
(14) Vertigo	—
(15) Abdominal discomfort	4.76
(16) Belch	—

Regarding the subjective questions, the medical students emphasize that the proposed environment stands out.

Positive Points. Positive points are as follows: being educational for health professionals and others, simulation in a suitable place rendering realistic effects, experience in understanding a psychotic patient's mind, reducing

Table 3: Questions and analysis of medical students' responses about the schizophrenia-related stigma evaluation.

Question/statement	No/nothing [%]					Very/completely [%]			
	1	2	3	4	5	6	7	8	9
I would feel sorry for José.	—	—	4.76	4.76	9.52	14.28	14.28	23.80	28.57
How dangerous do you think José is?	—	19.04	19.04	9.52	23.80	4.28	9.52	4.76	—
How scared would you feel with José?	19.04	14.28	23.80	9.52	9.52	9.52	4.76	9.52	—
I think José is guilty of his present condition.	90.47	—	9.52	—	—	—	—	—	—
I think it would be better for José's community that he be admitted to a psychiatric hospital.	52.38	19.04	4.76	—	9.52	4.76	4.76		4.76
How angry would you feel about José?	61.90	28.57	4.76	4.76	—	—	—	—	—
How likely is it that you will help José?	—	—	—	4.76	9.52	14.28	33.33	28.57	9.52
I would try to stay away from José.	33.33	19.04	9.52	4.76	—	19.04	14.28	—	—
Do you think José should be forced to take medical treatment, even against his will?	14.28	4.76	—	19.04	23.80	4.76	4.76	14.28	14.28

stigma and prejudice, showing the reality experienced by a schizophrenic, understanding the disease symptoms, interactivity being more attractive than the conventional information practice, and empathy with the schizophrenia symptoms.

Negative Points. Negative points were as follows: difficulty in putting glasses on the head, discomfort using the device, simulating in a more restless setting, difficulties in viewing for glasses users, voice-audio synchronization improvement, and possibility of causing uneasiness for some individuals.

Possibilities for Improvement. Possibilities for improvement include improving the external environment lighting, use of VR glasses with a better and more comfortable fitting and better closing of vision, adding real people in simulations, and figure-audio synchronization improvement.

In order to evaluate the impacts on the schizophrenia-related stigma, a questionnaire that evaluated questions about a fictional patient called "José" was applied, and these same questions were applied after using an augmented-reality environment, assessing the result changes. Appendix 2 of the questionnaire tells José's story. Questions and inquiries in the questionnaire comprised the following: "Would I feel sorry for José?," "How dangerous do you think José is?," "How scared would you feel with José?," "I think José is guilty of his present condition," "I think it would be better for José's community that he be admitted to a psychiatric hospital," "How angry would you feel about José?," "How likely is it that you will help José?," "I would try to stay away from José," and "Do you think José should be forced to take medical treatment, even against his will?" on a 1–9 scale, in which 1 corresponds to "no or nothing" and 9 corresponds to "very or completely."

During the results analysis of the application of the questionnaire related to the evaluation of the medical students' responses (Table 3) on the schizophrenia-related stigma, on a 1–9 scale of no/nothing and very/completely, 28.57% of the medical students gave value of 9; 23.80% considered 8; 14.28% chose 7; 6. 9.52% indicated value 5; 4.6% picked 4 and 3 for item "I would feel sorry for José," 4.76% of the medical students on a 1–9 scale of no/nothing and very/completely considered value 8, while 9.52% indicated 7; 14.20% recorded 6; 23.80% chose 5; 9.52% took 4 and 19.04% selected items 3 and 2 on the scale for item "How dangerous do you think José is?" Concerning the "How scared would you feel with José?" item, on a 1–9 scale of no/nothing and very/completely, 9.52% of the medical students scored values of 8, 6, 5, and 4; 4.76% indicated 7; 23.80% picked value 3; 14.28% chose value 2; and 19.04% scored 1. 9.52% of the medical students on a 1–9 scale of no/nothing and very/completely, item "I think José is guilty of his present condition" chose value of 3, and 90.47% picked value 1. Regarding item "I think it would be better for José's community that he be admitted to a psychiatric hospital" on a 1–9 scale of no/nothing and very/completely, 4.76% of the medical students pointed out values of 9, 7, 6, and 3. 9.52%, 19.04%, and 53.38% chose 5, 2, and 1, respectively. 4.76% of the medical students on a 1–9 scale of no/nothing and very/completely chose values 4 and 3, 28.57% selected 2, and 61.90% marked value 1 concerning item "How angry would you feel about José?" Values 9 and 5 were marked by 9.52% each. 28.57% selected value 8. 33.33% chose 7, 14.28% considered 6 and 4.76% scored 4 on a 1–9 scale of no/nothing and very/completely of item "How likely is it that you will help José?" In regard to "I would try to stay away from José," on a 1–9 scale of no/nothing and very/completely, 14.20% chose 7, while 19.04% selected 6 and 2; 4.76% considered 4. 9.52% chose 3 and 33.33% picked 1. On a 1–9 scale of no/nothing and very/completely relative to item "Do you think José should be forced to take medical treatment, even against his will?" 14.28% of the medical students considered values 9, 8, and 1, 4.76% selected 7, 6, and 2, 23.80% marked 5, and 19.04% pointed out 4. Table 3 shows the analysis of the medical students' responses about the schizophrenia-related stigma evaluation.

During the results analysis of the application of the questionnaire related to the evaluation of the medical students' answers (Table 4) on the evaluation of stigma after augmented-reality simulation, on a 1–9 scale of no/nothing and very/completely, 66.66% of the medical students marked value 9, 4.76% of the students considered 8, and 9.52% picked values 7, 6, and 5 concerning item "Would I feel sorry for José?" On a 1–9 scale of no/nothing and very/completely

Table 4: Questions and analysis of medical students' answers on the evaluation of stigma after augmented-reality simulation.

Question/statement	No/nothing [%]					Very/completely [%]			
	1	2	3	4	5	6	7	8	9
I would feel sorry for José.	—	—	—	—	9.52	9.52	9.52	4.76	66.66
How dangerous do you think José is?	4.76	14.28	14.28	9.52	9.52	9.52	19.04	19.04	—
How scared would you feel with José?	9.52	14.28	23.80	9.52	9.52	4.76	14.28	4.76	9.52
I think José is guilty of his present condition.	90.47	4.76	—	—	4.76	—	—	—	—
I think it would be better for José's community that he be admitted to a psychiatric hospital.	33.33	14.28	4.76	4.76	14.28	9.52	—	—	19.04
How angry would you feel about José?	76.19	4.76	14.28	4.76	—	—	—	—	—
How likely is it that you will help José?	—	—	—	—	9.52	14.28	14.28	9.52	52.38
I would try to stay away from José.	38.09	19.04	4.76	14.28	14.28	4.76	—	4.76	—
Do you think José should be forced to take medical treatment, even against his will?	4.76	14.28	4.76	—	23.80	—	9.52	14.28	28.57

of item "How dangerous do you think José is?", 19.04% of the medical students considered values 8 and 7, 9.52% chose values 6, 5, and 4, 14.28% marked values 3 and 2, and 4.76% scored 1. Concerning item "How scared would you feel with José?," on a 1–9 scale of no/nothing and very/completely, 9.52% scored 9, 5, 4, and 1, while 14.28% scored values 7 and 2; 4.76% of the medical students considered 8 and 6, and 23.80% selected value 3. On the 1–9 scale of no/nothing and very/completely of item "I think José is guilty for his present condition." 90.47% picked value 1, and 4.76% of the medical students considered values 5 and 2. In item "I think it would be better for José's community that he be admitted to a psychiatric hospital," on a 1–9 scale of no/nothing and very/completely, 19.04% of the medical students scored value 9. 9.52% chose value 6, 14.28% considered each 5 and 2, 4.76% scored 4 and 3, and 33.33% selected value 1. 4.46% of the medical students on a 1–9 scale of no/nothing and very/completely, for item "How angry would you feel about José?," chose values 4 and 2, 76.19% chose value 1, and 14.28% considered value 3. For item "How likely is it that you will help José?," on a 1–9 scale of no/nothing and very/completely, 9.52% of the medical students scored 8 and 5, 14.28% took 7 and 6, 52.38% scored value 9. 9.46% of the medical students considered, on a 1–9 scale of no/nothing and very/completely, values 8, 6, and 3, while 14.28% chose 5 and 4; 19.04% of the medical students chose 2; and 38.09% scored 1, for item "I would try to stay away from José." On a 1–9 scale of no/nothing and very/completely, 28.57% of the medical students considered value 9, 14.28% of the students chose 8 and 2, 9.52% chose 7, 23.80% scored value 5, and 4.76% chose values 3 and 1 for item "Do you think José should be forced to take medical treatment, even against his will?" Table 4 shows the analysis of the medical students' responses on the evaluation of stigma after the augmented-reality simulation.

After the simulation, as stated by the questionnaires, there was a trend to help the fictitious case patient. It is important to note that there was also an increase in the trend to hospitalize the patient and to treat him/her involuntarily.

These data indicate a change of posture after the simulation: while there was an increase in empathy, there was an apparent greater impression that the presented picture is serious. There was also an ascending trend after the simulation of considering José dangerous.

The results demonstrated an increase in the mean stigma score from 32.05 to 35.38 ($p = 0.004$), with statistical significance in pity, fear, and segregation. On the other hand, there was an increase in the average score referring to the probability of giving help, from 7.00 to 7.81 ($p = 0.034$). The tool had good acceptance, demonstrated by the average scores, for use as a teaching method (4.8), ability to increase the understanding of people with schizophrenia (4.57), realism of sound effects (4.29), realism of visual effects (3.81), and sensation of immersion in reality (3.71), on a scale from 1 (not at all) to 5 (extremely). In the analysis of the emotional impact of the tool on individuals submitted to the proposed environment, there was always some sort of symptom, and the most common one was the difficulty of maintaining focus and concentration.

Although this was an isolated intervention, there was an increase in the mean total stigma score; moreover, the simulation of psychotic symptoms through the augmented reality also resulted in increased scores of the possibility of helping a patient with psychosis. In general, the proposed system obtained a good overall evaluation. Notwithstanding these positive points, further improvements in the technique will be needed in order to decrease discomfort and improve concerns related to size and portability, so that the tool can have a large-scale usage. However, in its present form, the new tool can be used as an educational resource so that people can become more familiar with the symptoms of schizophrenia, and in doing so reducing its stigma and enhancing empathy for the patients.

The design of this study has limitations related to the long-term effect of VR in the change of attitude towards the bearer of schizophrenia. In cross-sectional analysis it is impossible to predict whether the experiment is capable of causing lasting stigma reduction.

4. Conclusion

This work presented the development of an augmented-reality environment simulating the schizophrenia psychotic

symptoms as an alternative tool to help reducing the schizophrenia-related stigma so that there is no delay at the beginning of treatment. We specifically addressed the use of an augmented-reality environment through Sony HMZ-T2 glasses, which proved useful for the simulation of visual and auditory effects, managing to transmit the visual effects well with few exceptions, such as people wearing glasses, who could not see appropriately. The Panasonic RP-BTGS10 headset, which uses bone tissue to transfer sound vibrations to the nervous system, is promising, lightweight, and affordable.

According to the results, the medical students and specialist/psychiatrist included the use of the augmented-reality environment as an educational resource for health professionals as well as for family members and society in search of reducing the disease-related stigma. In the analysis of the emotional impact of the tool on individuals submitted to the proposed environment, it shall be noticed that there was always some sort of symptom, while the difficulty of maintaining focus and concentration was the most common one.

The tool developed in this work showed very promising results, and can be applied in educational environments (groups of schools, colleges, and technical training), in hospitals and clinics, and in the training and awareness-raising of groups that may come into contact with psychosis-afflicted patients, such as police officers, municipal guards, and family members, amongst many other applications. It will be necessary to further improve the technique in order to decrease discomfort and improve concerns related to size and portability, so that it can have a large-scale application. In general, the new tool can be used as an educational resource so that people become more familiar with the schizophrenia symptoms, and in so doing reducing its stigma and enhancing empathy for the patients.

Longitudinal evaluation studies with one or multiple exposures to the RV tool can demonstrate if the effects of the experiment are lasting over time, as well as determining the need to repeat the experiment to consolidate the expected effect. Future studies may also indicate whether the effect of immersion experience can be reinforced by supplementary psychoeducation measures such as short lectures on schizophrenia, for example.

Disclosure

The funding sponsors had no role in the design of the study; in the collection, analyses, or interpretation of data; in the writing of the manuscript; or in the decision to publish.

Conflicts of Interest

All authors declare that they have no conflicts of interest.

Authors' Contributions

Rafael D. de C. Silva, Saulo G. C. Albuquerque, and Artur de V. Muniz designed the augmented-reality tool and performed the experiments, as well as investigation. Victor Hugo C. Albuquerque and Saulo G. C. Albuquerque analyzed the data. Victor Hugo C. Albuquerque, Sidarta Ribeiro, and Pedro P. Rebouças Filho are responsible for the funding acquisition and project administration. All authors contributed to and have approved the final manuscript.

Acknowledgments

VHCA acknowledges the sponsorship from the Brazilian National Council for Research and Development (CNPq) via Grant no. 301928/2014-2.

References

[1] WHO, "The world health report 2001," Mental Health: New UnderstanDing, New Hope, World Health Organization, 2001, http://www.who.int/whr/2001/en/whr01_djmessage_po.pdf.

[2] WHO, "Mental health," Schizophrenia, World Health Organization, 2017, http://www.who.int/mental_health/management/schizophrenia/en/.

[3] C. R. Bowie and P. D. Harvey, "Cognitive deficits and functional outcome in schizophrenia," *Neuropsychiatric Disease and Treatment*, vol. 2, no. 4, pp. 531–536, 2006.

[4] E. M. Joyce and J. P. Roiser, "Cognitive heterogeneity in schizophrenia," *Current Opinion in Psychiatry*, vol. 20, no. 3, pp. 268–272, 2007.

[5] P. Dalgalarrondo, "Psicopatologia e semiologia dos transtornos mentais, Artmed Editora, 2009".

[6] American Psychiatric Association, *Diagnostic And Statistical Manual of Mental Disorders (DSM-5)*, American Psychiatric Pub, 4th edition, 2013.

[7] N. C. Andreasen, "The diagnosis of schizophrenia," *Schizophrenia Bulletin*, vol. 13, no. 1, pp. 9–22, 1987.

[8] D. Freeman, "Studying and treating schizophrenia using virtual reality: a new paradigm," *Schizophrenia Bulletin*, vol. 34, no. 4, pp. 605–610, 2008.

[9] W. Veling, S. Moritz, and M. Van Der Gaag, "Brave new worlds - Review and update on virtual reality assessment and treatment in psychosis," *Schizophrenia Bulletin*, vol. 40, no. 6, pp. 1194–1197, 2014.

[10] N. Yee and J. N. Bailenson, "Walk a mile in digital shoes: the impact of embodied perspective-taking on the reduction of negative stereotyping in immersive virtual environments," in *Proceedings of Presence 2006: The 9th Annual International Workshop on Presence*, Cleveland, Ohio, USA, 2006.

[11] D. L. Penn, J. D. Ivory, A. Judge, and etal., "The virtual doppelganger: effects of a virtual reality simulator on perceptions of schizophrenia," *The Journal of nervous and mental disease*, vol. 198, no. 6, pp. 437–443, 2010.

[12] M. Rus-Calafell, J. Gutiérrez-Maldonado, and J. Ribas-Sabaté, "A virtual reality-integrated program for improving social skills in patients with schizophrenia: A pilot study," *Journal of Behavior Therapy and Experimental Psychiatry*, vol. 45, no. 1, pp. 81–89, 2014.

[13] S.-H. Park, J. Ku, J.-J. Kim et al., "Increased personal space of patients with schizophrenia in a virtual social environment," *Psychiatry Research*, vol. 169, no. 3, pp. 197–202, 2009.

[14] C. Hawco, L. Buchy, M. Bodnar et al., "Source retrieval is not properly differentiated from object retrieval in early schizophrenia: an fMRI study using virtual reality," *NeuroImage: Clinical*, vol. 7, pp. 336–346, 2015.

[15] K. Han, I. Young Kim, and J.-J. Kim, "Assessment of cognitive flexibility in real life using virtual reality: a comparison of healthy individuals and schizophrenia patients," *Computers in Biology and Medicine*, vol. 42, no. 8, pp. 841–847, 2012.

[16] S. Moritz, M. Voigt, U. Köther et al., "Can virtual reality reduce reality distortion? Impact of performance feedback on symptom change in schizophrenia patients," *Journal of Behavior Therapy and Experimental Psychiatry*, vol. 45, no. 2, pp. 267–271, 2014.

[17] R. M. E. M. Costa and L. A. V. De Carvalho, "The acceptance of virtual reality devices for cognitive rehabilitation: a report of positive results with schizophrenia," *Computer Methods and Programs in Biomedicine*, vol. 73, no. 3, pp. 173–182, 2004.

[18] M. Fornells-Ambrojo, C. Barker, D. Swapp, M. Slater, A. Antley, and D. Freeman, "Virtual reality and persecutory delusions: safety and feasibility," *Schizophrenia Research*, vol. 104, no. 1-3, pp. 228–236, 2008.

[19] J. Counotte, R. Pot-Kolder, A. M. van Roon, O. Hoskam, M. van der Gaag, and W. Veling, "High psychosis liability is associated with altered autonomic balance during exposure to Virtual Reality social stressors," *Schizophrenia Research*, vol. 184, pp. 14–20, 2016, http://www.sciencedirect.com/science/article/pii/S0920996416305187.

[20] P. Salgado-Pineda, R. Landin-Romero, F. Portillo et al., "Examining hippocampal function in schizophrenia using a virtual reality spatial navigation task," *Schizophrenia Research*, vol. 172, no. 1-3, pp. 86–93, 2016, http://www.sciencedirect.com/science/article/pii/S0920996416300895.

[21] M. J. Smith, M. F. Fleming, M. A. Wright et al., "Virtual reality job interview training and 6-month employment outcomes for individuals with schizophrenia seeking employment," *Schizophrenia Research*, vol. 166, no. 1-3, pp. 86–91, 2015, http://www.sciencedirect.com/science/article/pii/S0920996415002790.

[22] M. J. Smith, E. Ginger, M. Wright, K. Wright, M. Bell, and M. Fleming, "Poster #S266 virtual reality job interview training," *Schizophrenia Research*, vol. 153, 1, p. S186, 2014, http://www.sciencedirect.com/science/article/pii/S0920996414705456.

[23] W. Veling, R. Pot-Kolder, J. Counotte, and M. van der Gaag, "Psychosis liability, paranoia and distress in experimental virtual reality social environments," *Schizophrenia Research*, vol. 153, 1, pp. S377–S378, 2014.

[24] J. Counotte, R. Pot-Kolder, A. M. van Roon, O. Hoskam, M. van der Gaag, and W. Veling, "High psychosis liability is associated with altered autonomic balance during exposure to virtual reality social stressors," *Schizophrenia Research*, vol. 184, pp. 14–20, 2017.

[25] G. Thornicroft, E. Brohan, D. Rose, N. Sartorius, and M. Leese, "Global pattern of experienced and anticipated discrimination against people with schizophrenia: a cross-sectional survey," *The Lancet*, vol. 373, no. 9661, pp. 408–415, 2009.

[26] A. H. Crisp, M. G. Gelder, S. Rix, H. I. Meltzer, and O. J. Rowlands, "Stigmatisation of people with mental illnesses," *The British Journal of Psychiatry*, vol. 177, no. 1, pp. 4–7, 2000.

[27] D. L. Bower and W. G. Pettit, "The albuquerque police departments crisis intervention team," *FBI Law Enforcement Bulletin*, vol. 70, no. 2, pp. 1–6, 2001.

[28] N. Rüsch, K. Heekeren, A. Theodoridou et al., "Stigma as a stressor and transition to schizophrenia after one year among young people at risk of psychosis," *Schizophrenia Research*, vol. 166, no. 1-3, pp. 43–48, 2015.

[29] S. Sharples, S. Cobb, A. Moody, and J. R. Wilson, "Virtual reality induced symptoms and effects (VRISE): comparison of head mounted display (HMD), desktop and projection display systems," *Displays*, vol. 29, no. 2, pp. 58–69, 2008.

[30] J. Tichon, J. Banks, and P. Yellowlees, "The development of a virtual reality environment to model the experience of schizophrenia," in *Computational Science — ICCS 2003*, vol. 2659 of *Lecture Notes in Computer Science*, pp. 11–19, Springer, Berlin, Germany, 2003.

[31] P. W. Corrigan, S. B. Morris, P. J. Michaels, J. D. Rafacz, and N. Rüsch, "Challenging the public stigma of mental illness: a meta-analysis of outcome studies," *Psychiatric Services*, vol. 63, no. 10, pp. 963–973, 2012.

[32] F. Fernández-Aranda, S. Jiménez-Murcia, J. J. Santamaría et al., "Video games as a complementary therapy tool in mental disorders: playMancer, a European multicentre study," *Journal of Mental Health*, vol. 21, no. 4, pp. 364–374, 2012.

[33] J. K. Luiselli and A. J. Fischer, *Computer-Assisted and Web-Based Innovations in Psychology, Special Education, and Health*, Academic Press, Cambridge, Mass, USA, 2016.

[34] F. F. Rocha, C. M. de Lima, A. R. O. Guerra, and M. M. Marcelino, "Optimization of dense clouds to viewer softwares in virtual reality environment," in *Vi National Congress of Mechanical Engineering*, 2010.

[35] J. Carmigniani, B. Furht, M. Anisetti, P. Ceravolo, E. Damiani, and M. Ivkovic, "Augmented reality technologies, systems and applications," *Multimedia Tools and Applications*, vol. 51, no. 1, pp. 341–377, 2011.